RESPONSE OF ISOLATED STRUCTURES UNDER BI-DIRECTIONAL EXCITATIONS OF NEAR-FIELD GROUND MOTIONS

A THESIS SUBMITTED TO
THE GRADUATE SCHOOL OF NATURAL AND APPLIED SCIENCES
OF
MIDDLE EAST TECHNICAL UNIVERSITY

BY

GÖKHAN ÖZDEMİR

IN PARTIAL FULFILLMENT OF THE REQUIREMENTS
FOR
THE DEGREE OF DOCTOR OF PHILOSOPHY
IN
CIVIL ENGINEERING

MAY 2010

Approval of the thesis:

RESPONSE OF ISOLATED STRUCTURES UNDER BI-DIRECTIONAL EXCITATIONS OF NEAR-FIELD GROUND MOTIONS

submitted by **GÖKHAN ÖZDEMİR** in partial fulfillment of the requirements for the degree of **Doctor of Philosophy in Civil Engineering Department, Middle East Technical University** by,

Prof. Dr. Canan Özgen _____
Dean, Graduate School of **Natural and Applied Sciences**

Prof. Dr. Güney Özcebe _____
Head of Department, **Civil Engineering**

Assoc. Prof. Dr. Uğurhan Akyüz _____
Supervisor, **Civil Engineering Dept., METU**

Examining Committee Members:

Prof. Dr. Polat Gülkan _____
Civil Engineering Dept., METU

Assoc. Prof. Dr. Uğurhan Akyüz _____
Civil Engineering Dept., METU

Prof. Dr. Sinan Altın _____
Civil Engineering Dept., Gazi University

Assoc. Prof. Dr. Ahmet Yakut _____
Civil Engineering Dept., METU

Assist. Prof. Dr. Alp Caner _____
Civil Engineering Dept., METU

Date: _____

I hereby declare that all information in this document has been obtained and presented in accordance with academic rules and ethical conduct. I also declare that, as required by these rules and conduct, I have fully cited and referenced all material and results that are not original to this work.

Name, Last Name: Gökhan Özdemir

Signature :

ABSTRACT

RESPONSE OF ISOLATED STRUCTURES UNDER BI-DIRECTIONAL EXCITATIONS OF NEAR-FIELD GROUND MOTIONS

Özdemir, Gökhan

Ph.D., Department of Civil Engineering

Supervisor: Assoc. Prof. Dr. Uğurhan Akyüz

May 2010, 178 pages

Simplified methods of analysis described in codes and specifications for seismically isolated structures are always used either directly in special cases or for checking the results of nonlinear response history analysis (RHA). Important predictions for seismically isolated structures by simplified methods are the maximum displacements and base shears of the isolation system. In this study, the maximum isolator displacements and base shears determined by nonlinear RHA are compared with those determined by the equivalent lateral force (ELF) procedure in order to assess the accuracy of the simplified method in the case of bi-directional excitations with near-field characteristics. However, although there are currently many methods for ground motion selection and scaling, little guidance is available to classify which method is more appropriate than the others in any applications. Features of this study are that the ground motions used in analysis are selected and scaled using contemporary concepts and that the ground excitation is considered bi-

directional. The variations in response of isolated structures due to application of ground motions uni-directionally and bi-directionally are also studied by employing a scaling procedure that is appropriate for the bi-directional analysis. The proposed new scaling methodology is an amplitude scaling method that is capable of preserving the horizontal orthogonal components and it is developed especially for dynamic analysis of isolated structures. Analyses are conducted for two different symmetric reinforced concrete isolated structure for two different soil conditions in structural analysis program SAP2000. Effect of asymmetry in superstructure on isolator displacement is also investigated with further analyses considering 5% mass eccentricity at each floor level. Furthermore, once the significance of the orthogonal horizontal component on the response of isolation system is shown, the biaxial interaction of hysteretic behavior of lead rubber bearings is implemented in OpenSees by developing a subroutine which was not readily available.

Keywords: near-field records, bi-directional excitations, seismic isolation, lead rubber bearing, coupled behavior.

ÖZ

SİSMİK İZOLASYON UYGULANAN YAPILARIN YAKIN KAYNAKLI VE ÇİFT DOĞRULTULU DEPREM HAREKETLERİ ALTINDAKİ DAVRANIŞI

Özdemir, Gökhan
Doktora, İnşaat Mühendisliği Bölümü
Tez Yöneticisi: Doç. Dr. Uğurhan Akyüz

Mayıs 2010, 178 sayfa

Sismik izolasyon uygulanan binalar için şartnamelerde tariflenen basit hesap yöntemleri genellikle ya sınırlı özel durumlarda ya da doğrusal olmayan dinamik analiz sonuçlarının doğrulanmasında kullanılmaktadır. Sismik izolasyon uygulanan binalarda basitleştirilmiş yöntemler ile hesaplanmaya çalışılan iki önemli unsur maksimum izolatör deplasmanı ve maksimum kesme kuvveti değerleridir. Sunulan bu çalışmada sözü edilen iki unsurun basitleştirilmiş yöntem ile hesaplanmasının yakın kaynaklı depremlerin her iki doğrultuda da etkisi dikkate alındığında ne derece başarılı olduğu incelenmektedir. Bunun için doğrusal olmayan dinamik analizlerden elde edilen sonuçlar basitleştirilmiş yöntem yardımıyla hesaplanan değerler ile karşılaştırılmıştır. Ancak kullanılacak depremlerin seçimi ve ölçeklendirilmesi üzerine bir çok metot olmasına rağmen hangi metodun hangi şartlar altında kullanılacağına yönelik yeterli bilgi bulunmamaktadır. Bu çalışmanın önemli katkılarından birtanesi de kullanılan depremlerin seçiminde ve

ölçeklendirilmesinde güncel metotların uygulanması ve bunlar yapılırken de deprem kayıtlarının her iki yatay bileşeninin dikkate alınmasıdır. Bu çalışmada ayrıca geliştirilen deprem ölçeklendirme yöntemi kullanılarak sismik izolasyonlu yapıların tek ve çift doğrultulu deprem hareketleri altında davranışlarındaki değişimler de incelenmiştir. Analizler iki farklı simetrik betonarme bina ve iki farklı zemin sınıfı dikkate alınarak SAP2000 adlı yapısal analiz programı kullanılarak gerçekleştirilmiştir. Bunlara ek olarak, üst yapıdaki düzensizliğin izolatör deplasmanları üzerindeki etkisi her kat seviyesinde %5 kütle ekzantrikliği olduğu kabul edilerek incelenmiştir. Son olarak da çift doğrultulu deprem analizlerinin doğru bir şekilde analiz edilebilmesi amacıyla izolatörlerin her iki yatay doğrultudaki bağımlı hareketi OpenSees isimli programa modellenerek eklenmiştir.

Anahtar Kelimeler: Yakın kaynaklı depremler, çift doğrultulu analiz, sismik izolasyon, kurşun çekirdekli kauçuk yastık, bağımlı hareket

To my family and my wife…

ACKNOWLEDGEMENTS

I would like to express my appreciation to my supervisor Dr. Uğurhan Akyüz for his encouragement and friendship throughout the study.

I would also like to express my gratitude to Professor Michael Constantinou for his guidance and support during the course of this work. His constant availability for consultation and outstanding expertise in his research field combined ideally to provide me with an invaluable education experience.

I would further like to thank to Professor Julian Bommer for his guidance throughout the study. I am grateful to him for providing the documents I needed whenever I asked.

I also would like to extend my thanks to my friends for cheering me up. My deepest thanks goes to İbrahim Erdem, Sezgin Küçükçoban, Başar Özler, Cengiz Nergiz and Koray Sığırtmaç.

There are also a group of friends who in their own way made hours in METU more pleasant, such as: Nadide Seyhun, Pınar Onay Durdu, Seval Pınarbaşı, Emre Akın, Barış Erdil.

My special thanks goes to a computer guy Onur Soysal who I shared the house in Buffalo with. He means a lot to me for his devotion and his great helps.

There is also one I have to mention especially: Beyhan Bayhan. He is one of a kind person who makes most of the things more easier to me during the time I spend in METU. I deeply appreciate both his help and his friendship.

This study is funded by both the METU Scientific Research Projects Coordination Grant No: BAP-08-11-DPT2002K120510 and Scientific and Technological Research Council of Turkey (TUBITAK), which are also gratefully acknowledged.

Finally, I wish to dedicate this dissertation to my wife Aslı, to anne ve babam Hacer and Nüveren Özdemir, and to kardeşim Hakan. Their enduring love and

unconditional support and encouragement have been the real inspiration that I always felt during the course of this study.

TABLE OF CONTENTS

ABSTRACT iv
ÖZ. vi
ACKNOWLEDGEMENTS ix
TABLE OF CONTENTS xi
LIST OF TABLES xiv
LIST OF FIGURES xv
CHAPTER
1. INTRODUCTION 1
1.1 Seismic Isolation 1
1.2 History of Seismic Isolation 2
1.3 Types of Seismic Isolation Devices 5
1.3.1 Elastomeric Bearings 6
1.3.2 Sliding Isolation Systems 8
1.4 Response of Seismic Isolated Structures 9
1.5 Research Objective and Scope 15
1.6 Organization of the Dissertation 17
2. SELECTION AND SCALING OF GROUND MOTION RECORDS FOR DYNAMIC ANALYSIS 19
2.1 Introduction 19
2.2 Methods for Selection and Scaling of Ground Motion Records 19
2.2.1 Criteria for Selecting Ground Motion Records 21
2.2.1.1 Earthquake Magnitude 22
2.2.1.2 Distance to the Fault Rupture 23
2.2.1.3 Soil Classification 23
2.2.1.4 Additional Parameters in Selection of Records 24
2.2.2 Scaling of Ground Motion Records 24
2.2.2.1 Amplitude Scaling at Fundamental Period of Structure 26
2.2.2.2 Amplitude Scaling at a Range of Periods 26

2.2.3 Scaling Factor and Number of Ground Motions Considered..... 27
2.3 Selected Ground Motion Records 28
2.4 Scaling of Selected Ground Motion Records..... 33
3. MODELING OF ISOLATION SYSTEM AND SUPERSTRUCTURE..... 41
3.1 Introduction..... 41
3.2 Parameters Defining the Isolation System 41
3.3 Design of Isolation System 44
3.3.1 Damping Reduction Factor *B*..... 46
3.4 Modeling of Isolated Structures..... 49
3.4.1 Modeling of Superstructure..... 50
3.4.2 Modeling of Isolation System 54
4. EVALUATION OF EQUIVALENT LATERAL FORCE PROCEDURE IN ESTIMATING SEISMIC ISOLATOR DISPLACEMENTS AND SHEAR FORCES..... 65
4.1 Introduction..... 65
4.2 Analyses Conducted..... 67
4.2.1 Equivalent Lateral Force (ELF) Procedure..... 67
4.2.2 Nonlinear Response History Analysis (RHA) 68
4.3 Analysis Results..... 69
4.3.1 Maximum Isolator Displacements 69
4.3.1.1 Effect of Damping (Q/W Ratio)..... 74
4.3.1.2 Effect of Isolation Period T..... 76
4.3.2 Maximum Base Shear 76
4.3.2.1 Effect of Damping (Q/W Ratio)..... 78
4.3.2.2 Effect of Isolation Period T..... 79
5. RESPONSE OF ISOLATED STRUCTURES UNDER BI-DIRECTIONAL EXCITATIONS OF NEAR-FIELD GROUND MOTIONS 82
5.1 Introduction..... 82
5.2 Analyses Conducted..... 84
5.2.1 Non-linear Response History Analysis..... 84
5.3 Analysis Results..... 85
5.3.1 Response of Isolation System 86
5.3.1.1 Maximum Isolator Displacements 86

5.3.1.2 Maximum Base Shear 91
5.3.2 Response of Superstructure 93
5.3.2.1 Floor Accelerations 95
5.3.2.1.1 Effect of Isolation Period 96
5.3.2.1.2 Effect of Damping (Q/W Ratio) 99
5.3.2.2 Roof Displacements 106
5.3.2.3 Interstory Drifts 106
6. TORSIONAL AMPLIFICATIONS IN ISOLATOR DISPLACEMENTS DUE TO ASYMMETRIES IN THE SUPERSTRUCTURE 111
6.1 Introduction 111
6.2 Analyses Conducted 113
6.2.1 Non-linear Response History Analyses 113
6.2.2 Sensitivity Analyses 114
6.2.3 Effects of *Q*/*W* Ratio and Soil Condition 117
6.2.4 Evaluation of Simplified Method 121
7. IMPLEMENTATION OF BI-AXIAL INTERACTION OF HYSTERETIC FORCE-DEFORMATION RELATION OF ISOLATORS IN OPENSEES . 125
7.1 Introduction 125
7.2 OpenSees 126
7.3 CoupledMaterial Class 127
7.4 Verification of Implemented Material Model 130
7.4.1 Verification for Individual LRBs 130
7.4.2 Verification for LRBs Mounted Under Superstructure 134
7.5 Significance of Coupled Material Model 139
8. CONCLUSIONS AND RECOMMENDATIONS 144
8.1 Summary 144
8.2 Conclusions 145
8.3 Recommendations for Future Studies 149
REFERENCES 151
APPENDIX A. SOURCE CODE FOR COUPLED MATERIAL MODEL 161
CURRICULUM VITAE 177

LIST OF TABLES

TABLES

Table 1.1 History of seismic isolation (taken from lecture notes of Aseismic Base Isolation by Constantinou, 2009)..... 3
Table 2.1 Characteristics of near-field ground motions recorded at stiff soil..... 30
Table 2.2 Characteristics of near-field ground motions recorded at soft soil. 31
Table 2.3 Scale factors for stiff and soft soil records..... 38
Table 3.1 Values of damping reduction factor *B* in codes and specifications. 48
Table 3.2 Mechanical properties of concrete material 52
Table 3.3 Periods of the first three fixed-base modes of analyzed 3-story building..... 54
Table 3.4 Periods of the first three fixed-base modes of analyzed 7-story building..... 54
Table 3.5 Parameters for isolation systems considered in this study..... 57
Table 3.6 Properties of LRB modeled for 3S RC building at stiff soil..... 60
Table 3.7 Properties of LRB modeled for 3S RC building at soft soil. 60
Table 3.8 Properties of LRB modeled for 7S RC building at stiff soil..... 61
Table 3.9 Properties of LRB modeled for 7S RC building at soft soil. 61
Table 7.1 Data used in analysis of LRB1..... 131
Table 7.2 Data used in analysis of LRB2..... 131
Table 7.3 Characteristics of EE record. 133

LIST OF FIGURES

FIGURES

Figure 1.1 Effect of period shift in an isolated structure on accelerations (top) and displacements (bottom) (taken from Constantinou *et al*., 2007). 2
Figure 1.2 Early attempts for energy dissipation at Parthenon (taken from lecture notes of Aseismic Base Isolation by Constantinou, 2009). 4
Figure 1.3 Laminated RB (taken from Kunde and Jangid, 2003). 6
Figure 1.4 LRB (taken from Kunde and Jangid, 2003)..... 7
Figure 1.5 Multiple-core LRB (taken from Constantinou *et al*., 2007). 7
Figure 1.6 FPS (taken from Kunde and Jangid, 2003). 9
Figure 1.7 USC hospital building: elevation, plan, and sensor locations (taken from Nagarajaiah and Sun, 2000). 11
Figure 1.8 Recorded peak values of accelerations in EW (left) and NS (right) directions (adopted from Nagarajaiah and Sun, 2000). 11
Figure 1.9 Comparison between isolated and fixed-base cases in EW (top) and NS (bottom) directions (taken from Nagarajaiah and Sun, 2000). 12
Figure 2.1 Significance of forward directivity effect. 29
Figure 2.2 Near-field ground motion records of stiff soil bin: (a) velocity and (b) acceleration time histories. 32
Figure 2.3 Near-field ground motion records of soft soil bin: (a) velocity and (b) acceleration time histories. 33
Figure 2.4 Acceleration spectra of the selected ground motions and their mean spectra: (a) for stiff soil, (b) for soft soil. 35
Figure 2.5 Target MCE response spectra and mean SRSS spectra of scaled motions after first phase of scaling a) for stiff soil records, b) for soft soil records. 38

Figure 2.6 Target MCE response spectra and mean SRSS spectra of scaled motions after second phase of scaling for stiff (left side) and soft (right side) soil cases. 40
Figure 3.1 Bilinear force-deformation relation of an isolator. 42
Figure 3.2 Comparison of calculated *B* values of records in stiff soil bin with that of values presented in codes and specifications: for ASCE (top) and for Eurocode 8 (bottom). 50
Figure 3.3 Comparison of calculated *B* values of records in soft soil bin with that of values presented in codes and specifications: for ASCE (top) and for Eurocode 8 (bottom). 51
Figure 3.4 Idealized model of 3-story isolated RC building: (a) plan, (b) elevation, (c) 3D layout, and (d) isolation system. 53
Figure 3.5 Determination of isolator parameters by means of simplified method of analysis considering: normalized base shear (left) and isolator displacement (right). 56
Figure 3.6 Bi-linear force-deformation relation of a LRB in stiff soil for 3-story RC structure: a) $Q/W = 0.04$; b) $Q/W = 0.06$; c) $Q/W = 0.08$; d) $Q/W = 0.10$. ... 62
Figure 3.7 Bi-linear force-deformation relation of a LRB in soft soil for 3-story RC structure: a) $Q/W = 0.08$; b) $Q/W = 0.10$; c) $Q/W = 0.12$; d) $Q/W = 0.14$. ... 62
Figure 3.8 Bi-linear force-deformation relation of a LRB in stiff soil for 7-story RC structure: a) $Q/W = 0.04$; b) $Q/W = 0.06$; c) $Q/W = 0.08$; d) $Q/W = 0.10$. ... 63
Figure 3.9 Bi-linear force-deformation relation of a LRB in soft soil for 7-story RC structure: a) $Q/W = 0.08$; b) $Q/W = 0.10$; c) $Q/W = 0.12$; d) $Q/W = 0.14$. ... 63
Figure 3.10 3-D model of 3-story RC structure in SAP2000. 64
Figure 3.11 3-D model of 7-story RC structure in SAP2000. 64
Figure 4.1 Response spectra for design and maximum considered earthquakes of stiff and soft soil classifications (adopted from TEC(2007)). 68
Figure 4.2 Application of bi-directional ground motion excitations. 69
Figure 4.3 Comparison of displacements obtained by D_{ELF} and D_{RHA} for stiff (top) and soft (bottom) soil conditions. 71

Figure 4.4 Comparison of displacements obtained by D_{ELF} and D_{RHA} Code for: (a) stiff soil and (b) soft soil. 73
Figure 4.5 Ratio of D_{RHA} to D_{ELF} versus Q/W ratio at stiff soil conditions for MCE. 74
Figure 4.6 Ratio of D_{RHA} to D_{ELF} versus Q/W ratio at soft soil conditions for MCE. 75
Figure 4.7 Comparison of results of RHA and ELF procedure on isolation system shear force for stiff (top) and soft (bottom) soil conditions. 77
Figure 4.8 Ratio of V_{RHA} to V_{ELF} versus Q/W ratio at stiff soil conditions for MCE. 79
Figure 4.9 Ratio of V_{RHA} to V_{ELF} versus Q/W ratio at soft soil conditions for MCE. 80
Figure 5.1 Application of uni-directional and bi-directional ground motion excitations. 85
Figure 5.2 Variation of maximum isolator displacements with isolation period and damping for stiff soil condition. 87
Figure 5.3 Variation of maximum isolator displacements with isolation period and damping for soft soil condition. 88
Figure 5.4 Normalized isolator displacements obtained from bi-directional excitations for 3- and 7-story buildings and stiff and soft soil conditions. 89
Figure 5.5 Variation of D_{bi}/D_{uni} ratio versus Q/W ratio as a function of isolation period T for stiff (top) and soft (bottom) soil conditions 90
Figure 5.6 Variation of maximum base shears with isolation period and damping for stiff soil condition. 92
Figure 5.7 Variation of maximum base shears with isolation period and damping for soft soil condition 93
Figure 5.8 Variation of V_{bi}/V_{uni} ratio versus Q/W ratio as a function of isolation period T for stiff (top) and soft (bottom) soil conditions 94
Figure 5.9 Variations in Acc_{bi} of 3-story RC building as a function of isolation period T for various Q/W ratios under stiff soil condition 96

Figure 5.10 Variations in Acc_{bi} of 3-story RC building as a function of isolation period *T* for various *Q*/*W* ratios under soft soil condition. 97
Figure 5.11 Variations in Acc_{bi} of 7-story RC building as a function of isolation period *T* for various *Q*/*W* ratios under stiff soil condition..... 98
Figure 5.12 Variations in Acc_{bi} of 7-story RC building as a function of isolation period *T* for various *Q*/*W* ratios under soft soil condition. 99
Figure 5.13 Variations in Acc_{bi} of 3-story RC building as a function of *Q*/*W* ratios for various isolation periods *T* under stiff (left) and soft (right) soil conditions. 102
Figure 5.14 Variations in Acc_{bi} of 7-story RC building as a function of *Q*/*W* ratios for various isolation periods *T* under stiff (left) and soft (right) soil conditions. 103
Figure 5.15 Comparison of bi-directional and uni-directional accelerations of 3-story RC building for stiff (left) and soft (right) soil conditions. 104
Figure 5.16 Comparison of bi-directional and uni-directional accelerations of 7-story RC building for stiff (left) and soft (right) soil conditions. 105
Figure 5.17 Variation of roof displacements in isolated 3-story building for stiff (top) and soft (bottom) soil conditions. 107
Figure 5.18 Variation of roof displacements in isolated 7-story building for stiff (top) and soft (bottom) soil conditions. 108
Figure 5.19 Variation of interstory drift ratios with increasing *Q*/*W* ratio in 3-story RC building. 109
Figure 5.20 Variation of interstory drift ratios with increasing *Q*/*W* ratio in 7-story RC building. 110
Figure 6.1 Locations of eccentricity in superstructure. 115
Figure 6.2 Amplifications in isolator displacements due to isolation period under increasing *Q*/*W* ratios in 3-story superstructure. 116
Figure 6.3 Distribution of amplification in isolator displacements due to asymmetry in superstructure for each individual case of stiff soil conditions. 117
Figure 6.4 Distribution of amplification in isolator displacements due to asymmetry in superstructure for each individual case of soft soil conditions.. 118

Figure 6.5 Variation of D_{RHA}^{ECC}/D_{RHA} ratios due to increase in Q/W ratio for 3-story isolated structure for stiff (top) (T = 3.0 sec.) and soft (bottom) (T = 3.5 sec.) soil conditions. 119
Figure 6.6 Variation of D_{RHA}^{ECC}/D_{RHA} ratios due to increase in Q/W ratio for 7-story isolated structure for stiff (top) (T = 3.0 sec.) and soft (bottom) (T = 3.5 sec.) soil conditions. 120
Figure 6.7 Schematic view of parameters affecting torsional response of isolated structures..... 121
Figure 6.8 D_{RHA}^{ECC} versus D_{ELF}^{ECC} for 3-story superstructure in stiff (top) (T = 3.0 sec.) and soft (bottom) (T = 3.5 sec.) soil conditions. 122
Figure 6.9 D_{RHA}^{ECC} versus D_{ELF}^{ECC} for 7-story superstructure in stiff (top) (T = 3.0 sec.) and soft (bottom) (T = 3.5 sec.) soil conditions. 123
Figure 7.1 Material class hierarchy in OpenSees. 127
Figure 7.2 Analyzed isolator LRB1 (taken from Constantinou *et al*., 2007)..... 132
Figure 7.3 Analyzed isolator LRB2 (1 inch = 25.4 mm) (taken from Constantinou *et al*., 2007) 132
Figure 7.4 Acceleration spectra of EE record. 133
Figure 7.5 Force-displacement loops of isolator LRB1 135
Figure 7.6 Force-displacement loops of isolator LRB2 136
Figure 7.7 Variation of hysteretic components Z_x and Z_y with time for LRB1. 137
Figure 7.8 Variation of hysteretic components Z_x and Z_y with time for LRB2. 138
Figure 7.9 Symmetric 3S isolated RC building. 139
Figure 7.10 Comparison of coupled and uncoupled behavior of LRB1. 141
Figure 7.11 Comparison of coupled and uncoupled behavior of LRB2. 142
Figure 7.12 Comparison of coupled and uncoupled behavior of 3S isolated RC building. 143

CHAPTER 1

INTRODUCTION

1.1 SEISMIC ISOLATION

Seismic isolation is an innovative seismic design tool that provides protection for structures from probable damages of earthquakes. In this technique, the primary goal is to reduce the seismic demand rather than increasing the strength of the system. The basic idea behind the seismic isolation is to decouple the superstructure from the catastrophic effects of strong ground motions by shifting the fundamental period of the structure away from the dominant periods of the ground motions. This is achieved by providing necessary amount of flexibility and damping at the isolation level. Hence, the transmission of excessive effects of earthquake motion from ground level to the superstructure is reduced. The improvement in the seismic performance of the structure by decoupling the effects of ground motion from the structure yields to minimized floor accelerations and interstory drifts. Thus, seismic base isolation is one of the most effective methods which protect both the structural members and the valuable equipments inside.

The logic of period shift owing to isolation system is shown schematically in Figure 1.1. As it is shown, increasing the period of the system can yield reduced accelerations so that the structure will be subjected to low inertia forces. However, increasing the isolation period results in increased displacements. By increasing the damping in the isolation system, those excessive displacements can be limited.

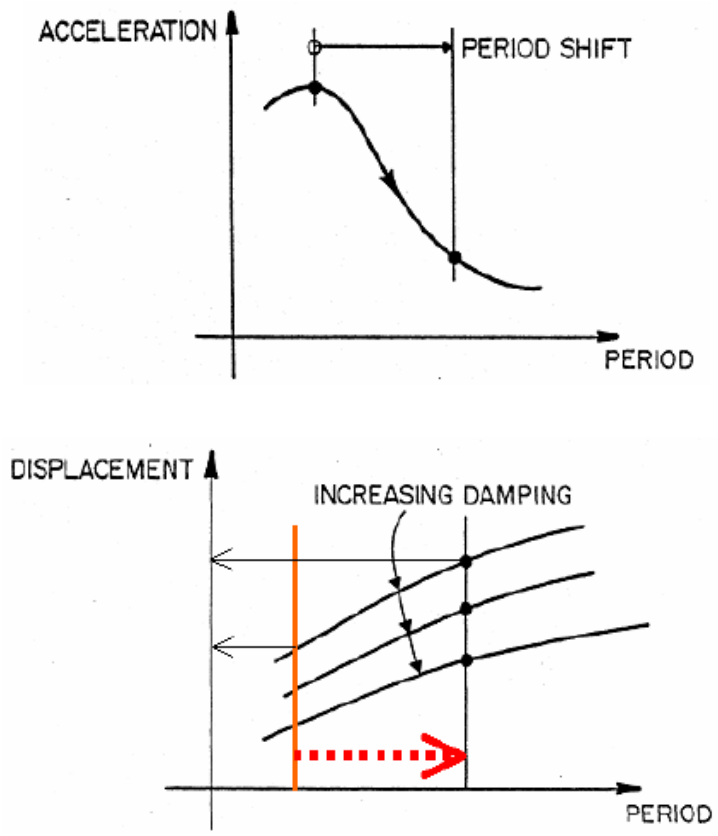

Figure 1.1 Effect of period shift in an isolated structure on accelerations (top) and displacements (bottom) (taken from Constantinou *et al*., 2007).

The need for superiority of seismic isolation in enhancing the performance of structures may arise under the following situations:

- Increased building safety and post earthquake operability is desired
- Reduced lateral design forces are desired
- An existing structure is not currently safe for earthquake loads.

1.2 HISTORY OF SEISMIC ISOLATION

Although seismic isolation has become a popular and effective technique in the seismic design of structures in the last two decades, primitive applications of

seismic isolation goes back to very early times in history. Development of seismic isolation concept is presented in Table 1.1.

Table 1.1 History of seismic isolation (taken from lecture notes of Aseismic Base Isolation by Constantinou, 2009).

440 BC	**Ancient Greece**	**Parthenon** DID THEY KNOW?
1320	**Kunya-Urgench, Turkmenistan**	**Minaret with reed mat foundation**
1870	**US**	**Touaillon of San Francisco obtains US Patent**
1907	**US**	**J. Bechtold of Germany obtains US Patent**
1909	**US**	**Dr. Calantarients of England applies for US Patent**
1909	**Italy**	**Messina-Reggio Commission considers seismic isolation**
1921	**Japan**	**Imperial Hotel, Tokyo designed by Frank Lloyd Wright**
1929	**US**	**Flexible first story (Mantel)**
1930	**New Zealand**	**de Montalk applies for Patent**
1959	**USSR**	**First engineered seismic-isolated building (cable suspended) in Ashkhabad, Turkmenistan**
1963	**USSR**	**Ellipsoid-shaped roller bearings Sevastopol**
1969	**Yugoslavia**	**Rubber isolation system, Skopje**
1970s	**France** **New Zealand** **US**	**EDF system, GAPEC isolators** **Lead/rubber bearings** **Prof. Kelly starts testing at UCB**
1980s	**US, Japan**	**Research, applications**

The basic idea behind the seismic isolation is to dissipate energy by means of implemented equipments instead of the structures's itself during the ground motions. In this sense, the ancient attempts for dissipation of energy was encountered in Pantheron at 440 BC, and used to connect the marbles in construction of columns of the structures. Connection detail of those marbles is given in Figure 1.2. In that primitive example of seismic isolation, marbles were connected by means of lead and iron plates permitting the relative movement of marbles through the height of the column. The energy dissipation is sustained by that movement. Displacements of marbles result in yielding of connection materials which provides the resisting force.

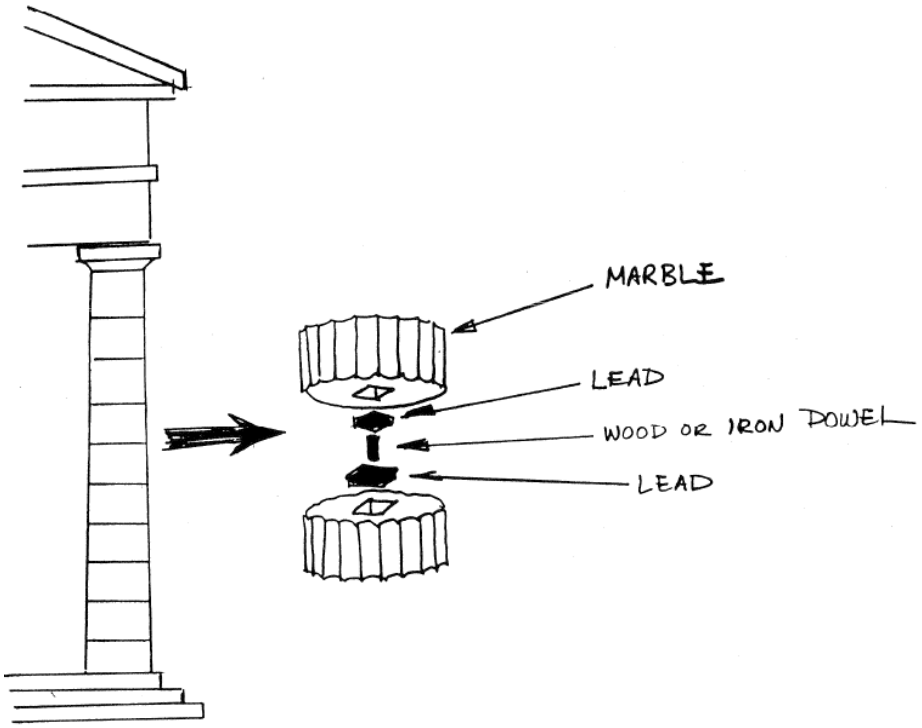

Figure 1.2 Early attempts for energy dissipation at Parthenon (taken from lecture notes of Aseismic Base Isolation by Constantinou, 2009).

The first example of seismic isolation system in modern times was proposed by Touaillon at 1870 and followed by Bechtold and Calantarients in the early 1900s.

Touaillon obtained a patent for his innovative design approach where the superstructure was mounted on spherical balls that are free to move in any direction. Touaillon stated that "*It will be seen that by this device the earthquake motion would be communicated to the superstructure without shock, and consequently no injury would result from such motion to a properly constructred building*". Similarly, the concept proposed by Calantarients in 1909 involved decoupling of the building form its foundation by introducing a talc layer in between (Naeim and Kelly, 1999). Parallel to initiation of seismic isolation approaches, Italian government considered the isolation as a seismic resistant design strategy in 1909, for the first time.

The concept of seismic isolation has become a practical reality within the last 40 years with the development of multilayer elastomeric bearings (Naeim and Kelly, 1999). In 1969, it was the first time that rubber isolation system was employed to protect a structure from earthquakes in Skopje, Macedonia. Since, there is not any reinforcement in the bearings used there, the horizontal and vertical stiffness of that system are more or less the same. As a result, the building will bounce and rock in case of an earthquake. That unwilling behavior of rubber bearings was enhanced by addition of thin steel plates to provide high vertical stiffness. Then, in New Zealand in 1975, it was proposed that a central lead plug be inserted into laminated rubber bearing to introduce additional vertical stiffness as well as damping characteristics in the bearing.

1.3 TYPES OF SEISMIC ISOLATION DEVICES

Being a well established technology now, seismic isolation has been used in many structures. Construction of isolation systems in those structures are mainly composed of two systems, i.e. elastomeric bearings and sliding systems. Regardless of the type of isolation system, what is expected from any kind of isolation system can be listed as follows (Skinner *et al*., 1993; Naeim and Kelly, 1999):

- Deformability under frequent static load (i.e. initial stiffness)

- Yielding force and displacement
- Capacity of self-centering after deformation
- Vertical stiffness.

1.3.1 Elastomeric Bearings

Most widely used elastomeric bearings are laminated rubber bearing (RB) and lead rubber bearing (LRB). The basic components of laminated RB system are steel and rubber plates built in the alternate layers as shown in Figure 1.3. Those internal reinforcing steel plates are referred as shims. Steel shims reduce the lateral bulging of the rubber and increase the vertical stiffness of the bearing. The dominant features of laminated RB system are the parallel action of linear spring and damping. The damping constant of the system varies considerably with the strain level of the bearing (Kunde and Jangid, 2003).

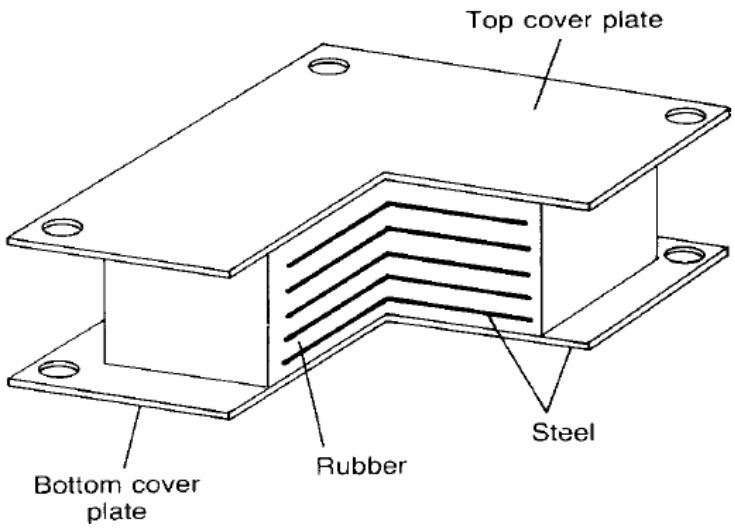

Figure 1.3 Laminated RB (taken from Kunde and Jangid, 2003).

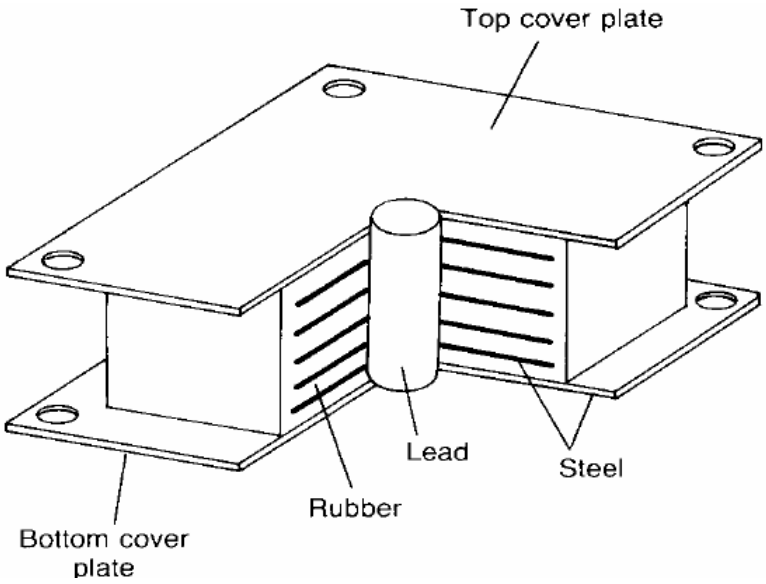

Figure 1.4 LRB (taken from Kunde and Jangid, 2003).

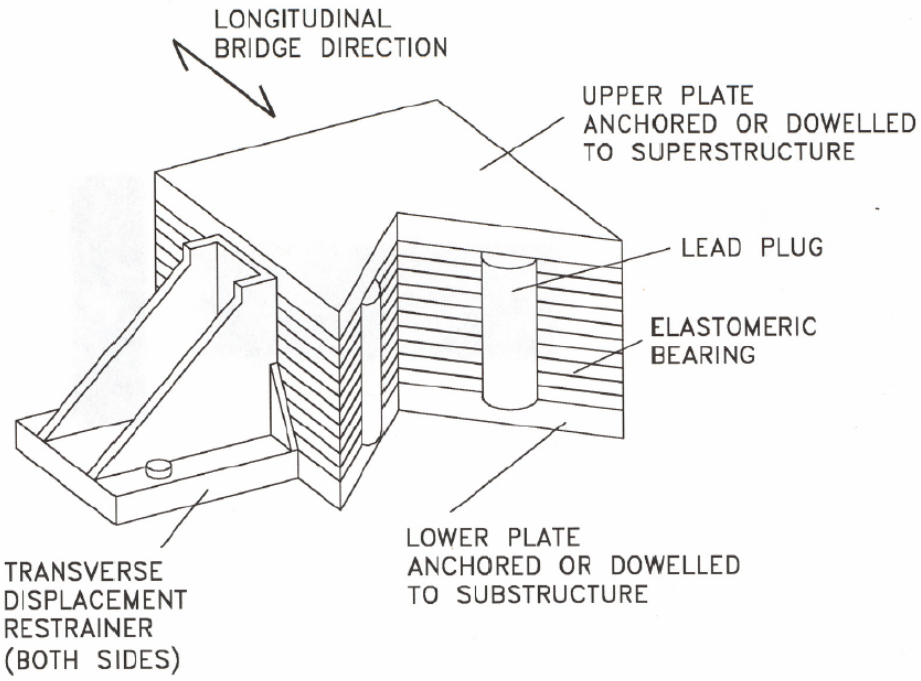

Figure 1.5 Multiple-core LRB (taken from Constantinou *et al*., 2007).

Schematic view of Lead-rubber bearing (LRB), which has the enhanced hysteretic behavior compared to laminated RB, is given in Figure 1.4. These bearings are similar to the laminated rubber bearing but a central lead core is used to provide an additional means of energy dissipation by increasing damping of the bearing. Kunde and Jangid (2003) stated that "*this system provides the combined features of vertical load support, horizontal flexibility, restoring force and damping in a single unit*".

LRBs have also been constructed using multiple lead cores. There are a few applications of multiple core LRBs in Japan and one in California, all in bridges (Kalpakidis, 2008). Figure 1.5 shows a view of multiple core LRB used for bridge applications in Japan.

1.3.2 Sliding Isolation Systems

Another seismic isolation technique is the application of sliding isolation devices. In those systems, isolation is achieved through sliding and friction. The main advantages of sliding isolation systems compared to elastomeric bearings are (i) frictional base isolation system is effective for a wide range of frequency input, (ii) frictional force is proportional to the mass of the structure and the center of mass and center of resistance of the sliding support coincides. Hence, the torsional effects produced by the asymmetric buildings are diminished.

When the notion of sliding bearings is combined with the concept of a pendulum type response, the obtained system is called friction pendulum system (FPS) (Zayas *et al*., 1990). In FPS (Figure 1.6), isolation is achieved through sliding of the articulated slider on the concave surface. Energy dissipation is provided by friction between the composite bearing material and the stainless steel overlay. The stainless steel overlay is attached to the concave plate. The sliding interface plays a crucial role in response of the FPS. Frictional response of the interface is affected by slider diameter, contact pressure, sliding velocity, and temperature. The key components of FPS are concave and housing plates, articulated slider, bearing material, and stainless steel overlay (Constantinou *et al*., 2007).

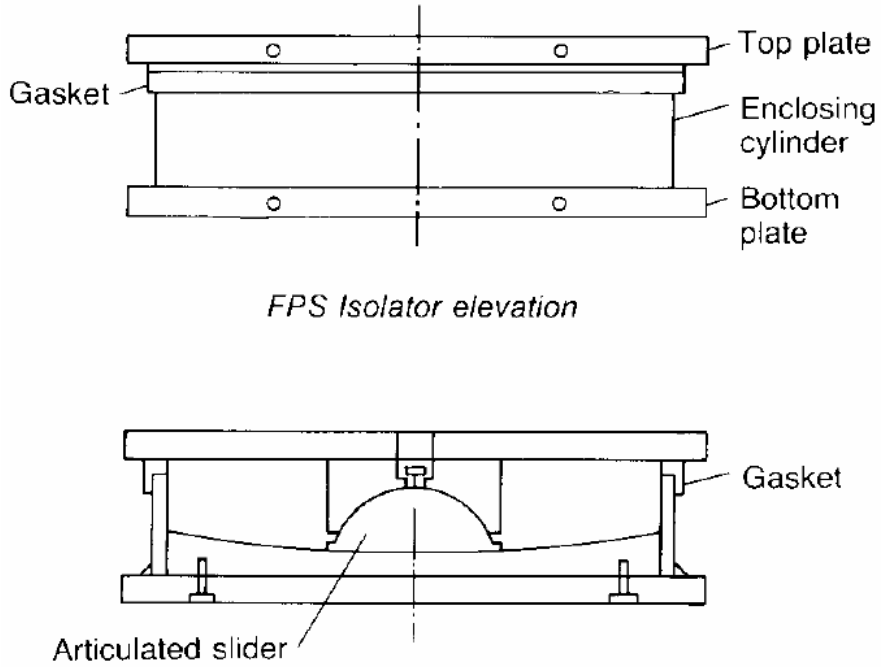

Figure 1.6 FPS (taken from Kunde and Jangid, 2003).

1.4 RESPONSE OF SEISMIC ISOLATED STRUCTURES

Numerous studies have demonstrated the benefits of seismic isolation for the mitigation or elimination of damage in structural and nonstructural components during severe earthquakes (Kelly, 1986; Buckle and Mayes, 1990; Jangid and Datta, 1995; Matsagar and Jangid, 2004; Huang *et al*., 2007). In addition, response of isolated structures subjected to far-field ground motions has also been studied by several researchers (Hwang, 1996; Hwang *et al*., 1997; Franchin *et al*., 2001; Dicleli and Buddaram, 2006). However, several seismologists have suggested that isolated structures are prone to large pulse type ground motions (Heaton *et al*. 1995; Hall *et al*. 1995). Ground motions which contain pulses in their velocity and displacement traces impose larger demands on structures than ordinary ground

motions. These ground motions are usually near-field ground motions with forward directivity effects (Alavi and Kravinkler, 2004). As the number of near-field records increases, the performance of the seismic isolation systems in near-field sites have been started to be questioned. It is reported that the existence of pulse type ground motions in the near-field sites decreases the performance of isolation systems. Because, pulse type ground motions result in a sudden burst of energy into the structure that must be dissipated immediately.

Although there are several analytical studies investigating the response of isolated structures, there are only a few cases where isolated structures have experienced significant ground shaking. The effectiveness of the isolation systems with LRB has been confirmed during the 1994 Northridge and 1995 Kobe earthquakes (Asher *et al*., 1997; Stewart *et al*., 1999; Nagarajaiah and Sun, 2000; Kani *et al*., 2006). One of the buildings that experienced the 1994 Northridge earthquake was University of Southern California (USC) hospital in which the used isolation system composed of 68 LRBs and 81 laminated RBs. USC hospital provided invaluable data because it was instrumented by the California Strong Motion Instrumentation Program (CSMIP) (Shakal *et al*., 1994) and placed several sensors through the plan and elevation of the building. Locations of the sensors placed in the USC hospital are given in Figure 1.7. The recorded absolute accelerations through the height of the building by means of those sensors are presented in Figure 1.8. Nagarajaiah and Sun (2000) performed an analytical study to investigate the efficiency of isolation system by comparing the recorded data with that of the fixed base simulation of USC hospital. Results in terms of maximum story shears and drift ratios are shown in Figure 1.9. Nagarajaiah and Sun (2000) stated that "*the fixed-base superstructure would experience three times more story shears and drifts than that of the superstructure in the isolated case*". Authors concluded that "*it is evident from the evaluation that the USC hospital performed well and base isolation was effective in reducing the response and providing earthquake protection*".

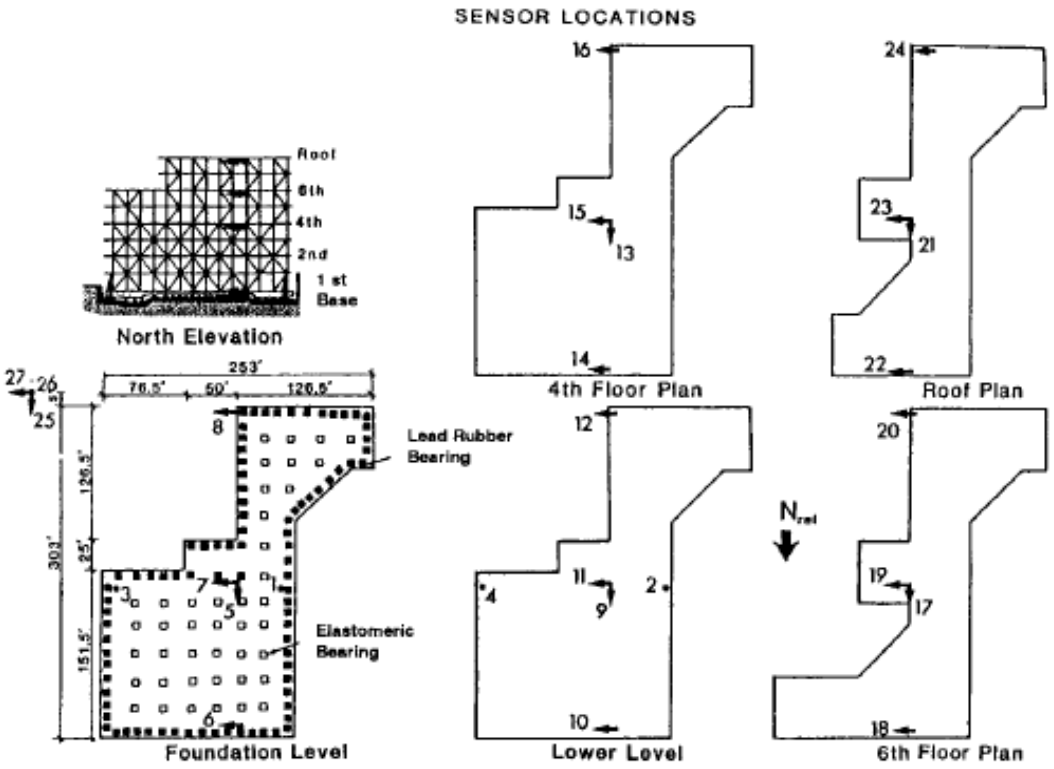

Figure 1.7 USC hospital building: elevation, plan, and sensor locations (taken from Nagarajaiah and Sun, 2000).

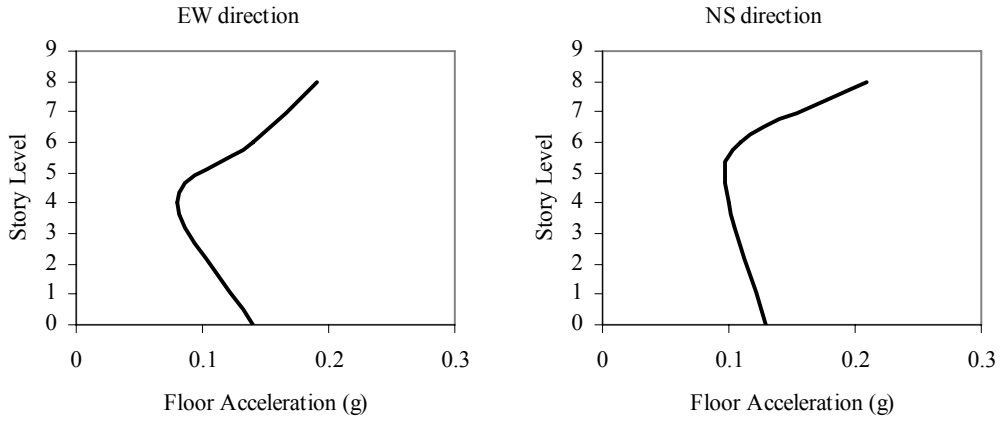

Figure 1.8 Recorded peak values of accelerations in EW (left) and NS (right) directions (adopted from Nagarajaiah and Sun, 2000).

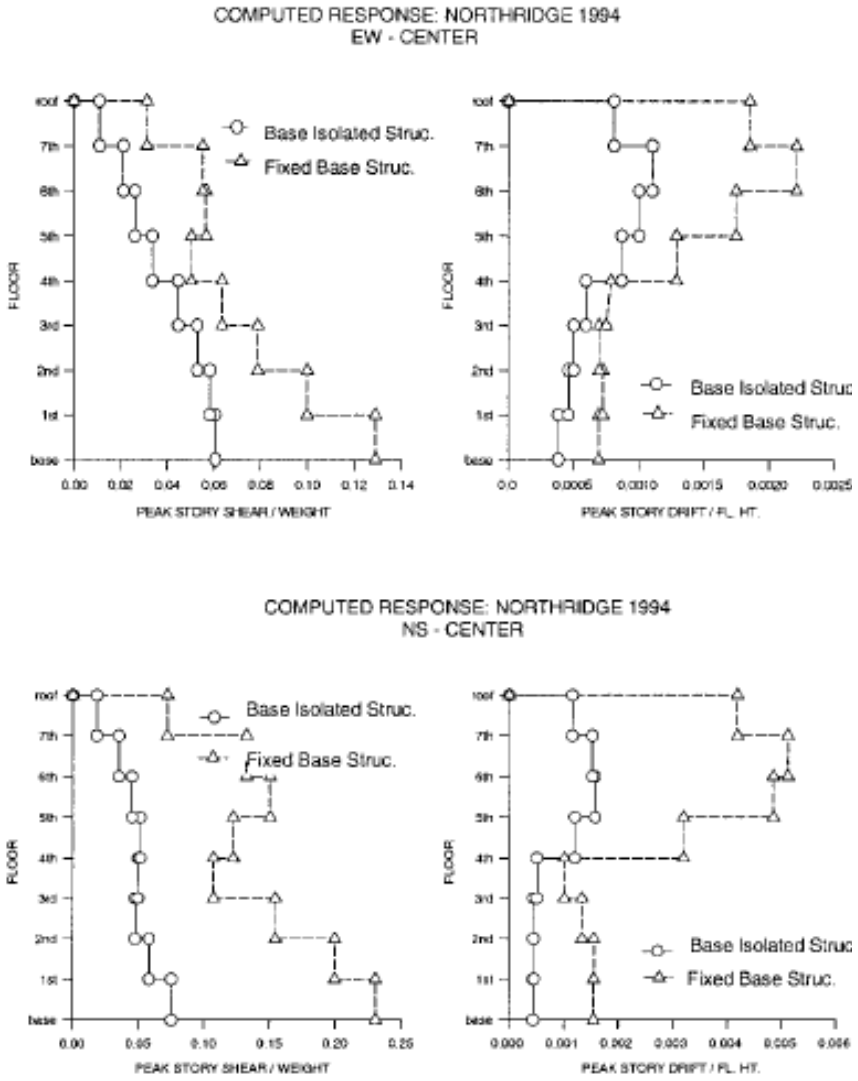

Figure 1.9 Comparison between isolated and fixed-base cases in EW (top) and NS (bottom) directions (taken from Nagarajaiah and Sun, 2000).

However, there are two cases where poor performance of seismic isolation has been observed (Constantinou *et al.*, 2007). First one was observed during the Kushiro-Oki earthquake in 1993 due to overloading in the bridge piers. Overloading has occurred because of stiffening in the seismic isolators due to very cold temperatures (Sato *et al.*, 1994). The second poor performance was observed at the Bolu Viaduct in the 1999 Duzce earthquake. The failure has occurred because the

displacement capacity of the isolation system was exceeded significantly (Roussis *et al*., 2003). Consequently, several researchers interested in the behavior of isolation systems under near-field ground motions and numerous analytical studies have been done (Makris and Chang, 2000; Jangid and Kelly, 2001; Dicleli and Buddaram, 2007).

Makris and Chang (2000) studied the efficiency of seismic isolation in protection of structures against pulse type near-field ground motions. Authors generated "*physically realizable trigonometric pulses*" to be representative of pulse type motions and they also verified the resemblance of generated motions by comparing with the real data of recorded near-field earthquakes. They considered 1-DOF and 2-DOF idealizations of seismic isolated structures. Makris and Chang (2000) concluded that seismic isolation is also beneficial under near-field conditions. Authors also revealed that yield displacement of the bilinear force-deformation relation of isolators is not an important parameter. Instead, Makris and Chang (2000) stated that the important parameter is the yield force.

In their study, Jangid and Kelly (2001) considered six pairs of records all of which contain a distinct pulse type behavior and grouped as fault-normal and fault-parallel. They investigated the response of a single DOF isolated system subjected to bi-directional excitations, simultaneously. In that study, isolation system was modeled with linear force-deformation behavior. Authors stated that "*fault-normal and fault-parallel components of near-field records are uncorrelated, with the fault-normal response significantly larger than the fault-parallel response*". Based on this phenomenon, authors further reported that the maximum isolator displacement will not be the vectorial sum of the maximum displacements in each horizontal direction, but simply the one in the fault-normal direction. Jangid and Kelly (2001) concluded that "*the resultant isolator displacement is not more than five percent of peak displacement due to the normal component of the near-field motion (for damping ratios greater than five percent and periods greater than 2 sec)*".

Being a very recent study, Dicleli and Buddaram (2007) focused on the accuracy of simplified method of analysis in prediction of maximum isolator

displacements in seismically isolated bridges. The evaluation of simplified method of analysis was conducted by comparing the seismic response quantities obtained from simplified method with that of nonlinear response history analysis (RHA). For analysis purpose, Dicleli and Buddaram (2007) simulated pulse type motions with decaying sinusoid. Considered isolators were modeled with a bilinear force-deformation relation. Authors concluded that simplified method generally overpredicts the maximum isolator displacements compared to that of nonlinear RHA. Dicleli and Buddaram (2007) also reported that the accuracy of simplified method in prediction of response in isolated bridges decreases as both the distance from fault and yield force of the bilinear force-deformation relation increases.

Although previous studies revealed invaluable outputs for understanding the response of isolated structures, most of them did not consider the effect of bi-directional excitations by applying the ground motions uni-directional. On the other hand, in recent years, it is stated that the coupling of the two orthogonal components of ground motions is important (Mosqueda *et al*., 2004). Although the number of ground motions (5) used is not enough and corresponds only to one soil group, in their study, Mosqueda *et al*. (2004) revealed that the maximum isolator displacements are underestimated when only one component of earthquake excitation is considered.

In addition, most of the previous studies also did not consider the variation in response of isolated structures due to soil condition. However, some recent studies made an emphasis on the response of isolation systems under near-field earthquake excitations when they are used in soft soil conditions (Chung *et al*., 1999; Pavlou and Constantinou, 2004). It was reported that the effectiveness of the isolation system decreases in soft soil conditions.

Even though there are numerous analytical and experimental studies regarding the response of isolation systems under uni-directional earthquake excitation, in contrast little data exist on the bi-directional response of isolated structures. Furthermore, the existing data is limited to implementation of ground motion in only one horizontal direction, ground motions recorded in a specific soil type or in a

specific region, and differentiation in the idealization of force-deformation behavior of the isolators. Thus, it is worthy to study the response of isolation systems including above mentioned approaches.

1.5 RESEARCH OBJECTIVE AND SCOPE

Having a highly nonlinear characteristic, response of isolated structures is highly dependent on the selection and scaling of the ground motions. Especially, procedure followed for scaling of records is crucial when pairs of motions are of concern. The issue of scaling time histories has been, and continues to be, the most troubling aspect of development and application of design ground motion criteria for seismic isolated structures. The way selected for scaling of the records may yield under-estimated or over-estimated performance of isolated structures by simplified method of analysis. Simplified method of analysis is an iterative analysis procedure and uses the effective stiffness, effective period and effective damping of the isolation system.

The first objective of this study is to propose a scaling procedure for recorded ground motions to be used in nonlinear RHA of isolated structures. The implemented scaling approach is consistent with contemporary practices in the representation of site-specific response spectra by the selected ground motion assemblies. The proposed method is then used to assess the accuracy of the simplified method of analysis, which is described in codes, in predicting the response quantities of isolated structures subjected to ground motions with near-field characteristics. Hence, maximum isolator displacements and maximum base shears calculated by simplified method of analysis are compared with that of the nonlinear RHA to achieve this first objective where both orthogonal horizontal components of the records are applied simultaneously. Conducted nonlinear RHA's consider a three story multi-degree-of-freedom (MDOF) reinforced concrete system and modeled to be representative of the application in Turkey.

The second objective is to investigate the effect of orthogonal horizontal components on the response of isolated structures when ground motions are applied

bi-directionally. Thus, a series of nonlinear RHA were conducted under both uni-directional and bi-directional excitations to obtain amplification in response quantities of isolated structures such as isolator displacements, base shears, roof displacements, floor accelerations, and drift ratios. Here, effect of superstructure on the response of isolated structures is also considered by conducting the nonlinear RHA with two different systems. Those two systems are composed of three- and seven-story reinforced concrete structures.

The third objective is to assess the accuracy of the procedure described in simplified method of analysis to incorporate the amplifications in isolator displacements due to asymmetry in the superstructure. For this purpose, eccentric three- and seven-story superstructures were isolated and subjected to bi-directional excitations. The amplified isolator displacements obtained from nonlinear RHA are compared with those calculated by simplified method.

All of the analyses performed to achieve the above listed objectives are conducted in two groups so that the effect of soil classification can be obtained clearly. These groups are classified according to shear wave velocities of the records. Average shear wave velocities of the first group are between 180 m/sec. and 360 m/sec. (site class D as per NEHRP) whereas ground motion records in the second group have shear wave velocities in the range of 360 m/sec. – 760 m/sec. (site class C as per NEHRP). Each group has eleven pairs of records where both of the horizontal components are considered.

The final objective of this study is to develop a material class that can capture the coupled behavior of isolation system with isolators having bilinear force deformation relation and implement it into OpenSees. The implemented model is also tested by comparing the results of the model with that of the structural analyses program SAP2000.

1.6 ORGANIZATION OF THE DISSERTATION

This dissertation is composed of eight main chapters with the brief contents given as follows:

Chapter 1: General overview of the seismic isolation and previous studies investigated the response of isolated structures under various parameters.

Chapter 2: Description of methods for selection and scaling of ground motion records used in literature. Selected near-field ground motions grouped according to soil classes. Explanation of the proposed new scaling method for pairs of records used in bi-directional analyses of isolated structures.

Chapter 3: Description and selection of parameters defining the isolation system. Definition of the iterative method of simplified analysis for design of isolators. Modeling of both isolation system and superstructures.

Chapter 4: Evaluation of the simplified method of analysis in prediction of response quantities of an isolated three-story RC structure.

Chapter 5: Comparison of response quantities of isolated three- and seven-story RC structures obtained under uni-directional and bi-directional excitations.

Chapter 6: Investigation of amplifications in the isolator displacements due to asymmetry in superstructure. Assessment of the accuracy of simplified methods in prediction of those amplified displacements.

Chapter 7: Implementation and verification of the biaxial material model for isolators that can capture the coupled behavior of isolation system under bi-directional excitations.

Chapter 8: A brief summary and the conclusions are given and recommendations for future studies are provided.

CHAPTER 2

SELECTION AND SCALING OF GROUND MOTION RECORDS FOR DYNAMIC ANALYSIS

2.1 INTRODUCTION

Understanding the selection and scaling of ground motion records becomes more crucial as the nonlinear RHA become common in practice. There are currently many methods for ground motion selection and scaling, but little guidance is available to classify which method is more appropriate than the others in any application. Hence, the choice of those methods mainly depends on researcher. The distributions of demand on structural and nonstructural components are directly affected by the procedures used to select and scale earthquake ground motions.

The information presented in this chapter summarizes procedures available for researchers during the selection and scaling of records. Important points that should be kept in mind during the selection and scaling of records are emphasized in Section 2.2. Then, Section 2.3 presents the selected ground motions where as Section 2.4 describes the new scaling method proposed in this study for dynamic analysis of isolated structures.

2.2 METHODS FOR SELECTION AND SCALING OF GROUND MOTION RECORDS

The general way of representing the ground motions for design of earthquake resistant structures is handled by the use of response spectrum of accelerations or displacements. Codified procedures address to a specific spectra to be used in

simplified methods such as equivalent lateral force or spectral modal methods. Those spectra are mostly achieved by scaling an elastic spectrum. Nevertheless, there can be some conditions where scaling the elastic response spectrum to obtain the structural response is not suitable. Those cases can be classified as: irregular structures (both in elevation and plan); structures where contribution of higher modes are more likely; structures with special features like isolation systems. In such cases, one may need to employ dynamic analysis (ASSHTO, 1999; ASCE, 2005; EN, 2005).

The basic requirement of a dynamic analysis is to use a suitable set of ground motion records. However, there is little guidance to engineers for selecting and scaling the ground motion records. This section aims to present widely used procedures for selecting and scaling the records.

The initial step of dynamic analysis is to obtain acceleration time series. There are basically three ways of obtaining acceleration time series. First option is to generate artificial records. This approach requires shortly generation of a response spectrum by a power spectral density function and derivation of numerous sinusoidal signals with different amplitudes. Then, those sinusoidal motions are summed to match the target response spectrum. This procedure can result in records which are very close to elastic design spectrum. On the other hand, use of artificial records is accepted to be inconvenient. This consensus is especially valid for nonlinear analyses (Bommer and Acevedo, 2004). The main inconvenience in generating artificial records is the existence of unrealistically high number of strong motion cycles. Another problem in this approach is the matching of the elastic design spectrum (Reiter, 1990; Bommer *et al*., 2000). About this approach, Naeim and Lew (1995) stated that generating artificial records compatible with a design spectrum is not suitable.

The second option is the use of synthetic records. Generation of these records is based on seismological source models. These models also consider the effect of site conditions. There are various freeware public programs developed to generate synthetic records (Zeng *et al*., 1994; Beresnev and Atkinson, 1998; Boore, 2003).

However, this approach needs expertise on engineering seismology to define the related parameters that can highly affect the generated ground motions (Bommer and Acevedo, 2004).

Finally, the third option is to use the original recorded accelerograms. Being the original recorded data, the problems addressed in generating artificial records are automatically discarded. Moreover, in the last decade, accessing the ground motion records through the public databases becomes easier. The straightforward procedures to handle with the selection of those records make it simpler to use in analyses. The simplicity in manipulating the original records also eliminates the need for expertise in engineering seismology. The use of recorded ground motions become worldwide as accessibility of records can be achieved through several internet sites (Wald, 1997). These sites allow the users to download the earthquake records in digital form.

Two widely referred websites that provide searching and downloading of ground motion records are COSMOS (http://db.cosmos-eq.org) and PEER (http://peer.berkeley.edu/smcat). These websites allow the users to conduct searches considering magnitude of the record, distance to fault rupture, peak ground acceleration (PGV), peak ground velocity (PGV), peak ground displacement (PGD) and site conditions. The data available at COSMOS website are in both uncorrected and/or corrected format. Also, in most of the cases, there is not sufficient information about correction method. On the other hand, the data presented at PEER website are all in corrected format. Moreover, Bommer and Acevedo (2004) stated that PEER records are more reliable than records of COSMOS when especially the long-period response is of concern.

2.2.1 Criteria for Selecting Ground Motion Records

As the accessibility of the ground motion records increases, the use of dynamic analysis becomes more popular in the last decades. However, the ease in obtaining the ground motion records comes up with a serious question: How reliable is the way an engineer use the records to acquire the response of a structure under

dynamic analysis? Since the selection and scaling of the records highly affects the response, one should be very careful about the parameters used in both selection and scaling.

When selecting ground motion records, there are basically three parameters that affect the sensitivity of the nonlinear dynamic analyses. These are magnitude of the earthquake, distance to the fault rupture, and soil classification at the site. Nevertheless, there is little information about those issues in literature. In the following paragraphs, some recent studies that investigate the record selection are summarized. It should be kept in mind that any of the reviewed studies did not address the near field effects by discarding the directivity (pulse-type effect).

2.2.1.1 Earthquake Magnitude

The magnitude of the ground motion is one of the parameters that its importance in the selection of records is questioned in the literature. Some studies reported that it is not an important parameter when a proper scaling is provided (Shome *et al*., 1998; Baker and Cornell, 2005; Iervolino and Cornell, 2005) while some others stated that it strongly affects the response (Stewart *et al*., 2001; Bommer and Acevedo, 2004).

Shome *et al*. (1998) studied the response of nonlinear multi degree of freedom (MDOF) systems to shed light on the effect of magnitude of earthquakes on selection of records. Authors concluded that the better way of using the records for nonlinear analyses is to scale them to a spectrum of a scenario earthquake. Hence, sensitivity of response to earthquake magnitude can be ignored. However, Shome *et al*. (1998) also recommended that magnitudes of records should be "*roughly the same*". Similarly, Bazzurro and Cornell (1994a and 1994b), Shome (1999), Carballo (2000), Luco (2002), Medina (2002), Jalayer (2003), Baker and Cornell (2005), and Iervolino and Cornell (2005) stated that earthquake magnitude has limited or no effect on nonlinear response of structures.

Opinions supporting the earthquake magnitude as an important parameter, depends their claim on the severe effect of magnitude on duration of motion (number of cycles) and on the shape of response spectrum (Stewart, 2001; Bommer and Acevedo, 2004). Hence, they recommend selecting the records in a magnitude range as narrow as possible.

2.2.1.2 Distance to the Fault Rupture

Distance of the site to the fault rupture is the second parameter that was studied by detail in the literature for selection of ground motion records. Apart from the effect of magnitude, there is a consensus on sensitivity of response of structures to distance. It was reported that its effect on response of structures is even less than magnitude (Shome *et al*., 1998; Bommer and Acevedo, 2004; Baker and Cornell, 2005). It is stated that if the required number of records can not be obtained by a narrow range of magnitude, the range of distance can be extended to increase the number of records. However, this generalization is not valid for records selected from soft soil class and ground motions containing near field effects (Bommer and Acevedo, 2004).

2.2.1.3 Soil Classification

The third parameter is the soil classification at the site. Soil classification highly affects the records in terms of amplitude and shape of response spectrum. Hence, it should be considered during the selection of records in an appropriate manner. However, solely trusting on the soil classification may not be suitable all the time (Bommer and Acevedo, 2004). It should be kept in mind that the classification of soil classes is based on the properties of the uppermost 30 m at the site. On the other hand, deeper soil deposit can highly affect the classification of site (Boore, 2004). Bommer and Acevedo (2004) recommended that one can use a record from a site to be representative of upper or lower soil classes in case there is not enough number of records.

2.2.1.4 Additional Parameters in Selection of Records

Although mainly they are not considered as a parameter in selection of ground motion records due to lack of number of records to be considered, there are two more factors that can limit the selection of records. These factors are: (i) mechanism of the fault rupture, (ii) domination of a set of records by a single ground motion. Bommer and Acevedo (2004) reported that the difference between records obtained from both normal and strike-slip fault mechanisms is not significant. However, there is common agreement on higher amplitudes of records generated by reverse-fault mechanism. On the other hand, degree of highness in amplitude of a record is unsettled (Douglas, 2003). On this topic, Bommer *et al*. (2003b) concluded that type of faulting mechanism is not crucial on selection of records. Using a number of records that will dominate the results of conducted analyses is not proper because results will not be representative of a general case. Instead, it is dominated by the characteristics of that specific record.

2.2.2 Scaling of Ground Motion Records

There are basically two methods described in the current codes and specifications for scaling of ground motion records. These methods are used to match a uniform target spectrum. First method was developed for analysis of (elastic) nuclear power plant structures (Huang, 2008). This procedure involves an amplitude and/or frequency scaling of ground motions based on only one horizontal component.

The second method was developed in the early 1990s for nonlinear analysis of seismically isolated structures (Huang, 2008). This method is an amplitude scaling method. Rather than individual single-components of ground motions, pairs of components are considered by this procedure. Each pair of motions are scaled such that for periods between $0.5T_D$ and $1.25T_M$, the average of the square root of the sum of the squares (SRSS) of the 5% damped spectral ordinates from all ground motion pairs does not fall below 1.3 times the corresponding 5% damped target spectrum by more than 10% (ASCE, 2005). Periods T_D and T_M are defined as the effective

periods in the design earthquake (DE) and the maximum considered earthquake (MCE), respectively. One can use at least three or seven or more ground motions in RHA. If three pairs are used, the maximum response of the parameter of interest must be used. If seven or more pairs are used, the average value of the response parameter of interest can be used (ASCE, 2005).

In addition to restriction that the average SRSS should not be less than the specified value, the maximum displacements and base shear obtained by dynamic analyses should not be less than a percentage of the corresponding values calculated by simplified elastic procedures (i.e. equivalent lateral force procedure). This percentage is reported to be 90% by Constantinou *et al*. (2007) while it is stated as in the range between 70%-90% (Bommer and Acevedo, 2004). Hence, scaling of the records becomes more important to provide results from dynamic analyses compatible with that limitation.

There are numerous studies in the literature that discussed the subject of scaling and its effects on the response of nonlinear structures (Shome *et al*., 1998; Baker and Cornell, 2005; Hancock *et al*., 2008). The main agreement in the literature on scaling of ground motion records is that the response of nonlinear structures highly depends on the procedures followed for scaling. Results may be over- or under-predicted depending on the method of scaling (Huang *et al*, 2006; Huang, 2008).

In a recent study, Huang *et al*. (2006) investigated the impact of two scaling techniques on response of nonlinear structures. Authors first used spectrally matched records and compare the results when response is obtained by using amplitude scaling. Huang *et al*. (2006) concluded that spectrally matched records underestimate the response in highly nonlinear structures. This inspection is also observed by Carballo and Cornell (2000). Moreover, Huang *et al*. (2006) strongly recommended that one should not use spectrally matched records when distribution of accelerations and displacements are of concern.

Two widely used amplitude scaling procedures are summarized in the following paragraphs and suitability of those methods is addressed accordingly.

2.2.2.1 Amplitude Scaling at Fundamental Period of Structure

This method implies that a set of selected records should be scaled such that spectral accelerations of each record are matched with that of the design or target spectrum at fundamental period of the structure (Shome *et al*., 1998). However, the basic drawback of this method is that it considers only the fundamental period. In most of the times, there are uncertainties in prediction of period. Moreover, as damage initiates in the structure, period of the structures elongates instantly. Furthermore, if contribution of higher mode effects on the response of structure is expected to be significant, then higher mode periods, which are smaller than the fundamental period, will be of interest.

2.2.2.2 Amplitude Scaling at a Range of Periods

Incidence of damage in a structure increases the fundamental period. The elongated period due to initiation of damage may be considerably high. Haselton and Baker (2006) stated that the degree of increase in period depends on the nonlinearity of the structure. In their study, Haselton and Baker (2006) implied the importance of scaling records in a range of periods rather than at a single period. This conclusion is also addressed in study of Bommer and Acevedo (2004). Scaling of records at a range of periods is performed by minimizing the sum of the squared errors between a target spectrum and spectral ordinates of each record.

When both of the horizontal components of a record need to be used, the same procedure should be employed for geometric mean of two components to minimize the sum of the squared errors (Huang, 2008). This method is referred as geo-mean scaling. The scale factor obtained by geo-mean scaling is used for both of the components. This is especially important for records with near field effects to preserve the difference between the components (Stewart *et al*., 2001).

In this method, one can decide on the period range for scaling. Moreover, this method preserves the spectral shape and correlation between the horizontal

components of ground motions. This procedure is studied in Section 2.4 in more detail.

2.2.3 Scaling Factor and Number of Ground Motions Considered

An important research subject is the limitation for the scaling factor in order not to introduce any bias on results. According to study of Krinitzsky and Chang (1977), records with a scale factor higher than four should not be used. In a similar study, Vanmarcke (1979) stated that the limit for scale factors should be two for liquefaction analyses. Moreover, Malhotra (2003) stated in his study that 5.84, which is one of the scale factors he came up with, is higher than the normally accepted upper limit of four for a scaling factor. In a recent study, Hancock *et al*. (2008) investigated the effect of scaling factor by considering several damage measures. Authors reported that there is not any steady increase or decrease in response of the structures with scaling factors up to ten. They also stated that the probable bias may be observed due to inappropriate selection of records which are not compatible with magnitude and spectral shape.

Another key issue is the number of records. What codes recommend engineers to do is (i) to select at least three records and get the maximum response from analyses results of those three records; (ii) to select seven or more records and get the average of the results. However, the number of records to be used in dynamic analyses is of concern in several researches. Shome *et al*. (1998) stated that any proper scaling of records may reduce the number of analyses needed to obtain the response by a factor of four. This conclusion is also supported by Hancock *et al*. (2008). Bommer and Acevedo (2004) also reported that the required number of records for dynamic analysis can be reduced by proper scaling and selection. Recently, Huang (2008) conducted a study about the required number of records for performing unbiased dynamic analyses. Author concluded that eleven records are enough to obtain successful estimates for the response.

2.3 SELECTED GROUND MOTION RECORDS

In the light of previous studies, selection of ground motion records was carried out such that magnitude, distance, and soil classification of the records are similar. In this sense, two sets of near-field ground motions were selected. These ground motion sets are, respectively, composed of stiff soil (Bin1) and soft soil records (Bin2). A set of 22 pairs of near-field ground motion records has been compiled from well known and extensively studied seismic events occurred in United States, Turkey, Iran, Taiwan, and former USSR.

The classification of those ground motion sets basically depends on the average shear wave velocity at the upper 30 m soil profile. Bin1 is roughly composed of ground motions recorded at sites with an average shear wave velocity in between 360 m/s and 750 m/s. The corresponding average shear wave velocity for Bin2 is in the range of 180 m/s and 360 m/s. This classification is done as per NEHRP and shear wave values are taken from ASCE. Each Bin has eleven pairs of records. The number of considered ground motion records was decided based on the previous studies. As already mentioned, eleven records were reported to be enough as being representative of a target spectrum with a proper scaling method (Huang, 2008).

Since, the near-field response of isolated structures is of concern in this study, the selection of ground motion records was performed so that the records contain clear pulse signals. Significance of pulse signals in near-field records is regarded as the topic of researches in the last few decades (Housner and Trifunac, 1967; Boore and Zoback, 1974; Somerville *et al*., 1997; Abrahamson, 2000; Iwan *et al*., 2000; Cuesta *et al*., 2003; Akkar *et al*., 2005a). Metin (2006) indicated that "*fault rupture propagating towards site at high velocities would result a dominant high amplitude pulse in the fault-normal direction*". This is called as forward directivity effect. Mavroeidis (2004) defined the characteristics of records with forward directivity effect as follows: "*most of the elastic energy arrives coherently in a single, intense, relatively long-period pulse at the beginning of the record, representing the cumulative effect of almost all the seismic radiation from the fault*". In contrast, if the fault rupture propagates away from the site, strong ground motion pulses are not

observed. This phenomenon is illustrated in Figure 2.1. It shows the fault normal velocity time histories recorded at Lucerne Valley and Joshua Tree stations during 1992 Landers earthquake. It is clear that Lucerne Valley record, which is at the forward direction of rupture front, has a significant pulse. On the contrary, Joshua Tree record, which is located at backward direction of rupture front, is considerably weak. Hence, selection of ground motions with near-field effect needs special care. Information on the selection of these motions was obtained from previous studies carried out by Somerville *et al*. (1997), Akkar and Gulkan (2002), Pavlou and Constantinou (2004) and Metin (2006).

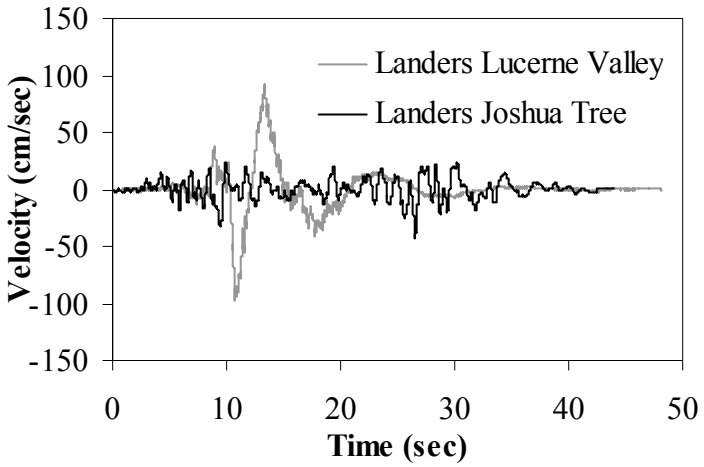

Figure 2.1 Significance of forward directivity effect.

The digital records of considered ground motions and summaries of their characteristics were downloaded from PEER Strong Motion Database. Selected ground motion records and their characteristics are listed in Tables 2.1 and 2.2 for Bin1 and Bin2, respectively. These characteristics include the moment magnitude M_W, the closest distance to the fault rupture d, the peak ground acceleration (PGA), peak ground velocity (PGV) and the peak ground displacement (PGD).

Table 2.1 Characteristics of near-field ground motions recorded at stiff soil.

Earthquake	Station	Magnitude (M_w)	d (km)	Component	PGA (g)	PGV (cm/sec)	PGD (cm)
Chi Chi (CC057)	TCU057	7.6	11.8	N	0.09	42.6	56.2
				W	0.12	35.2	56.7
Cape Mendocino (CMP)	Petrolia	7.0	8.2	0	0.59	48.4	21.7
				90	0.66	89.7	29.6
Duzce (DB)	Bolu	7.1	12	0	0.73	56.4	23.1
				90	0.82	62.1	13.6
Gazli (GK)	Karakyr	6.8	5.5	0	0.61	65.4	25.3
				90	0.72	71.6	23.7
Kocaeli (KG)	Gebze	7.5	10.9	0	0.24	50.3	42.7
				270	0.14	29.7	27.5
Kocaeli (KI)	Izmit	7.5	7.2	180	0.15	22.6	9.8
				90	0.22	29.8	17.1
Landers (LL)	Lucerne	7.3	2.2	275	0.72	97.6	70.3
				0	0.79	31.9	16.4
Northridge (NN)	Newhall	6.7	5.9	90	0.58	75.5	17.6
				360	0.59	97.2	38.1
Northridge (NR)	Rinaldi	6.7	6.5	228	0.84	166.1	28.8
				318	0.47	73.0	19.8
Northridge (NS)	Sylmar	6.7	5.4	52	0.61	117.4	53.5
				142	0.90	102.8	47.0
Tabas (TT)	Tabas	7.4	2.1	LN	0.84	97.8	36.9
				TR	0.85	121.4	94.6

Although it is mentioned in the previous studies that magnitude and distance to fault rupture are not of vital importance, it should be kept in mind that those studies did not consider the near-field effects. Apart from those conclusions, the selection of ground motion records tried to be handled in as narrow range as possible in terms of both magnitude and distance to fault rupture. The magnitudes of the considered

motions are in between 6.0 and 7.6 and the distances to the fault rupture are less than 15 km.

Table 2.2 Characteristics of near-field ground motions recorded at soft soil.

Earthquake	Station	Magnitude (M_w)	d (km)	Component	PGA (g)	PGV (cm/sec)	PGD (cm)
Chi Chi (CC101)	TCU101	7.6	2.1	N	0.25	49.4	35.1
				W	0.20	67.9	75.4
Erzincan (EE)	Erzincan	6.7	4.4	NS	0.52	83.9	27.4
				EW	0.50	64.3	22.8
Imperial Valley (IVA4)	Array 4	6.5	7.1	140	0.49	37.4	20.2
				230	0.36	76.6	59.0
Imperial Valley (IVA5)	Array 5	6.5	4.0	140	0.52	46.9	35.4
				230	0.38	90.5	63.0
Imperial Valley (IVA6)	Array 6	6.5	1.4	140	0.41	64.9	27.7
				230	0.44	109.8	65.9
Imperial Valley (IVA10)	Array 10	6.5	6.2	50	0.17	47.5	31.1
				320	0.22	41.0	19.4
Kocaeli (KD)	Duzce	7.5	15.4	180	0.31	58.8	44.1
				270	0.36	46.4	17.6
Kocaeli (KY)	Yarimca	7.5	4.8	60	0.27	65.7	57.0
				330	0.35	62.1	51.0
Loma Prieta (LPCor)	Corralitos	6.9	3.9	0	0.64	55.2	10.9
				90	0.48	45.2	11.4
Loma Prieta (LPSar)	Saratoga	6.9	8.5	0	0.51	41.2	16.2
				90	0.32	42.6	27.5
Parkfield (PC)	Cholame 2	6.0	14.3	90	0.60	63.3	14.1
				360	0.37	44.1	8.9

Figures 2.2 and 2.3 illustrate the velocity and acceleration time histories of the ground motions presented in Tables 1 and 2 in a more visual manner for stiff and soft soil bins, respectively.

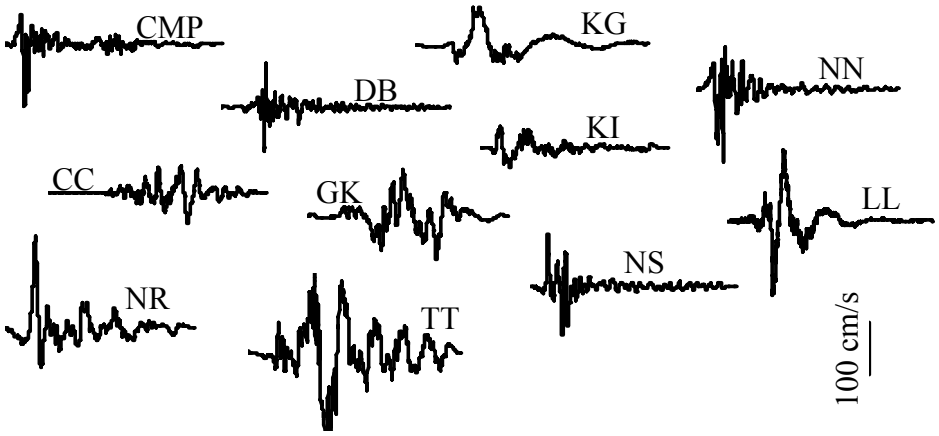

(a)

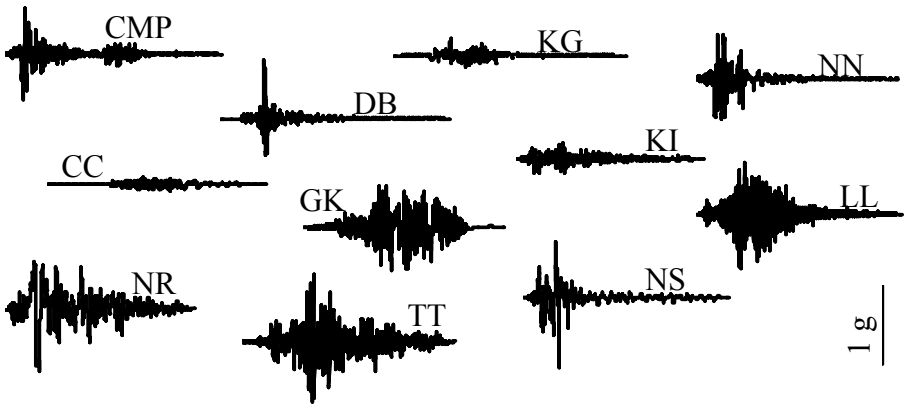

(b)

Figure 2.2 Near-field ground motion records of stiff soil bin: (a) velocity and (b) acceleration time histories.

To provide sufficient number of records in each bin, as suggested in Bommer and Acevedo (2004), some records from lower soil class as per NEHRP (according

to average shear wave velocities) were assigned as stiff soil. For instance, although the average shear wave velocities are around 280 m/s for records from Northridge earthquake (Newhall, Rinaldi, and Sylmar records), they are considered as stiff soil.

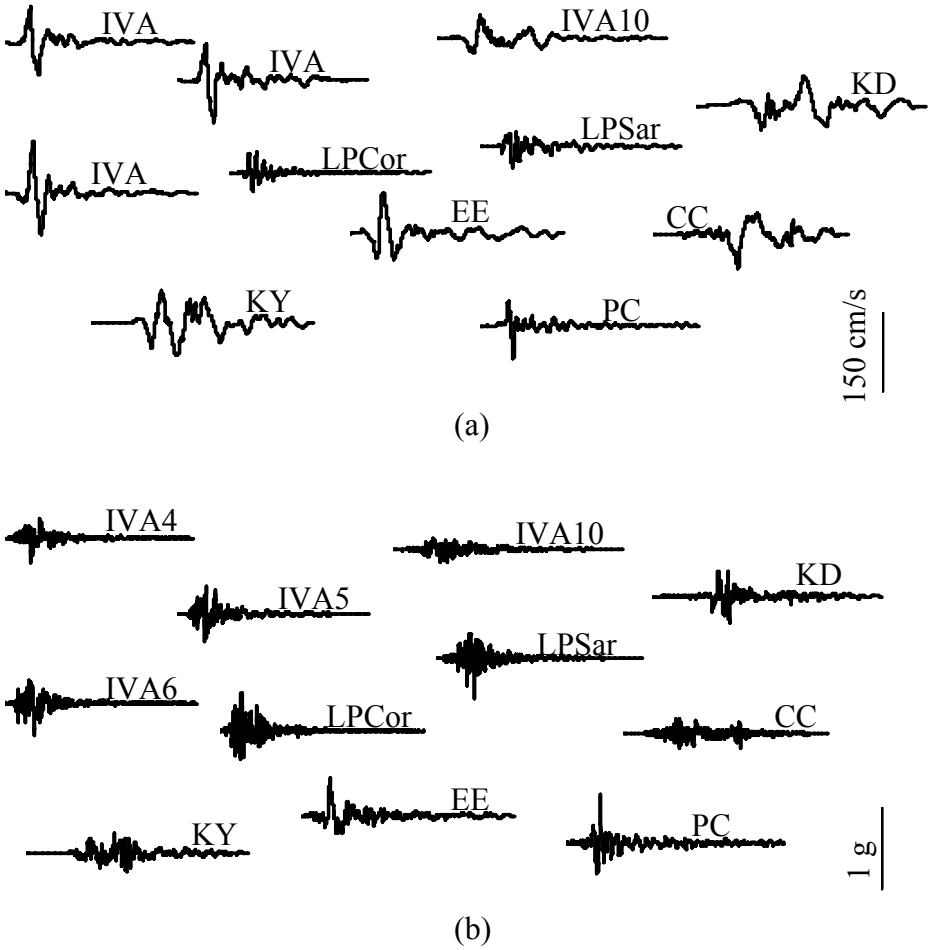

Figure 2.3 Near-field ground motion records of soft soil bin: (a) velocity and (b) acceleration time histories.

2.4 SCALING OF SELECTED GROUND MOTION RECORDS

As it is discussed in Section 2.2.2, performance of nonlinear structures is highly sensitive to the selected scaling procedure. It may yield under-estimation or over-

estimation results depending on the chosen scaling procedure. One should be very careful on selection of the appropriate method for scaling. In the light of previous studies, some key points in determining the optimal scaling procedure can be listed as follows (Shome *et al*., 1998; Bommer and Acevedo, 2004; Baker and Cornell, 2005; Hancock *et al*., 2008):

- It should be independent of structural period
- It should cover a period range rather than considering only one period
- The number of the considered ground motion records should be as small as possible to determine seismic demands of the structure
- Its applicability should not be limited only for far-field records but also includes near-field records
- The distribution in the earthquake shaking for the selected characterization of the hazard (spectrum or annual probability of exceedance of a spectral ordinate) should be preserved for the site of interest
- The effect of orthogonal horizontal components of the record should be considered
- Scale factors should not be too high. It should be less than four.

In this sense, scaling of the selected near-field ground motion pairs was carried out in two phases. In the first part, the selected ground motion records become compatible with the target spectrum whereas the second part assures the requirement of the codes for dynamic analyses. The first phase is according to method described by Huang (2008) and also utilized in study of Constantinou *et al*. (2007) and known as geo-mean scaling. This method is an amplitude scaling method (it does not involve spectral matching procedures) which seeks to minimize a sum (ε) of the weighted squared errors between the geometric mean of the two horizontal components and the target spectral values at various periods. Error ε is defined as:

$$\varepsilon = \sum_{i=1}^{n} b_i \left(a \cdot y_i - y_{Ti} \right)^2 \qquad (2.1)$$

where b_i is the weighting factor for the squared error at period T_i; a is the scaling factor for the pair of ground motions of interest; y_i is the geometric mean of the spectral ordinates for the pair at period T_i; y_{Ti} is the target spectral ordinate at period T_i; and n is the number of target spectral values considered (Huang, 2008). In Figure 2.4, acceleration spectrum of each ground motion is calculated by taking the geometric mean of the acceleration spectra of the two horizontal ground motion components. The acceleration spectra of all the ground motions and their mean are also presented in Figure 2.4.

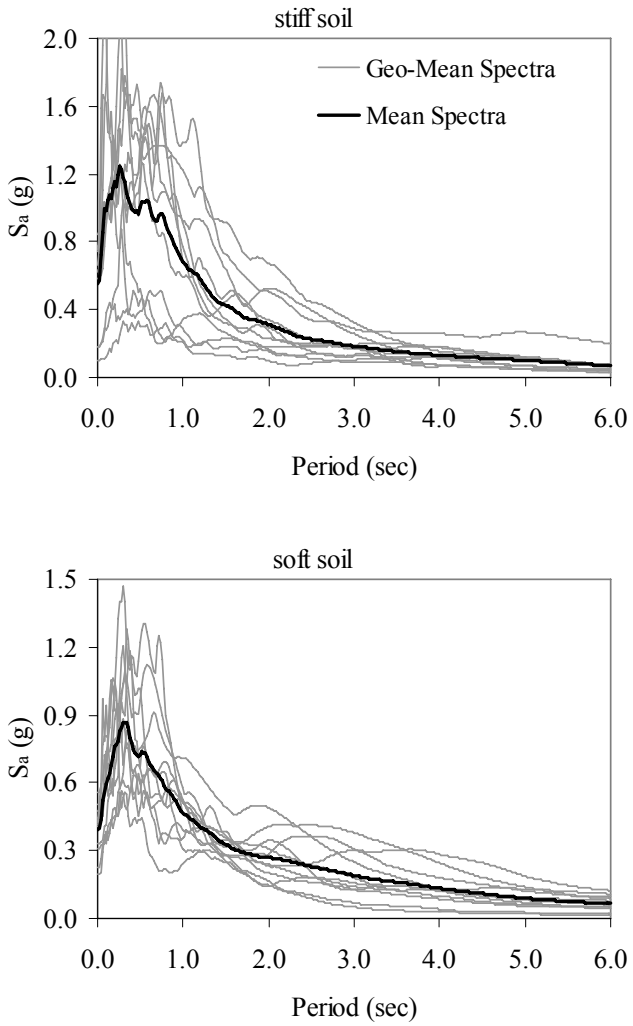

Figure 2.4 Acceleration spectra of the selected ground motions and their mean spectra: (a) for stiff soil, (b) for soft soil.

The scaling factor (a) that results in the minimum value of ε is calculated by setting the derivative of Eq. (2.1) equal to zero with respect to a. The result is

$$\frac{\partial \varepsilon}{\partial a} = 0 \Rightarrow \sum_{i=1}^{n} 2b_i y_i \left(a \cdot y_i - y_{Ti}\right) = 0 \qquad (2.2)$$

$$a = \frac{\sum_{i=1}^{n} b_i \cdot y_i \cdot y_{Ti}}{\sum_{i=1}^{n} b_i \cdot y_i^2} \qquad (2.3)$$

The above mentioned geo-mean scaling method was developed first by Somerville *et al*. (1997) for the offshore oil industry and used in SAC steel project. Then, Huang (2008) modified that method to be used in assesment of nuclear power plants. Author applied the geo-mean scaling method by considering multiple periods which are 0.3 sec., 0.6 sec., and 2 sec. However, these selected periods are not adequate to be used for analysis of isolated structures. Because, fundamental periods of the isolated structures are mostly greater than 2 sec. and matching the spectrum for periods less than 2 sec. is meaningless for dynamic analysis of isolated structures. Hence, the new proposed scaling method is developed by modifying the period range used in the scaling which is appropriate for dynamic analysis of seismic isolated structures.

Since, an appropriate scaling procedure should cover a wide set of periods rather than only one period; the period range considered in the proposed method is also wide. The scaling is based on five target periods (T_i): 1, 2, 3, 4, and 5 sec. The weighting of factors are determined such that the scaled spectra have the most compatible shape with that of the design spectra under consideration. To achieve this goal, a series of combinations of weight factors were tested and best combination was chosen. As a result, weight factors for the periods of concern are selected to be 0.1, 0.1, 0.2, 0.3, and 0.3, respectively. These weight factors are same for all of the ground motion records considered (Ozdemir and Constantinou, 2010).

Target spectra for maximum considered earthquake (MCE) and design earthquake (DE) for two sites, one characterized by stiff soil and the other by soft soil conditions are used. Both of the spectra for MCE and DE are selected as described in Turkish Earthquake Code (TEC) (2007) for the two soil conditions. The spectrum characteristic periods of target spectra for MCE are: T_A = 0.15sec, and T_B = 0.4sec for stiff soil; and T_A = 0.2sec, and T_B = 0.6sec for soft soil. The corresponding spectral ordinates for MCE are selected to be 1.5 times the ordinates of DE spectra (ASCE, 2005; TEC, 2007). For both of the soil conditions, the spectral accelerations are calculated in accordance with TEC (2007). It is calculated simply by following the relation of $A(T) = A_o I S(T)$. Here, $A(T)$ is the spectral acceleration coefficient, A_o is the effective ground acceleration coefficient, I is the building importance factor, $S(T)$ is the spectrum coefficient. By choosing A_o = 0.4 (seismic zone 1 to be representative of near-field conditions), I = 1.0 (for structures such as residential or office buildings, and $S(T)$ = 2.5 (for $T_A \leq T \leq T_B$), $A(T)$ corresponding to 5% damped design spectrum normalised by the acceleration gravity is obtained as 1g between the spectrum characteristic periods. Thus, $A(T)$ when MCE is of concern is calculated as 1.5g between the spectrum characteristic periods in accordance with TEC (2007). Figure 2.5 compares the target MCE spectra to the mean SRSS of the spectral components of the scaled ground motions after the first phase of scaling.

The second phase of the scaling was performed to assure the requirements of ASCE (2005). Hence, each pair of motions was further scaled such that for each period between $0.5T_D$ and $1.25T_M$, the average of the SRSS spectra from all ground motion pairs does not fall below 1.3 times the corresponding ordinate of the target response spectrum by more than 10%. Periods T_D and T_M are defined as the effective periods in the DE and the MCE, respectively.

The final scaling factor for each ground motion is the product of two factors obtained in two scaling phases. However, different isolation systems considered have different periods T_D and T_M, so that the scale factors slightly differed for each system considered. For simplicity, one scaling factor was selected for each ground

motion record and used for all considered isolation systems (Ozdemir and Constantinou, 2010). These final scaling factors are presented in Table 2.3 for the two soil conditions.

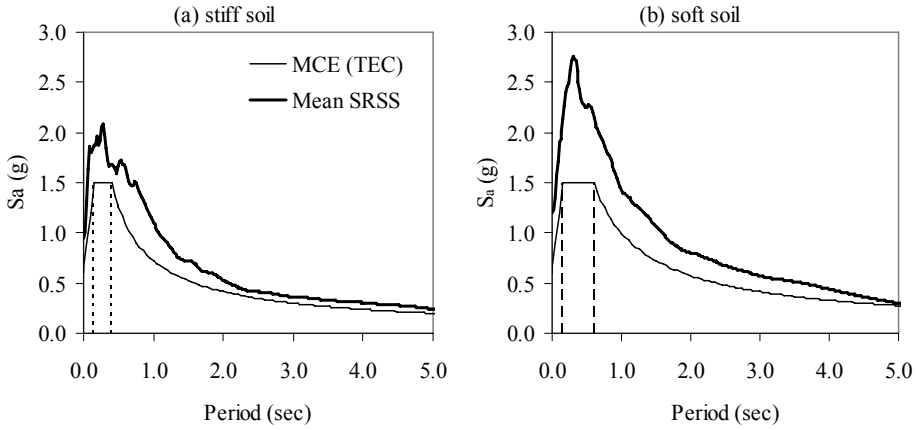

Figure 2.5 Target MCE response spectra and mean SRSS spectra of scaled motions after first phase of scaling a) for stiff soil records, b) for soft soil records.

Table 2.3 Scale factors for stiff and soft soil records.

Stiff Soil			Soft Soil		
Ground Motion	Scale Factor		Ground Motion	Scale Factor	
	DE	MCE		DE	MCE
CC057	1.54	2.31	CC101	1.62	2.43
CMP	0.74	1.10	EE	0.83	1.24
DB	0.62	0.93	IVA4	1.17	1.75
GK	0.87	1.31	IVA5	0.99	1.48
KG	1.73	2.60	IVA6	0.83	1.24
KI	1.79	2.69	IVA10	1.80	2.70
LL	1.14	1.71	KD	1.16	1.74
NN	0.62	0.93	KY	0.93	1.39
NR	0.45	0.68	LPCor	1.47	2.20
NS	0.40	0.60	LPSar	1.61	2.41
TT	0.60	0.90	PC	1.15	1.73

Previous studies concluded that the scale factors should not be too high. Krinitzsky and Chang (1977) reported that it should be less than four, whereas Hanckok *et al*. (2008) stated that scale factors up to ten can be used without any bias in the results. Final scale factors presented in Table 2.3 are all less than four and compatible with the previous studies.

Figure 2.6 compares the target MCE spectra, scaled in accordance with ASCE (2005), to the mean SRSS of the spectral components of the scaled ground motions after final scaling. Each of the graphs in Figure 2.6 corresponds to a different isolation system characterized with different values of periods T_D and T_M, which are shown by dashed lines on each graph. Note that the acceptance criteria of ASCE (2005) are met for each isolation system in the period range of $0.5T_D$ to $1.25T_M$. Although characteristics of isolation systems are studied in detail in Chapter 3, in Figure 2.6, Q is the characteristic strength of the bearing (Figure 3.1) and W is the weight acting on the isolators.

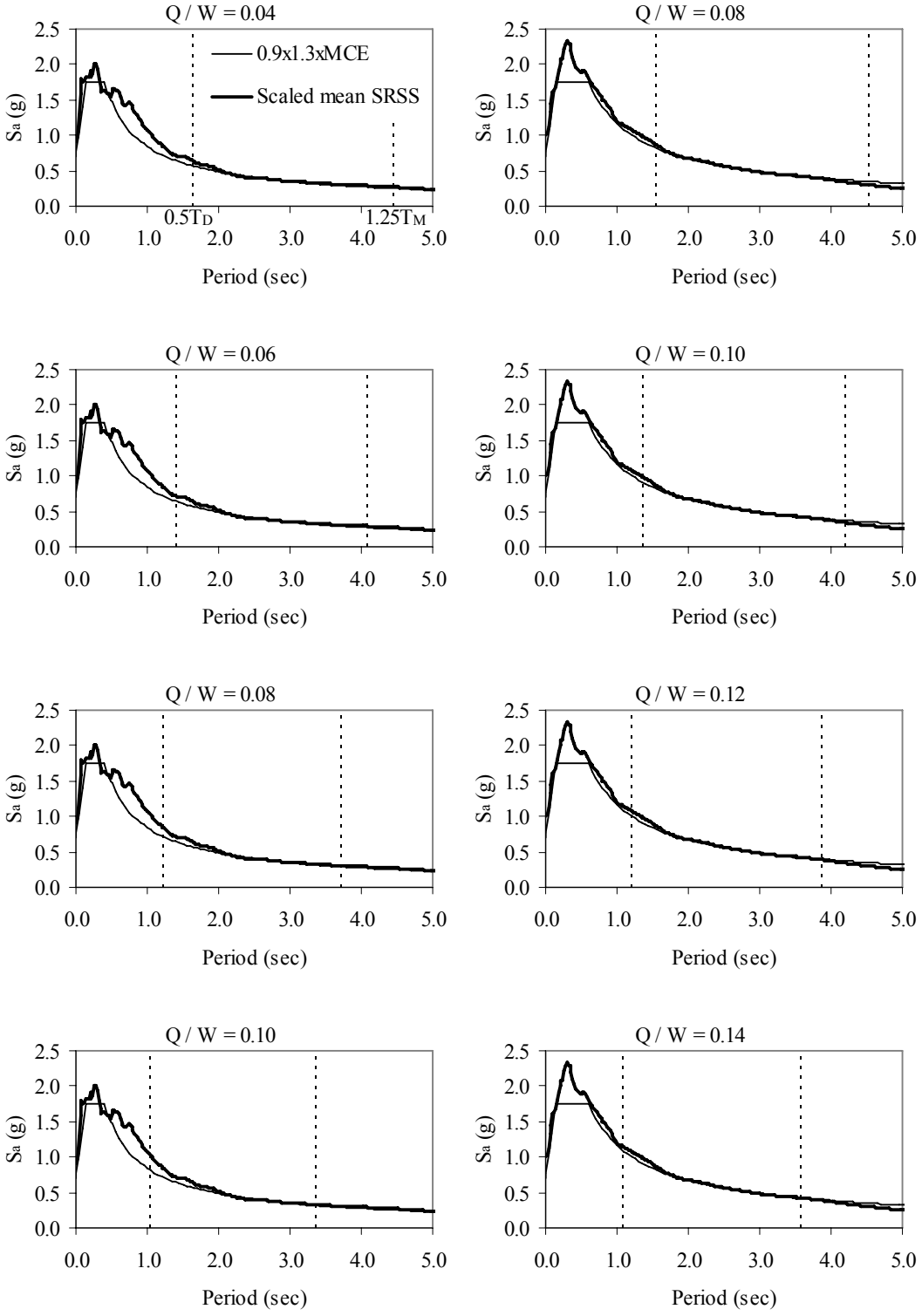

Figure 2.6 Target MCE response spectra and mean SRSS spectra of scaled motions after second phase of scaling for stiff (left side) and soft (right side) soil cases.

CHAPTER 3

MODELING OF ISOLATION SYSTEM AND SUPERSTRUCTURE

3.1 INTRODUCTION

In this chapter, the modeling of both the isolation system and superstructure is discussed. First, parameters that delineate the force-deformation relation of isolators are defined. Then, the procedures described in codes for design of isolators are discussed in detail. Finally, the characteristics and modeling of both the superstructures and isolators are presented.

3.2 PARAMETERS DEFINING THE ISOLATION SYSTEM

Considering non-linear isolation systems, most of them can be represented by a bi-linear force-deformation relation. Lead rubber bearings (LRB), steel energy dissipaters and lead-extrusion dampers (Skinner *et al*., 1993; Naeim and Kelly, 1999) are among the systems that can be represented by bi-linear models.

The isolation systems considered in this study are composed of LRBs and represented by a generic bi-linear hysteretic representation without considerations for cycle-to-cycle deterioration of properties. Figure 3.1 illustrates the idealized force-deformation relation, in which Q is the characteristic strength, k_d is the post-yield stiffness (directly related to stiffness of rubber), and k_e is the initial elastic stiffness. F_y and D_y are the yield force and yield displacement, respectively. Only three of these parameters are needed for the description of the model, which herein are selected to be Q, k_d and D_y. In Figure 3.1, D represents the maximum lateral

isolator displacement and *F* represents the corresponding maximum lateral force carried by the isolator.

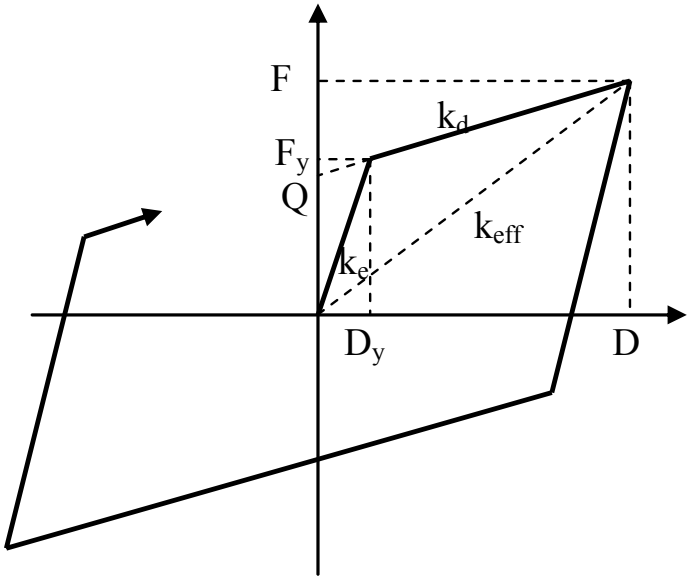

Figure 3.1 Bilinear force-deformation relation of an isolator.

Unlike the post yield stiffness, which is essentially a physical property of the isolator, the initial stiffness is open to interpretation because the transition from initial to yielded state in actual bearing tests is gradual. However, the general procedure suggests a fixed value for the ratio of post yield stiffness to initial stiffness (Skinner at al., 1993; Naeim and Kelly, 1999). To shed light on determination of the initial stiffness, Makris and Chang (2000) conducted a parametric study to find out the effect of D_y on the response of isolated structures. Authors selected a range of yield deformations to be representative of both sliding bearings (0.2 mm) and lead rubber bearings (10 and 20 mm). Their study revealed that "*the benefits by hysteretic dissipation are nearly indifferent to the level of the yield displacement of the hysteretic mechanism*". It has been concluded that fixing k_e/k_d to a constant value is inappropriate, since this assumption leads to variation of

yield deformation D_y with yield strength (Makris and Chang, 2000). A similar study was carried out by Ryan and Chopra (2004). They stated that the yield displacement of bi-linear force-deformation relation should be fixed rather than fixing k_e/k_d and their suggestion is 10 mm for LRBs.

The issue of determining the initial stiffness k_e is discussed here in detail. As being composed of both rubber and lead, the initial stiffness k_e of a LRB is equal to sum of the stiffnesses of rubber (k_d) and lead (k_l) (prior to yielding). k_l and k_d can be determined from the following expressions:

$$k_l = \frac{G_l \times A_l}{h_r} \tag{3.1}$$

$$k_d = \frac{G_r \times A_r}{h_r} \tag{3.2}$$

where, G_l and A_l are shear modulus and cross sectional area of the lead; G_r and A_r are shear modulus and cross sectional area of the rubber, respectively; and h_r is the total height of the rubber.

As it is seen clearly in Figure 3.1, D_y can simply be calculated as defined in Equation (3.3). Furthermore, F_y can be obtained by Equation (3.4). Inserting Equation (3.4) into Equation (3.3) yields the definition of D_y as presented in Equation (3.5).

$$D_y = \frac{F_y}{k_e} = \frac{F_y}{k_l + k_d} \tag{3.3}$$

$$F_y = Q + k_d \times D_y \tag{3.4}$$

$$D_y = \frac{Q}{k_e - k_d} = \frac{Q}{k_l} \tag{3.5}$$

As mentioned before, Q is the characteristic strength and it is equal to yield strength of the lead. Q can be calculated by multiplication of A_l and yield stress (σ_l) of lead. By inserting Equation (3.1) and Q in terms of A_l and σ_l into Equation (3.5), yield displacement D_y is obtained as defined in Equation (3.6).

$$D_y = \frac{\sigma_l \times h_r}{G_l} \tag{3.6}$$

It is obvious through Equations (3.1)-(3.6) that D_y is not sensitive to the change in k_e/k_d ratio and should stay constant unless characteristic properties of lead (σ_l and G_l) and total rubber height (h_r) change. Therefore, D_y should be fixed to a constant value instead of fixing the k_e/k_d ratio.

In the current study, a fixed value of 10 mm is assigned to the yield displacement, which is more representative of lead-rubber isolation systems rather than sliding systems for which this value should be at least one order less. On the other hand, the value of the yield displacement does not have any important effect on the isolation system displacement calculation and, consequently, on the isolation shear force.

3.3 DESIGN OF ISOLATION SYSTEM

Procedures defined in design of isolation systems are based on an iterative method to predict both the maximum isolator displacement and shear force carried by isolators. That iterative method can be summarized as follows:

Simplified method of analysis defined in ASCE (2005) starts with an assumption for the displacement D of isolator. The assumed value of displacement D is then used to calculate the effective stiffness k_{eff} of a single-degree-of-freedom (SDOF) system which is a representation of the isolated structure as described in Equation (3.7).

$$k_{eff} = \frac{Q}{D} + k_d \tag{3.7}$$

Post-yield stiffness k_d of the isolator can be calculated from Equation (3.2). k_d can also be defined by using a target isolation period T as in Equation (3.8). Calculation of k_{eff} is followed by the prediction of effective damping β_{eff}. It starts with obtaining the area of hysteretic loop from Equation (3.9). This area represents the energy dissipation at each cycle. Then, the effective damping ratio β_{eff}, which produces the same amount of energy dissipation with that of the hysteretic energy dissipated at each cyclic motion of the LRB, is expressed as by Equation (3.10). The calculated effective stiffness k_{eff} is then used to calculate the effective period T_{eff} as in Equation (3.11).

$$T = 2 \cdot \pi \sqrt{\frac{W}{k_d \cdot g}} \tag{3.8}$$

$$ED = 4 \cdot Q \cdot (D - D_y) \tag{3.9}$$

$$\beta_{eff} = \frac{4 \cdot Q \cdot (D - D_y)}{2 \cdot \pi \cdot k_{eff} \cdot D^2} \tag{3.10}$$

$$T_{eff} = 2 \cdot \pi \sqrt{\frac{W}{k_{eff} \cdot g}} \tag{3.11}$$

Once T_{eff} and β_{eff} are obtained, the next step is the determination of the displacement. The displacement of isolation system is then calculated from the modified response spectrum for damping β_{eff} by using the damping reduction factor B to account for the effects of damping higher than 5% for period T_{eff}. Accordingly, the displacement is calculated as

$$D = \frac{gS_a T_{eff}^2}{4\pi^2 B} \tag{3.12}$$

The process is iterative until the assumed value and the calculated value of displacement are sufficiently close. Herein the value of *B* in ASCE (2005) has been used (see Table 3.1).

3.3.1 Damping Reduction Factor *B*

The damping reduction factor *B* enables the use of simplified elastic methods by modifying the 5% damped elastic response spectrum for increased damping values. Elastic spectrum for damping values greater than 5% can simply be obtained by dividing the 5% spectrum by factor *B*:

$$S_a(T,\beta) = \frac{S_a(T,5\%)}{B} \tag{3.13}$$

where $S_a(T,\beta)$ is the spectral acceleration at period *T* and damping ratio β. It worths to mention that the spectral acceleration in Equation (3.13) is the acceleration at maximum displacement (pseudo-acceleration). It does not have to be the maximum acceleration (no contribution from any viscous force) (Constantinou *et al*., 2007). Hence, it is related to the spectral displacement S_d through Equation (3.14). Therefore, *B* can be calculated by using both spectral acceleration and spectral displacement as shown in Equation (3.15).

$$S_d = \frac{T^2}{4\pi^2} S_a \tag{3.14}$$

$$B = \frac{S_a(T,5\%)}{S_a(T,\beta)} = \frac{S_d(T,5\%)}{S_d(T,\beta)} \tag{3.15}$$

Calculation of damping reduction factor *B* is based on statistical processing of results obtained by Equation (3.15) for the selected ground motions. First, factor *B* is calculated for each individual record and then the average or median values of the results are considered. Hence, selection of ground motions affects factor *B*. Consequently, the values for factor *B* given in codes and specifications are typically on the conservative side (Constantinou *et al*., 2007).

In Table 3.1, values of factor *B* are presented in accordance with the following codes and specifications: 1999 AASHTO (American Association of State Highway and Transportation Officials, 1999), 2003 NEHRP (Building Seismic Safety Council, 2003), 2005 ASCE (American Society of Civil Engineers, 2005), Eurocode 8 (European Committee for Standardization, 2005) and recommendations in FEMA 440 (Applied Technology Council, 2005).

Apart from the others, FEMA 440 and Eurocode 8 employ equations for calculation of factor *B*. Others present the values of factor *B* in a tabular format for different damping values. In case of using damping ratios other than given in tabular format, damping reduction factor can be calculated by linear interpolation. In Table 3.1, values of factor *B* are calculated by Equations (3.16) and (3.17) for FEMA 440 (2005) and Eurocode 8 (2005), respectively, and rounded to the nearest number with one decimal accuracy.

B suggested in FEMA 440 is

$$B = \frac{4}{5.6 - ln(100\beta)} \tag{3.16}$$

B suggested in Eurocode 8 is

$$B = \sqrt{\frac{0.05 + \beta}{0.10}} \tag{3.17}$$

Table 3.1 Values of damping reduction factor *B* in codes and specifications.

β %	AASHTO, ASCE	NEHRP	FEMA 440	EUROCODE 8
≤ 2	0.8	0.8	0.8	0.8
5	1.0	1.0	1.0	1.0
10	1.2	1.2	1.2	1.2
20	1.5	1.5	1.5	1.6
30	1.7	1.7 or 1.8	1.8	1.9
40	1.9	2.1	2.1	2.1
50	2.0	2.4	2.4	2.3

As it is seen in Table 3.1, there is no distinction in values of factor *B* due to soil conditions where structures are located. Codes and specifications do not address the effect of soil conditions on *B* factor. There are some recent studies focused on factor *B* such as Lin and Chang (2004), Lin (2007), and Lin and Miranda (2009) that investigated the sensitivity of factor *B* to soil types.

Lin and Chang (2004) considered more than 1000 records to study the effect of site classes on factor *B*. Their conclusion was that there is no significant difference in *B* at low damping values for stiff and soft soil conditions. However, at higher damping values (β > 30%), there occurred minor variations, up to 10%, between stiff and soft soil conditions. Although that study revealed invaluable results, small number of near field records in the overall dataset considered is questionable to come up with a decision about near field records. Similarly, Lin (2007) studied the similar concepts considering only the records from Chi Chi 1999 earthquake. Distances of the records to the fault rupture are in the range of 25 km and 170 km. Even though the conclusions of Lin (2007) were the same as Lin and Chang (2004), still near-field concept was not considered directly. On the other hand, Pavlou and Constantinou (2004) studied the applicability of *B* values presented in codes and specifications for near-field records. Authors stated that *B* values presented in codes are generally conservative for near-field records regardless of the soil type. However, they also reported that *B* values in codes become unconservative when

damping values are higher than 40%. But, they also declared that damping values exceeding 40% are related to higher modes where the periods are low.

Figures 3.2 and 3.3 show the calculated *B* values of the selected ground motion records presented in Tables 2.1 and 2.2 together with the suggested *B* values presented in ASCE (2005) and Eurocode 8 (2005) for stiff and soft soil bins, respectively. In these two figures, black lines represents the values of *B* suggested by codes, while grey lines stands for the calculated *B* values by using Equation (3.18). To be able to reflect the effect of both of the horizontal components on factor *B*, first pseudo-acceleration spectrum of each component were obtained individually. This is done by an analysis program called SeismoSignal (2009). Then, geometric means of obtained spectra were calculated at each period. This process was repeated for all of the eleven records in each ground motion bins. Calculated *B* values are obtained by taking the average of eleven records at different damping levels. Figure 3.2 demonstrates that both ASCE (2005) and Eurocode 8 (2005) give conservative values of *B* for records at stiff soil bin at almost all damping ratios and periods. However, in Figure 3.3, suggested values of ASCE (2005) for *B* are observed to be conservative while values in Eurocode 8 are unconservative for records at soft soil bin. The degree of unconservatism increases as period increases especially in the range of 20% and 40% damping ratios. Hence, values of *B* are taken from ASCE (2005) in modeling of isolators. Constantinou *et al*. (2007) also used the values for *B* given in ASCE (2005).

3.4 MODELING OF ISOLATED STRUCTURES

Modeling of the isolated structures is composed of two phases: (i) modeling of superstructure, (ii) modeling of isolation system. In the following subsections, modeling aspects of both superstructure and isolators considered in the present study are discussed in detail.

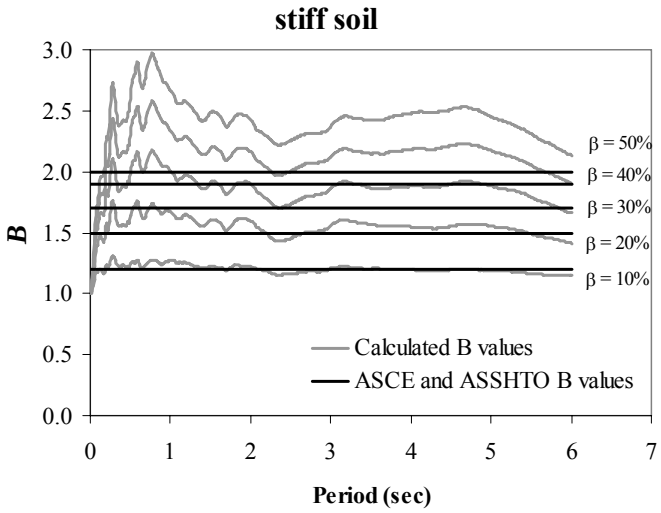

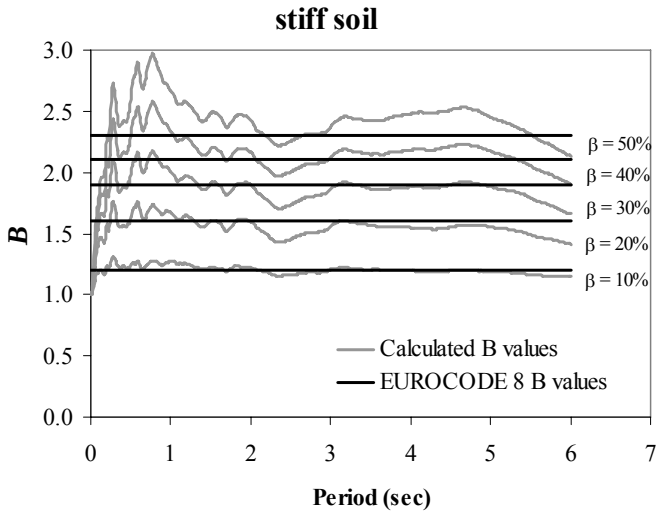

Figure 3.2 Comparison of calculated *B* values of records in stiff soil bin with that of values presented in codes and specifications: for ASCE (top) and for Eurocode 8 (bottom).

3.4.1 Modeling of Superstructure

The building stock in Turkey is mainly comprised of low- to mid-rise reinforced concrete (RC) buildings. Knowing this fact, in a recent study, a detailed research

was carried out to report the characteristics of the RC buildings in Istanbul, Turkey (Yakut, 2008). The obtained data shows the average plan area, column orientation through the plan, number of bays in both long and short directions of the plan, and story heights for numerous RC buildings.

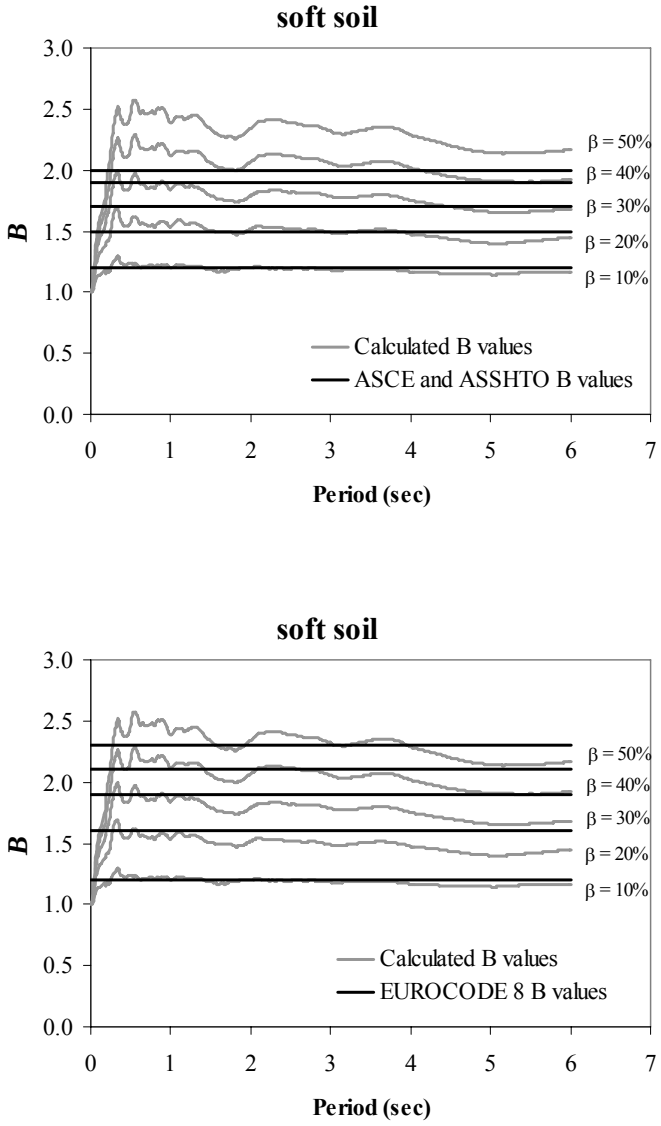

Figure 3.3 Comparison of calculated *B* values of records in soft soil bin with that of values presented in codes and specifications: for ASCE (top) and for Eurocode 8 (bottom).

In the light of that study, two RC buildings with different story heights, 3-story (3S), and 7-story (7S), are modeled in 3-D. All of the RC buildings under consideration have four identical bays in long direction and three identical bays in short direction. The plan dimensions of the RC buildings with 3- and 7-story are 16mx10.5m, and 18mx12m, respectively. Story heights of the structures are 2.9 m and equal at each story level. Idealized model of 3S RC frame is depicted in Figure 3.4.

Structures are regular in elevation and symmetric with respect to two main orthogonal axes both in mass and stiffness. In accordance with the study of Yakut (2008), both of the buildings were designed so that half of the columns are oriented in their strong direction while the other half in their weak directions. Column dimensions of 3S and 7S RC structures are 35cmx50cm and 40cmx55cm, respectively. Typical beam dimensions are 30cmx50cm and 30cmx60cm for 3S and 7S buildings, respectively. The concrete is selected to have a compressive strength f_c of 25 MPa with material properties presented in Table 3.2. The distributed dead and live load values are 500 kg/m^2 and 200 kg/m^2, respectively in accordance with the TEC (2008). Thus, total weights of the structures are 3420 kN and 9190 kN for 3S and 7S buildings, respectively.

Table 3.2 Mechanical properties of concrete material

Modulus of elasticity, E	30000 MPa
Poisson ratio, ν	0.2
Compression strength, f_c	25 MPa

For the nonlinear RHA, the structural analysis program SAP2000 (2008) is used to predict the responses of the isolated structures. Modeling of the superstructure is based on the following assumptions:

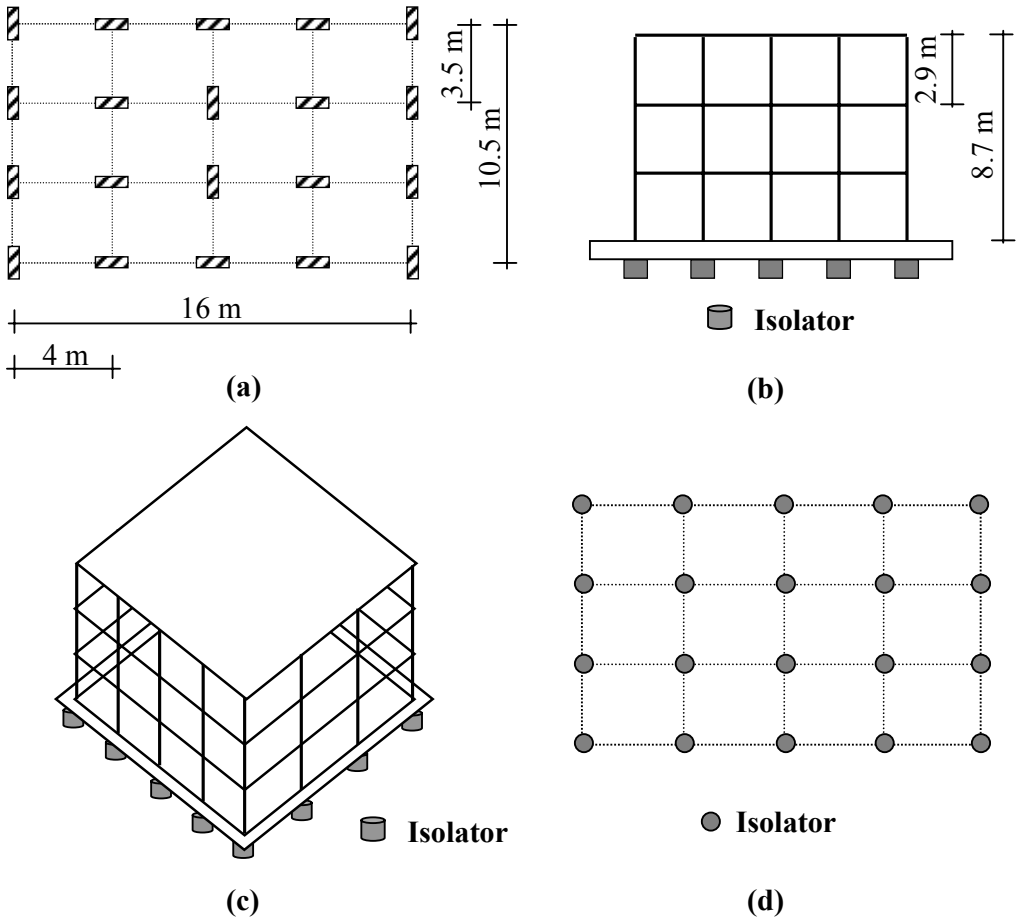

Figure 3.4 Idealized model of 3-story isolated RC building: (a) plan, (b) elevation, (c) 3D layout, and (d) isolation system.

- Since the isolation system reduces the earthquake response by dissipating the energy through hysteretic loops, superstructure remains within the elastic range. Hence, frame members of the superstructure are modeled as elastic
- Floors at each story level of the superstructure are modeled as rigid in their own plane. Consequently, each floor has three degree of freedoms: two translations and one rotation
- Columns providing the lateral stiffness are inextensible and weightless
- Mass of a floor is equally distributed among the joints of that floor level

- Effects of soil-structure interaction are not taken into consideration
- Eccentricities (actual or accidental) in the structure are not considered (not valid for the study presented in Chapter 6).

Tables 3.3 and 3.4 present the periods of the first three fixed-base modes of the buildings under elastic conditions. Since the structural models are symmetric in stiffness and mass, mode shapes obtained by SAP2000 (2008) are purely translational and rotational.

Table 3.3 Periods of the first three fixed-base modes of analyzed 3-story building.

MODE	PERIOD (sec.)
1 (Translation – in long direction)	0.20
2 (Translation – in short direction)	0.20
3 (Rotation)	0.19

Table 3.4 Periods of the first three fixed-base modes of analyzed 7-story building.

MODE	PERIOD (sec.)
1 (Translation – in long direction)	0.43
2 (Translation – in short direction)	0.43
3 (Rotation)	0.41

3.4.2 Modeling of Isolation System

As being an iterative method, design of isolators were carried out according to the procedure presented in Section 3.3. Values of the isolation system parameters considered in this study are presented in Table 3.5. The parameters used are the

ratio of strength Q to weight W supported by isolators, the period T based on the post-elastic stiffness (Equation (3.8)).

Selection of the two parameter namely, isolation period T and Q/W ratio is very crucial. Since, in an isolated structure, the results of the analyses are directly affected by these two parameters. There are several studies that attributed their study to the selection of effective isolation period (Equation (3.11)) in the range of 1.5 – 3.0 sec. (Makris, 1997; Jangid and Kelly, 2001; Alhan and Gavin, 2004; Tena-Colunga and Osornia, 2006; Providakis, 2008) regardless of the design spectrum. However, it is believed that determining the isolation period T without considering the design spectrum is not a realistic approach. Because, there is no way to determine the effectiveness of isolation period T in reducing the base shears without considering a spectrum. In this study, the period range of isolation period T is selected so that the base shear of the superstructure is not more than a specific value. The limit for base shear is chosen as 30% of the weight of the superstructure in MCE (Constantinou, 2009). This selection is conducted by following the simplified method of analysis defined in codes (ASCE, 2005). Calculation of the base shear V_b by simplified method of analysis was performed by means of Equation (3.18).

$$V_b = K_d \times D \tag{3.18}$$

where

$$K_d = \sum k_d \tag{3.19}$$

Figure 3.5 presents the estimations made by simplified method of analysis in terms of maximum isolator displacements and normalized base shears. It is clear that the isolation period T should be higher than 3.0 sec. and 3.5 sec for stiff and soft soil conditions, respectively when 30% limitation is of concern. It should be mentioned that the simplified method of analysis does not consider the superstructure, but based on calculations of an isolated single-degree-of-freedom

(SDOF) system where the weight of the superstructure is assigned the joints at top of the isolators itself. Hence, the effect of superstructure flexibility is not adressed here.

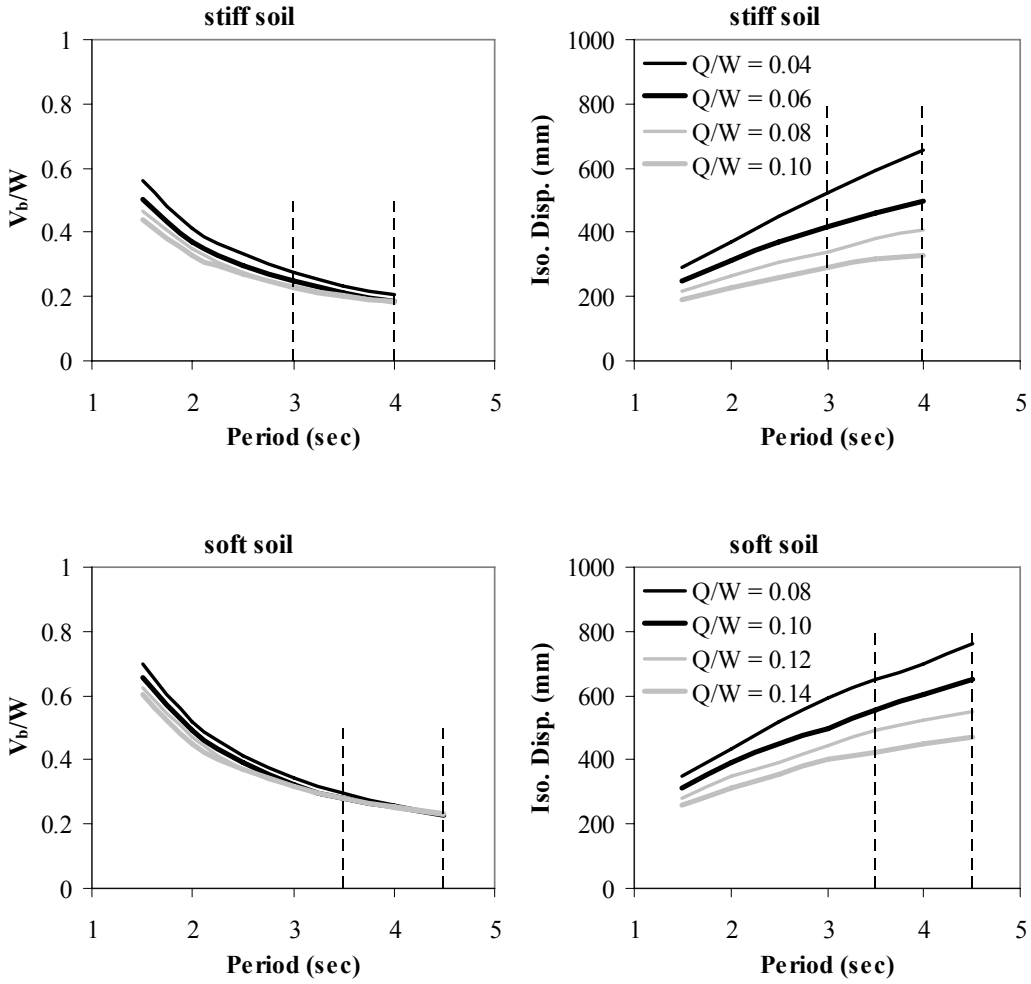

Figure 3.5 Determination of isolator parameters by means of simplified method of analysis considering: normalized base shear (left) and isolator displacement (right).

Selection of *Q*/*W* ratio is limited by considering two further parameters. One is the maximum isolator displacement and the other is the effective damping of corresponding isolation system. Maximum isolator displacement is used to

determine the lowest Q/W ratio. On the left side of Figure 3.5, maximum isolator displacements are calculated by simplified method of analysis under MCE. The basic limitation in determining the isolation systems is the buckling of isolator at maximum design displacements. To eliminate the buckling of isolators used in this study, maximum isolator displacements are limited by 800 mm (Constantinou, 2009). With that limitation and using the isolation periods obtained earlier, the corresponding minimum Q/W ratios are 0.04 and 0.08 for stiff and soft soil conditions, respectively. On the other hand, maximum values of Q/W ratios are determined by restricting the effective damping of the isolators at maximum design displacements. Although the codified procedures allow the use of simplified method of analysis up to 50% effective damping, the maximum value for effective damping is limited so that it does not exceed 40% in MCE (Constantinou, 2009). Hence, upper limits for Q/W ratios are obtained as 0.10 and 0.14 for stiff and soft soil conditions, respectively. These realistic parameters of isolation systems are given in Table 3.5.

Table 3.5 Parameters for isolation systems considered in this study.

Period, T (sec)	3.0, 3.5, 4.0 (for stiff soil)
	3.5, 4.0, 4.5 (for soft soil)
Strength to Weight Ratio,	0.04, 0.06, 0.08, 0.10 (for stiff soil)
Q/W	0.08, 0.10, 0.12, 0.14 (for soft soil)

Properties of the designed isolators are given through Tables 3.6-3.9. Those tables are grouped according to soil conditions and story height of the RC buildings. Each table presents the isolation period T, ratio of strength Q to weight W, yield force F_y, initial stiffness k_e, post yield stiffness k_d, target design displacement D, and corresponding effective damping β_{eff}. Note that, D and β_{eff} values are calculated for both MCE and DE. DE is defined as the design spectra having a probability of

exceedance of 10% in 50 years (475 years return period), whereas MCE is defined as the design spectra with probability of exceedance of 2% in 50 years (2500 years return period).

It is important to indicate that the effective values obtained by simplified method of analysis are not used for nonlinear RHA and isolators are modeled with their real behavior. For this purpose, nonlinear link elements of SAP2000 (2008) are utilized to model bi-linear force-deformation relations of isolators. Each link element (with zero length) has two joints: one is fixed to the ground and the other is connected to the superstructure. Parameters needed for utilizing the link elements are F_y, k_e, and ratio of post yield stiffness k_d to initial stiffness k_e. Both of the RC buildings are supported by twenty isolators as illustrated in Figure 3.4. All isolators have identical properties. Hysteresis loops of the isolators with the characteristics given through Tables 3.6-3.9 are presented in Figures 3.6-3.9 for different soil conditions and buildings.

Employed link elements in SAP2000 (2008) have coupled plasticity properties for both of the deformations in orthogonal horizontal directions. The two dimensional bi-linear hysteretic model in SAP2000 (2008) was developed by Park *et al*. (1986). This model was tested and verified to produce acceptable results on the behavior of isolators in bi-directional motion (Nagarajaiah *et al*., 1989; Mokha *et al*., 1993). According to the model developed by Park *et al*. (1986), if the isolators behave nonlinearly in both of the horizontal directions, forces assembled with due account for bi-directional interaction effects are computed by the following equations:

$$\begin{Bmatrix} F_X \\ F_Y \end{Bmatrix} = r \cdot \begin{bmatrix} \dfrac{F_y}{D_y} & 0 \\ 0 & \dfrac{F_y}{D_y} \end{bmatrix} \cdot \begin{Bmatrix} D_X \\ D_Y \end{Bmatrix} + (1-r) \cdot \begin{bmatrix} F_y & 0 \\ 0 & F_y \end{bmatrix} \cdot \begin{Bmatrix} Z_x \\ Z_y \end{Bmatrix} \quad (3.23)$$

$$Y \cdot \begin{Bmatrix} \dot{Z}_x \\ \dot{Z}_y \end{Bmatrix} = \left(A \cdot [I] - B \cdot [\Omega]\right) \cdot \begin{Bmatrix} \dot{D}_X \\ \dot{D}_Y \end{Bmatrix} \tag{3.24}$$

$$[\Omega] = \begin{Bmatrix} Z_x^2 \cdot \left[sgn\left(\dot{D}_X \, Z_x \right) + 1 \right] & Z_x Z_y \left[sgn\left(\dot{D}_Y \, Z_y \right) + 1 \right] \\ Z_x Z_y \left[sgn\left(\dot{D}_X \, Z_x \right) + 1 \right] & Z_y^2 \left[sgn\left(\dot{D}_Y \, Z_y \right) + 1 \right] \end{Bmatrix} \tag{3.25}$$

where r is post-yield to initial stiffness ratio; D_X and D_Y are displacements of isolators in orthogonal horizontal directions; and $\dot{D}_X$ and $\dot{D}_Y$ are the corresponding relative velocities in orthogonal horizontal directions at the isolator; Z_x and Z_y are hysteretic dimensionless quantities that account for the direction and the biaxial interaction of hysteretic forces (Park *et al*., 1986). A and B in Equation (3.24) are dimensionless quantities and equal to 1 and 0.5, respectively to satisfy the relation of A=2B (Constantinou and Adnane, 1987). This assumption is essential because it assures that the force and displacement vectors are in the same direction.

Figures 3.10 and 3.11 show the idealized 3-D models of isolated 3S and 7S RC structures in SAP2000 (2008). Superstructures are supported on the isolators located at the base level.

Table 3.6 Properties of LRB modeled for 3S RC building at stiff soil.

T (sec.)	Q/W	F_y (N)	k_e (N/mm)	k_d (N/mm)	MCE		DE	
					D (mm)	β_{eff} (%)	D (mm)	β_{eff} (%)
3.0	0.04	7600	760	76.6	523	9.1	281	14.8
	0.06	11020	1102	76.6	419	15.1	211	23.6
	0.08	14440	1444	76.6	340	21.3	168	30.9
	0.10	17860	1786	76.6	290	26.8	136	36.7
3.5	0.04	7400	740	56.5	589	10.7	310	17.4
	0.06	10820	1082	56.5	461	17.7	231	26.9
	0.08	14240	1424	56.5	376	24.4	179	34.6
	0.10	17660	1766	56.5	314	30.3	142	40.4
4.0	0.04	7270	727	42.8	655	12.2	333	20.0
	0.06	10690	1069	42.8	496	20.3	248	30.0
	0.08	14110	1411	42.8	406	27.3	187	37.9
	0.10	17530	1753	42.8	333	33.6	150	43.1

Table 3.7 Properties of LRB modeled for 3S RC building at soft soil.

T (sec.)	Q/W	F_y (N)	k_e (N/mm)	k_d (N/mm)	MCE		DE	
					D (mm)	β_{eff} (%)	D (mm)	β_{eff} (%)
3.5	0.08	14240	1424	56.5	652	17.0	327	26.3
	0.10	17660	1766	56.5	555	22.1	269	32.5
	0.12	21080	2108	56.5	488	26.7	225	37.6
	0.14	24500	2450	56.5	427	31.1	193	41.5
4.0	0.08	14110	1411	42.8	703	19.5	350	29.4
	0.10	17530	1753	42.8	604	24.9	284	35.8
	0.12	20950	2095	42.8	522	29.8	235	40.8
	0.14	24370	2437	42.8	452	34.4	204	44.3
4.5	0.08	14020	1402	33.6	760	21.8	370	32.3
	0.10	17440	1744	33.6	647	27.4	294	38.8
	0.12	20860	2086	33.6	550	32.7	248	43.3
	0.14	24280	2428	33.6	472	37.3	212	46.6

Table 3.8 Properties of LRB modeled for 7S RC building at stiff soil.

T (sec.)	Q/W	F_y (N)	k_e (N/mm)	k_d (N/mm)	MCE		DE	
					D (mm)	β_{eff} (%)	D (mm)	β_{eff} (%)
3.0	0.04	20430	2043	206	523	9.1	281	14.8
	0.06	29620	2962	206	419	15.1	211	23.6
	0.08	38810	3881	206	340	21.3	168	30.9
	0.10	48000	4800	206	290	26.8	136	36.7
3.5	0.04	19890	1989	151.2	589	10.7	310	17.4
	0.06	29080	2908	151.2	461	17.7	231	26.9
	0.08	38270	3827	151.2	376	24.4	179	34.6
	0.10	47460	4746	151.2	314	30.3	142	40.4
4.0	0.04	19540	1954	115.5	655	12.2	333	20.0
	0.06	28730	2873	115.5	496	20.3	248	30.0
	0.08	37920	3792	115.5	406	27.3	187	37.9
	0.10	47110	4711	115.5	333	33.6	150	43.1

Table 3.9 Properties of LRB modeled for 7S RC building at soft soil.

T (sec.)	Q/W	F_y (N)	k_e (N/mm)	k_d (N/mm)	MCE		DE	
					D (mm)	β_{eff} (%)	D (mm)	β_{eff} (%)
3.5	0.08	38270	3827	151.2	652	17.0	327	26.3
	0.10	47460	4746	151.2	555	22.1	269	32.5
	0.12	56650	5665	151.2	488	26.7	225	37.6
	0.14	65840	6584	151.2	427	31.1	193	41.5
4.0	0.08	37920	3792	115.5	703	19.5	350	29.4
	0.10	47110	4711	115.5	604	24.9	284	35.8
	0.12	56300	5630	115.5	522	29.8	235	40.8
	0.14	65490	6549	115.5	452	34.4	204	44.3
4.5	0.08	37670	3767	90.5	760	21.8	370	32.3
	0.10	46860	4686	90.5	647	27.4	294	38.8
	0.12	56050	5605	90.5	550	32.7	248	43.3
	0.14	65240	6524	90.5	472	37.3	212	46.6

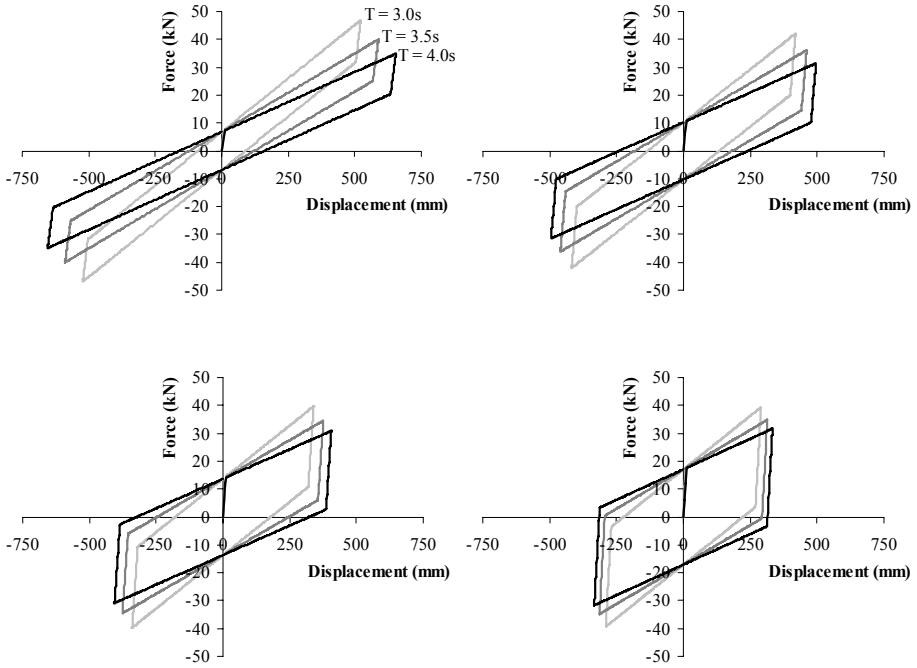

Figure 3.6 Bi-linear force-deformation relation of a LRB in stiff soil for 3-story RC structure: a) $Q/W = 0.04$; b) $Q/W = 0.06$; c) $Q/W = 0.08$; d) $Q/W = 0.10$.

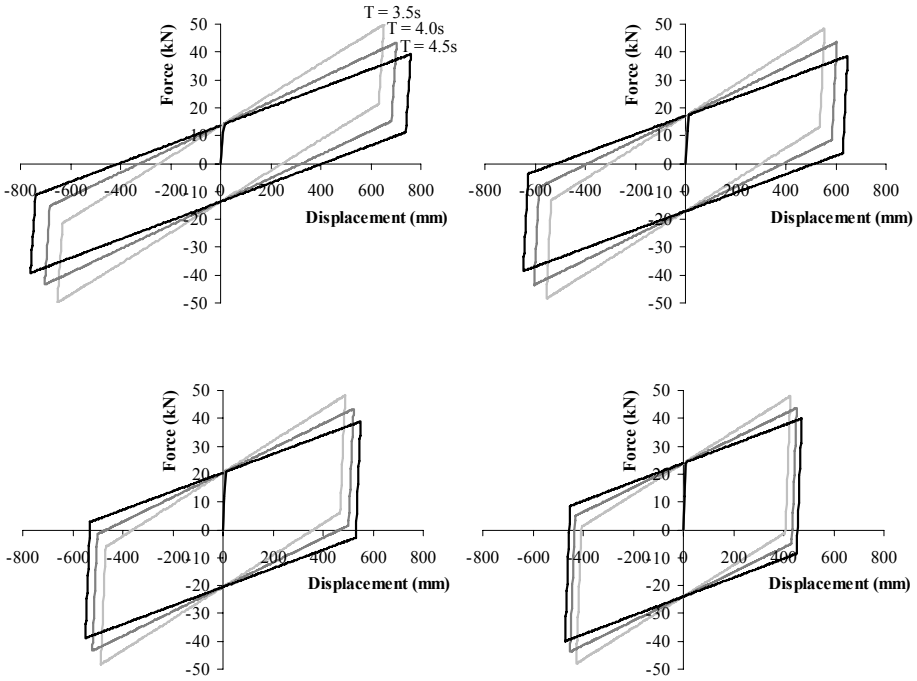

Figure 3.7 Bi-linear force-deformation relation of a LRB in soft soil for 3-story RC structure: a) $Q/W = 0.08$; b) $Q/W = 0.10$; c) $Q/W = 0.12$; d) $Q/W = 0.14$.

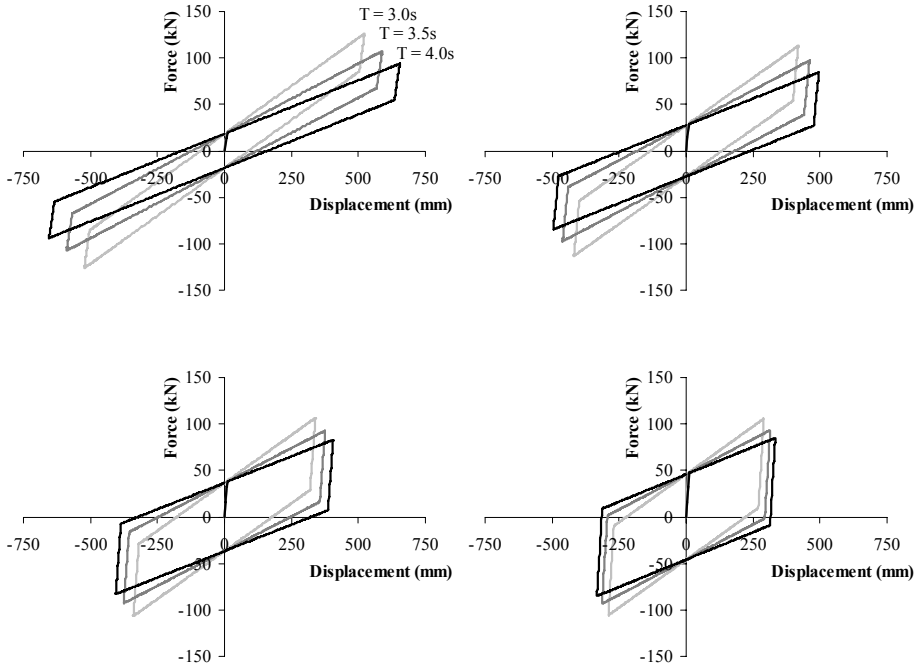

Figure 3.8 Bi-linear force-deformation relation of a LRB in stiff soil for 7-story RC structure: a) $Q/W = 0.04$; b) $Q/W = 0.06$; c) $Q/W = 0.08$; d) $Q/W = 0.10$.

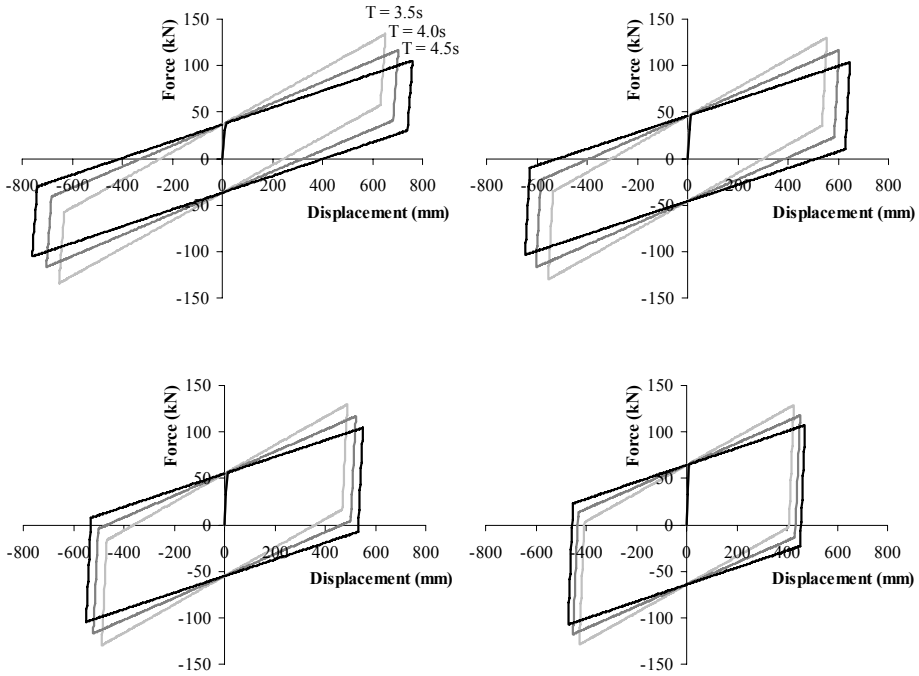

Figure 3.9 Bi-linear force-deformation relation of a LRB in soft soil for 7-story RC structure: a) $Q/W = 0.08$; b) $Q/W = 0.10$; c) $Q/W = 0.12$; d) $Q/W = 0.14$.

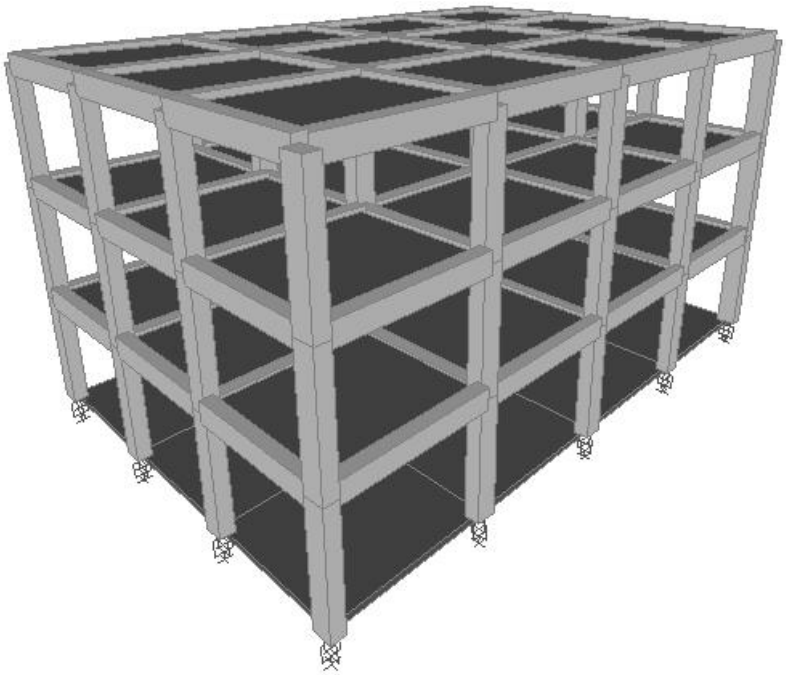

Figure 3.10 3-D model of 3-story RC structure in SAP2000.

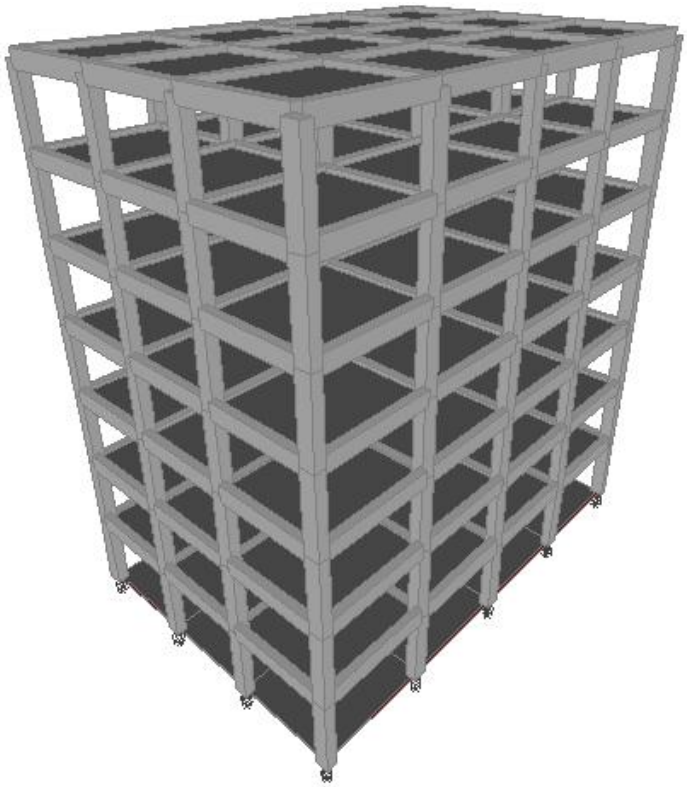

Figure 3.11 3-D model of 7-story RC structure in SAP2000.

CHAPTER 4

EVALUATION OF EQUIVALENT LATERAL FORCE PROCEDURE IN ESTIMATING SEISMIC ISOLATOR DISPLACEMENTS AND SHEAR FORCES

4.1 INTRODUCTION

Simplified methods of analysis are described in codes and specifications for seismically isolated structures (e.g., AASHTO (1999), ASCE (2005), Eurocode 8 (2005)). These simplified methods of analysis are either directly used in restricted cases (e.g., symmetric structures, height less than four stories, away from a fault) or are used as gage or criteria for the results of nonlinear RHA, that is typically used in the analysis of seismically isolated structures.

Important predictions for seismically isolated structures by simplified methods are the maximum resultant displacement of the isolation system and the maximum shear force in the isolation system. This study concentrates on the prediction of these two quantities by the equivalent lateral force (ELF) procedure of ASCE (2005) (which is virtually identical to AASHTO (1999) and Eurocode 8 (2005)). In ELF procedure, the structure is represented by a single-degree-of-freedom system with stiffness equal to secant or effective stiffness (Figure 3.1) and viscous damping represented by effective damping at the calculated displacement. The method utilizes code-specific or site-specific 5% damped spectra after modification for the effects of effective damping higher than 5%. The difference between the simplified analysis procedures of ASCE (2005), AASHTO (1999) and EN (2005) is only

based on the description of the modification of the 5%-damped spectrum for higher damping ratios.

Several studies evaluated the simplified methods of analysis (Iwan and Gates, 1979; Kircher and Lashkari, 1989; Theodossiou and Constantinou, 1991; Winters and Constantinou, 1993; Tsopelas *et al*., 1997; Chopra and Goel, 1999; Ramirez *et al*., 2002; Pavlou and Constantinou, 2004; Warn and Whittaker, 2004; Guyader and Iwan, 2006; Fadi and Constantinou, 2009). Those studies considered one-directional ground excitation, with the exception of the studies of Kircher and Lashkari (1989), Theodossiou and Constantinou (1991), Winters and Constantinou (1993) and Warn and Whittaker (2004) which concentrated on seismically isolated structures subjected to bi-directional ground excitation. In the studies of Kircher and Lashkari (1989), Theodossiou and Constantinou (1991) and Winters and Constantinou (1993) the calculated displacement in RHA was the maximum among the two components along the two principal directions and not the resultant displacement. This may have not been an important difference because of the motions used in RHA were far-field motions without a significant difference between the maximum one-directional component of displacement and the resultant displacement.

The study of Warn and Whittaker (2004) compared predictions of the simplified analysis procedure to the peak resultant displacement calculated in RHA and the conclusion was that the simplified analysis method under-predicts the displacement demand. This conclusion contradicts the conclusions of the related studies of Kircher and Lashkari (1989), Theodossiou and Constantinou (1991), Winters and Constantinou (1993), Tsopelas *et al* (1997), Ramirez *et al* (2002), Pavlou and Constantinou (2004) and Fadi and Constantinou (2009). Two characteristics of the Warn and Whittaker (2004) study differed from the other aforementioned studies:

1) The motions used in RHA were not scaled to represent a particular response spectrum. Rather large bins of motions were used and the median spectrum of the motions in each bin was used as the response spectrum to use in the simplified analysis. The spectral acceleration value at 1 second period of each median spectrum was used directly in simplified analysis calculations

per AASHTO (1999) by assuming that to be equal to quantity AS_i. Inspection of the spectra reported in Warn and Whittaker (2004) reveals that the median spectra of all components generally followed the inverse of period rule as presumed in AASHTO (1999), although median spectra of some bins did not.

2) The motions used were from either near-field or large magnitude earthquakes.

It is believed that these two characteristics affected the RHA calculated in Warn and Whittaker (2004). Accordingly, the study reported herein also concentrated on motions with near-field characteristics but implemented a selection and a new scaling method proposed for dynamic analysis of isolated structures (see Section 2.4) that is consistent with contemporary practices in the representation of site-specific response spectra by ground motion assemblies. The RHA and the ELF procedure were implemented as described in ASCE (2005) and as they would be used in the analysis of seismically isolated buildings today.

4.2 ANALYSES CONDUCTED

Evaluation of simplified method of analysis is based on the comparison of results obtained by ELF procedure with the results obtained by nonlinear RHA. RHA were conducted under bi-directional earthquake excitations. Considered superstructure is a 3-story symmetric RC building as illustrated in Chapter 3 (Figure 3.4).

4.2.1 Equivalent Lateral Force (ELF) Procedure

ELF procedure is an iterative method that is based on modification of 5% damped spectrum due to higher effective damping values at the isolation level. This iterative approach is defined in Section 3.3 of Chapter 3 in detail.

Evaluation of ELF procedure was performed for two different levels of ground motions: DE and MCE. Corresponding 5% damped response spectra are given in Figure 4.1 for both stiff and soft soil conditions (TEC, 2007).

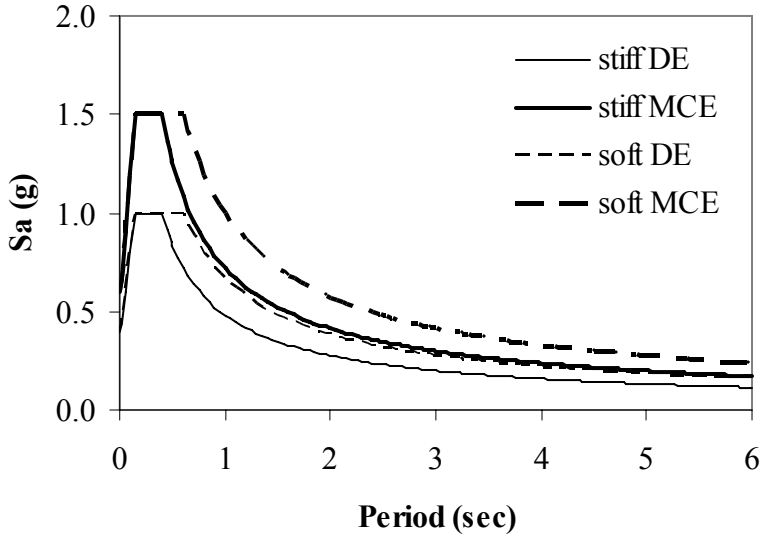

Figure 4.1 Response spectra for design and maximum considered earthquakes of stiff and soft soil classifications (adopted from TEC(2007)).

Considering the isolator properties presented in Table 3.5 of Chapter 3, forty eight different iterative analyses were conducted: half of them were for DE and the other half for MCE. Results of ELF procedure for the selected isolator parameters were given through Tables 3.6-3.7.

4.2.2 Nonlinear Response History Analysis (RHA)

A total of 528 nonlinear RHA were conducted under bi-directional earthquake excitations in structural analysis program SAP2000 (2008). Details of selection of records and proposed new scaling method for records was given in Section 2.4 of Chapter 2.

The isolated structure is subjected to both horizontal orthogonal components simultaneously (Figure 4.2 (a) or (b)). As a consequence of having a completely symmetric system, maximum displacements of the isolators under bi-directional loading conditions depicted in Figures 4.2(a) and 4.2(b) are exactly the same. This observation yields the reduction of required number of simulations by 50%.

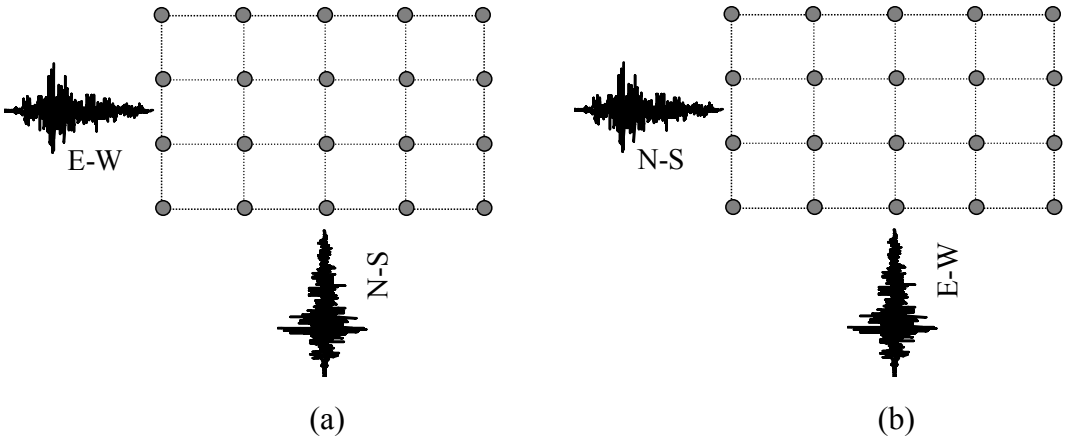

Figure 4.2 Application of bi-directional ground motion excitations.

4.3 ANALYSIS RESULTS

The results of the analyses are discussed in two groups: (i) maximum isolator displacements and (ii) maximum base shear carried by isolators. Each group has two further subsections to differentiate between the effects of damping (Q/W ratio) and isolation period T.

4.3.1 Maximum Isolator Displacements

A comparison of isolator displacements calculated by the ELF procedure with displacements determined by nonlinear RHA, where the proposed new scaling method is used, for both of the site classes are presented in Figure 4.3. The horizontal axis in these graphs represents the displacement calculated by equivalent

lateral force procedure (D_{ELF}). The vertical axis represents the maximum resultant isolator displacements calculated in the nonlinear RHA (D_{RHA}). The solid lines in these figures are the reference lines with slope equal to one. Any point located below these lines indicates conservative estimation of the isolator displacement by the ELF procedure. The superiority of the proposed new scaling method is also indicated by Figure 4.4 where only the code requirements for scaling of records is employed for nonlinear RHA of isolated building.

The iterative way of ELF procedure to predict maximum isolator displacements does not consider the contribution of horizontal orthogonal component. Analysis should be independently performed in the two orthogonal directions and results be combined by 100%+30% rule. This rule indicates that the maximum isolator displacement is equal to vectorial sum of the isolators due to longitudinal and transverse earthquake components. This displacement can be calculated as $\sqrt{D^2 + (0.3D)^2} \approx 1.05D$. Here, D is the response in strong direction of the motion. Hence, D_{ELF}, in which effect of bi-directional excitation is considered, is equal to 1.05 times the displacement calculated by the ELF procedure. The maximum isolator displacements of the isolated structures in nonlinear RHA are calculated by taking the SRSS of displacements in both horizontal orthogonal directions at each time step. Once the maximum displacements are obtained for all of the eleven analyses in each earthquake bin (Tables 2.1 and 2.2), results are processed to represent the mean values of those eleven analyses. The data presented under the name of D_{RHA} are the mean values.

Results presented in Figure 4.3 consider the observations for both DE and MCE. Data presented by solid geometric shapes reprent the results for DE, while results for MCE are represented by the ones that are hollow. Presentation of the corresponding data is not grouped according to Q/W ratios. However, it should be stated that D_{ELF} decreases as Q/W ratio increases.

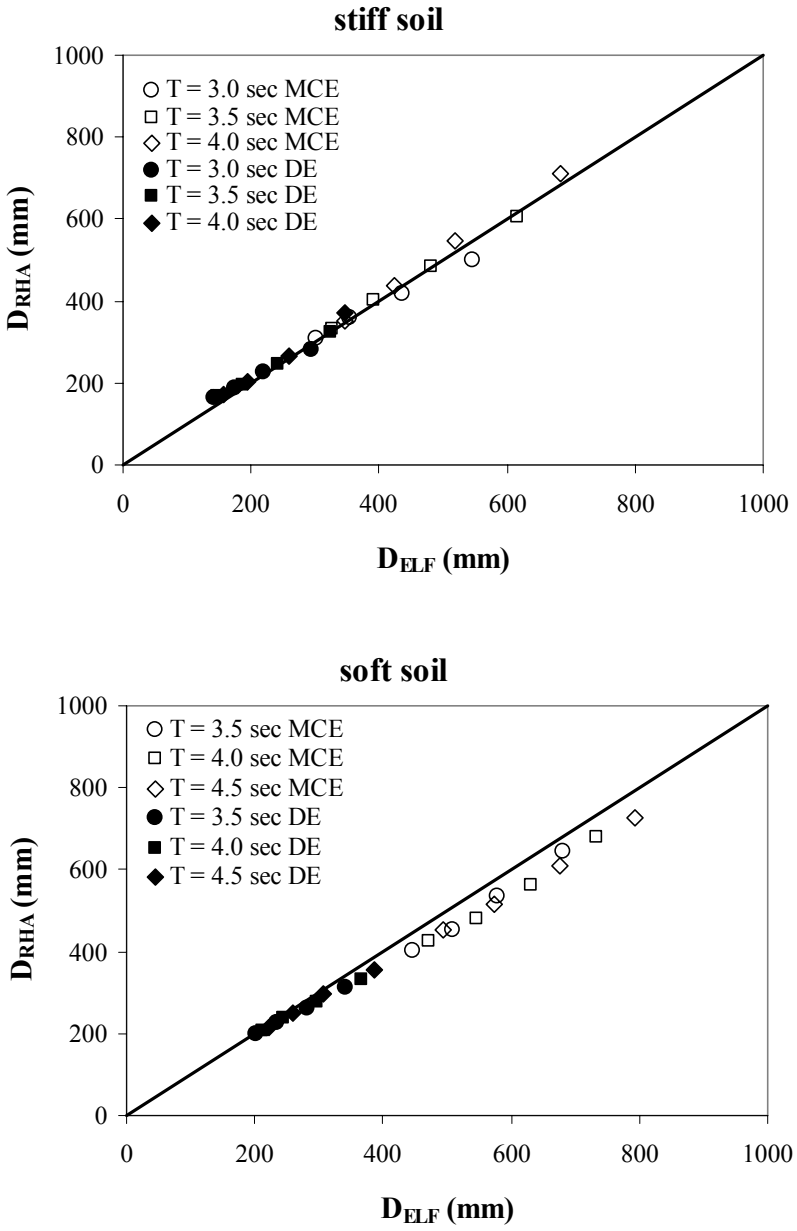

Figure 4.3 Comparison of displacements obtained by D_{ELF} and D_{RHA} for stiff (top) and soft (bottom) soil conditions.

Figure 4.3 demonstrate that the ELF procedure predicts the isolator displacement with acceptable accuracy. For stiff soil records, the simplified method slightly underestimates the displacement demands when the isolation period *T* is

greater than 3.5 sec. The maximum amount of underestimation is not greater than 5% when it is MCE, which is acceptably low. On the other hand, the amount of underestimation may be up to 13% for DE (i.e. Q/W = 0.10). Corresponding effective damping ratio for those cases are above 40%. For soft soil records, the ELF procedure overestimates the displacement demands, although the degree of overestimation does not exceed about 12%. It is on the safe side regardless of the considered earthquake (DE or MCE). The degree of conservatism reduces for DE compared to MCE.

To indicate the success of proposed method for scaling ground motion records, an additional series of nonlinear RHA were also conducted for MCE by using only the scaling procedure defined in ASCE (2005). Method used for scaling the records described in ASCE (2005) simply involves constructing average SRSS spectra from all horizontal component pairs that does not fall below 1.3 times the corresponding ordinate of the design response spectrum by more than 10%. Figure 4.4 presents the comparison of displacements calculated by ELF (D_{ELF}) and obtained from nonlinear RHA in accordance with the code (D_{RHA} Code). Comparisons were done for stiff and soft soil conditions separately.

Figure 4.4a shows that the predictions of ELF method are always unsafe for stiff soil condition regardless of the isolation period. Although the predictions become closer as the isolation period increases, the best estimate of D_{ELF} is about 5% less than that of D_{RHA}. The degree of under-prediction varies in between 5% - 20% depending on the Q/W ratio. As Q/W ratio increases, prediction of ELF method gets more inappropriate. The maximum erroneous prediction which corresponds to the case where Q/W = 0.10 and T = 3.0 sec. is 20% less than the displacements obtained by nonlinear RHA.

The same comparisons were done for soft soil condition in Figure 4.4b. It is clear that for higher isolation periods, ELF procedure and nonlinear RHA results are almost equal to each other. However, for the cases with isolation period T = 3.5 sec., ELF procedure is not enough to predict the maximum isolator displacements.

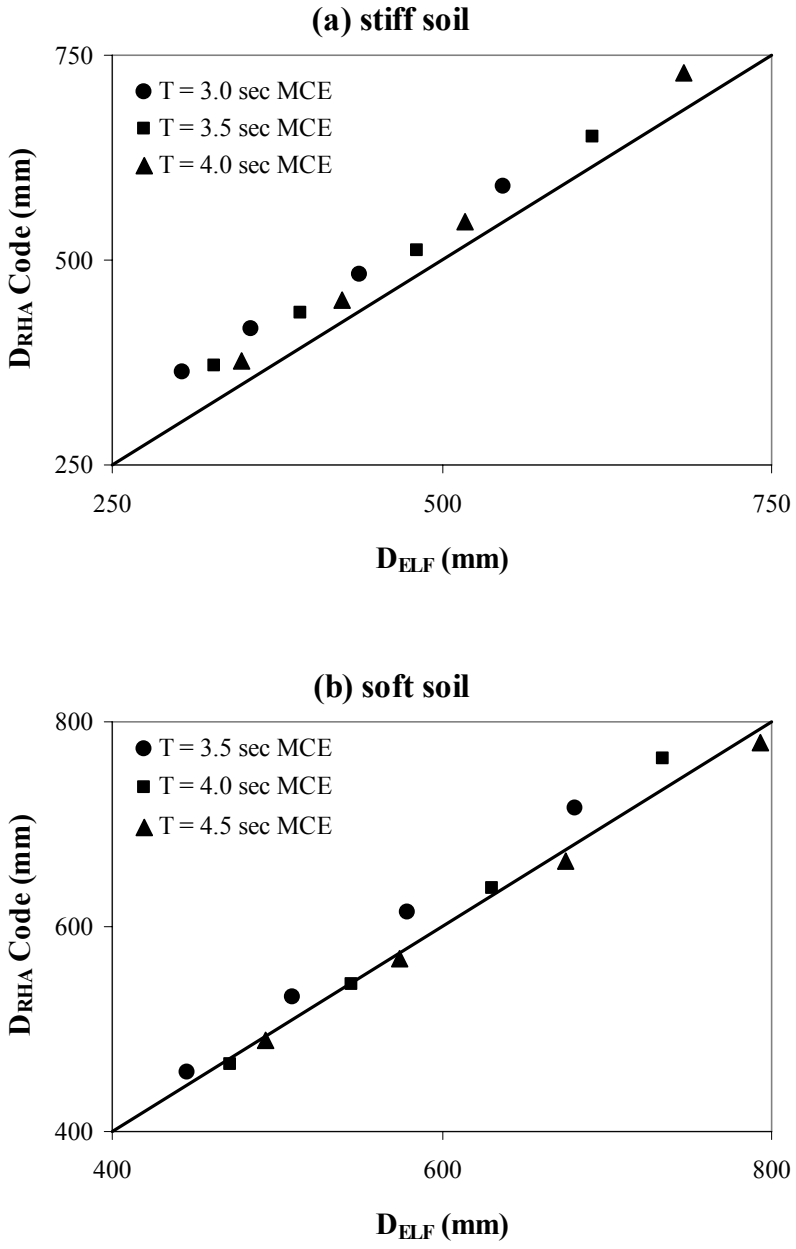

Figure 4.4 Comparison of displacements obtained by D_{ELF} and D_{RHA} Code for: (a) stiff soil and (b) soft soil.

Comparison of Figures 4.3 and 4.4 shows the reason why the proposed method of scaling is more adequate when bi-directional ground motion excitations are of concern. The effects of both horizontal components are adequately considered and

scaled to become compatible with the corresponding design spectrum by means of proposed scaling method. This is important because scaling pairs of records is crucial for comparison of bi-directional analysis results with that of uni-directional ones. The proposed method of scaling preserves the difference between the two horizontal components of a record which is especially important for records with near-field effects (Stewart *et al*., 2001).

4.3.1.1 Effect of Damping (Q/W Ratio)

In this section, variation of D_{RHA}/D_{ELF} is investigated to indicate the success of ELF method under the effect of Q/W ratio. Thus, D_{RHA}/D_{ELF} ratios are plotted against considered Q/W ratios in Figures 4.5 and 4.6 for stiff and soft soil conditions, respectively. Comparisons are done only for MCE, because the most important thing in an isolation system is the prediction of maximum isolator displacement for design purposes. And, it is clear that the displacements obtained from MCE are higher than that of DE.

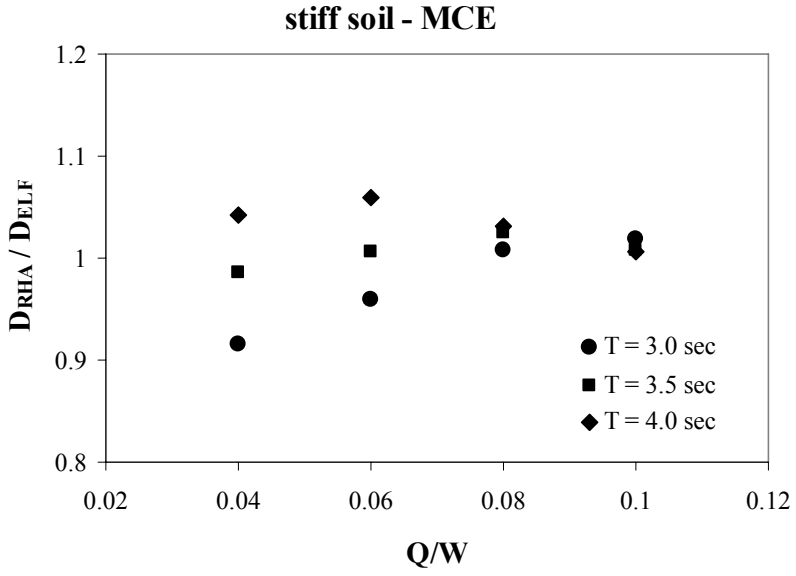

Figure 4.5 Ratio of D_{RHA} to D_{ELF} versus Q/W ratio at stiff soil conditions for MCE.

In Figure 4.5, results for MCE demonstrate that the effect of Q/W ratio on D_{RHA}/D_{ELF} ratio is not same for all of the selected isolation periods. D_{RHA}/D_{ELF} ratio increases with an increase in Q/W ratio for the system with isolation period of 3 sec. Variation of D_{RHA}/D_{ELF} ratio is in between 0.9 and 1.0 for those systems. On the other hand, D_{RHA}/D_{ELF} ratio seems to be insenstive to variation in Q/W ratio for the systems where isolation period is 3.5 sec. It is almost identical for all of the considered Q/W ratios. Predictions of maximum isolator displacements by ELF procedure give safe results for isolation systems with periods of 3 and 3.5 sec. in stiff soil conditions. However, although the degree of underestimation is slight, when isolation period is 4 sec. there occurs some underestimation depending on the Q/W ratio. At lower Q/W ratios, where effective damping values at maximum isolator displacements are in between 10%-20%, the simplified method of analysis underestimates the maximum isolator displacements with a variation in D_{RHA}/D_{ELF} ratio up to 1.05. Nevertheless, D_{RHA}/D_{ELF} ratio then decreases for further increase in Q/W ratio and provides that simplified method of analysis gives safe predictions compared to nonlinear RHA results.

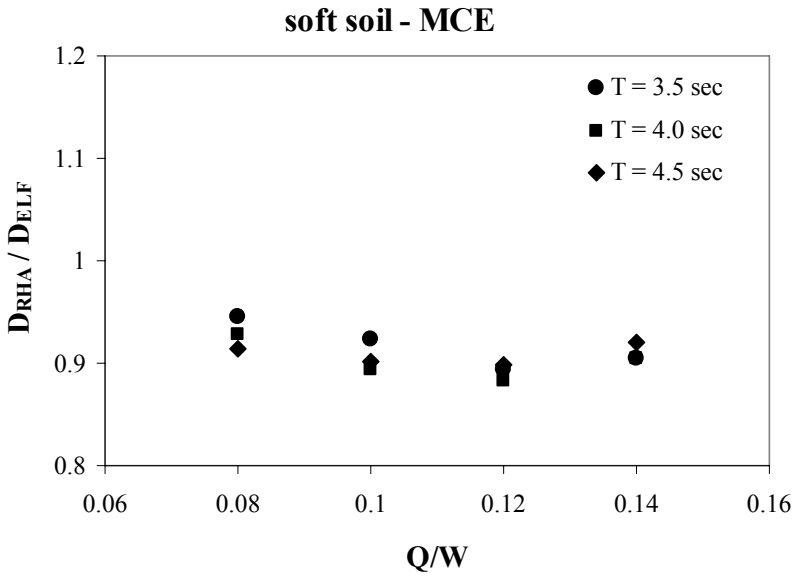

Figure 4.6 Ratio of D_{RHA} to D_{ELF} versus Q/W ratio at soft soil conditions for MCE.

Data presented in Figure 4.6 reveal that tendency of D_{RHA}/D_{ELF} ratio due to alteration in Q/W ratio under soft soil conditions is opposite to that of stiff soil conditions. D_{RHA}/D_{ELF} ratio decreases with increasing Q/W ratio having a minimum at $Q/W = 0.12$. Then, it slightly increases when Q/W raised to 0.14. As D_{RHA}/D_{ELF} ratio being less than one regardless of the Q/W ratio, predictions of simplified method are safe up to about 10%.

4.3.1.2 Effect of Isolation Period T

Figures 4.5 and 4.6 are also used to comprehend the effect of isolation period T on efficiency of predictions of ELF procedure by presenting D_{RHA}/D_{ELF} ratios for results obtained under stiff and soft soil conditions, respectively.

In Figure 4.5, it is observed that the accuracy of ELF procedure to predict maximum isolator displacements depends on isolation period T for Q/W ratios less than and equal to 0.06. On the other hand, when Q/W ratios are greater than 0.06, isolation period becomes an ineffective parameter for accuracy of the ELF procedure. D_{RHA}/D_{ELF} ratios are almost identical for all of the considered isolation periods.

When the same comparison is done for isolation systems under soft soil conditions in Figure 4.6, it is clear that variation in isolation system T has no effect on D_{RHA}/D_{ELF} ratios for all of the isolation systems under consideration. This indicates that prediction of maximum isolator displacement by means of simplified method of analysis is not sensitive to alteration of isolation period for soft soil condition regardless of the Q/W ratio.

4.3.2 Maximum Base Shear

Evaluation of ELF procedure in predicting the maximum base shear of the isolated structure is done by comparing the base shears calculated by ELF procedure and obtained by nonlinear RHA. Comparison results are presented in Figure 4.7 for both stiff and soft soil conditions.

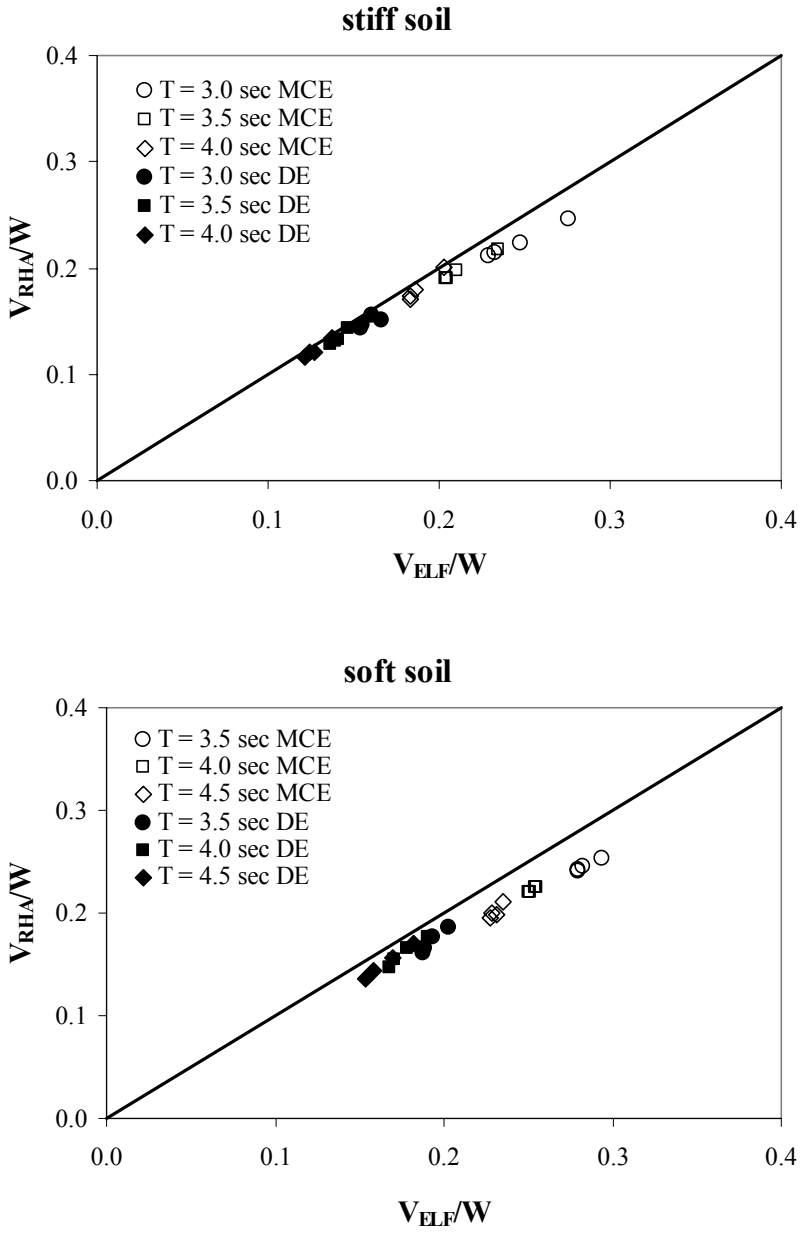

Figure 4.7 Comparison of results of RHA and ELF procedure on isolation system shear force for stiff (top) and soft (bottom) soil conditions.

In Figure 4.7, both horizontal and vertical axes are normalized by the total weight of the superstructure. Base shears obtained from nonlinear RHA and ELF procedure are represented by V_{RHA} and V_{ELF}, respectively. Similar to Figure 4.3,

solid line stands for the cases where simplified analyses results are equal to that of nonlinear dynamic analyses. Any point below that line shows that prediction by simplified method of analysis (ELF procedure) is safe.

Since, force based design of structures considers only the response under uni-directional representation of ground motions, comparisons are done accordingly. Hence, V_{ELF} is the maximum shear force in any horizontal orthogonal direction of the isolation system (x or y) without consideration of any bi-directional effect. V_{RHA} is the mean value, among the eleven analyses, of the maximum x-direction shear forces, or the y-direction shear forces under bi-directional ground motion excitation.

Figure 4.7 shows that predictions of ELF procedure are accurate enough when compared to results from nonlinear dynamic analyses. Furthermore, they are on the safe side for all of the cases considered.

4.3.2.1 Effect of Damping (Q/W Ratio)

Sensitivity of predictions of simplified method of analyses are studied in terms of variations in V_{RHA}/V_{ELF} under considered Q/W ratios in this section. To shed light on this topic, V_{RHA}/V_{ELF} ratios versus Q/W ratios are presented in Figures 4.8 and 4.9 for stiff and soft soil conditions. Comparisons are again conducted for MCE, because prediction of maximum base shear by ELF procedure is of concern.

Figure 4.8 shows that variations in V_{RHA}/V_{ELF} ratios due to alteration of Q/W ratio is very similar to variations of D_{RHA}/D_{ELF} ratios as presented in Figure 4.5. Although it is very limited, V_{RHA}/V_{ELF} ratio increases with an increase in Q/W ratio for the system with isolation period equals to 3 sec. The minimum and maximum values for V_{RHA}/V_{ELF} ratios are around 0.89 and 0.92 for those systems, respectively. On the other hand, V_{RHA}/V_{ELF} ratios of the systems with an isolation period of 3.5 sec. are observed to be insenstive to variation in Q/W ratio. They are almost identical for all of the considered Q/W ratios. When the systems with isolation period T equals to 4 sec. are of concern, V_{RHA}/V_{ELF} ratio decreases as Q/W ratio increases from 0.04 to 0.08. However, for further increase of Q/W ratio to

0.10, Figure 4.8 shows that there is a minor increase in V_{RHA}/V_{ELF} ratio which can be neglected. It is clear in Figure 4.8 that the maximum base shears calculated by simplified method of analysis are safe and in good aggreement with the ones obtained by nonlinear RHA under stiff soil conditions.

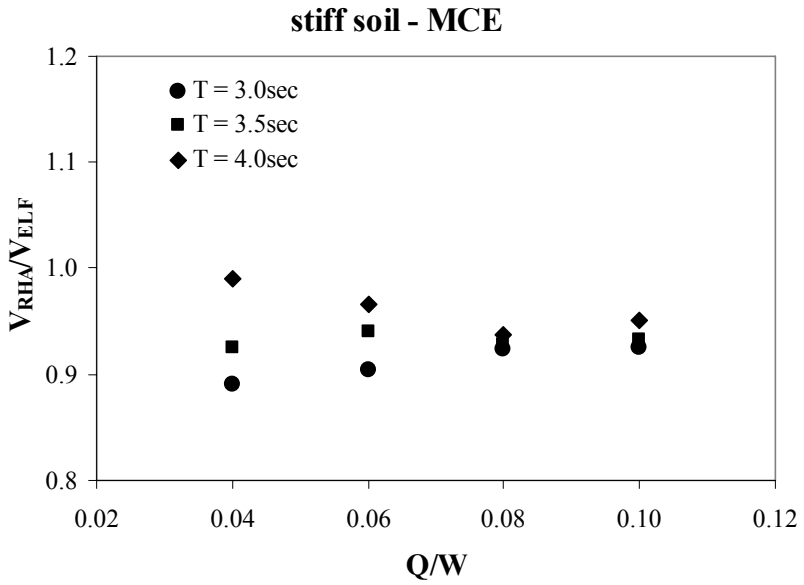

Figure 4.8 Ratio of V_{RHA} to V_{ELF} versus *Q*/*W* ratio at stiff soil conditions for MCE.

Apparently, variation of V_{RHA}/V_{ELF} ratio is not affected by any change in *Q*/*W* ratio under soft soil conditions as depicted in Figure 4.9. V_{RHA}/V_{ELF} ratios of the considered isolation systems almost lay on a horizontal line for all of the *Q*/*W* ratios. This indicates that the prediction of maximum base shears by ELF procedure is not sensitive to change in damping ratios in the isolation level.

4.3.2.2 Effect of Isolation Period T

Figures 4.8 and 4.9 are visited one more time and investigated to observe the effect of isolation period *T* on prediction of maximum base shears by simplified

method of analysis. And, variations in V_{RHA}/V_{ELF} ratios due to change in isolation periods are discussed in this section.

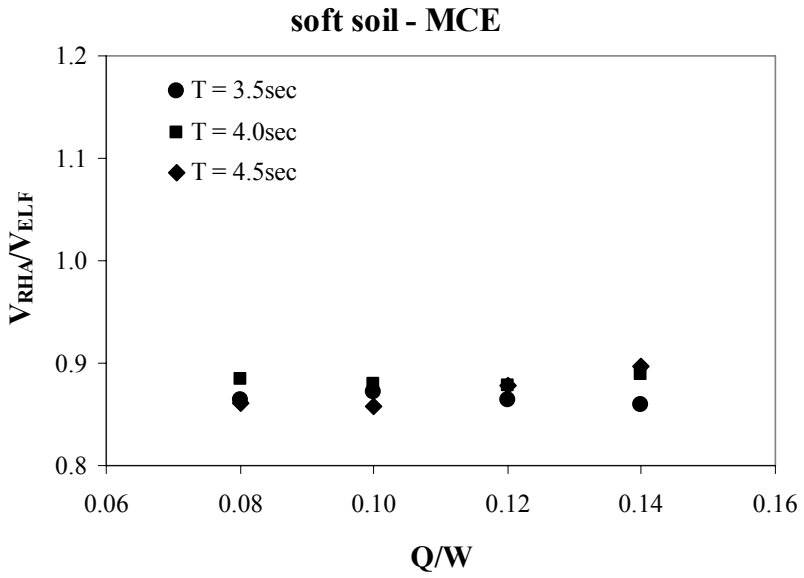

Figure 4.9 Ratio of V_{RHA} to V_{ELF} versus Q/W ratio at soft soil conditions for MCE.

As it is seen in Figure 4.8, effect of isolation period T should be studied in two groups. Since, there is a region where the isolation period is not effective but there is another region where isolation period directly affects the V_{RHA}/V_{ELF} ratios. In the first group ($Q/W \leq 0.06$), effective damping ratios of the isolators are in between 20% to 30%. It can be concluded that the prediction of maximum base shears by means of ELF procedure is sensitive to change in isolation period in the range of 20% - 30% effective damping. However, for the second group ($Q/W > 0.06$), isolation period is obtained to be ineffective in predicting the maximum base shears by looking at the differences between V_{RHA}/V_{ELF} ratios presented in Figure 4.8.

Apart from discussions made for stiff soil condition, V_{RHA}/V_{ELF} ratio is obtained to be insensitive to change in isolation period regardless of the damping ratio at

isolation level under soft soil conditions. Figure 4.9 shows that variation in V_{RHA}/V_{ELF} ratio due to change in isolation period is negligible.

CHAPTER 5

RESPONSE OF ISOLATED STRUCTURES UNDER BI-DIRECTIONAL EXCITATIONS OF NEAR-FIELD GROUND MOTIONS

5.1 INTRODUCTION

Most of the design codes recommend two approaches to consider the effects of orthogonal ground motions on the response of structures. One is the SRSS rule, and the other is the percentage rule. The percentage rule is simply the application of 100%+30% combination. This method is first recommended by Rosenblueth and Contreras (1977). They made linear approximation during the modeling of orthogonal ground motion components in terms of elastic spectral accelerations. The suggested 30% increment in the response of structures is implied to cover the errors initiated by the linear approximation (Menun and Der Kiureghian 1998).

The percentage rule for combination of effect of multi-component ground motions do not consider neither the dynamic characteristics of response of structure (linear or nonlinear) nor the soil conditions (rock, soft soil). However, some recent studies made an emphasis on the response of isolation systems under soft soil and near-field conditions (Chung *et al*., 1999; Pavlou and Constantinou, 2004). Jangid and Kelly (2001) studied the response of linear isolation systems to near-field motions under bi-directional earthquake excitations and concluded that the resultant displacement of the isolators can be obtained simply by increasing the displacement under uni-directional excitation by 5% to incorporate the effect of orthogonal component. However, being composed of linear systems, that conclusion was open

to further investigation. Hence, Mosqueda *et al*. (2004), Warn and Whittaker (2004), and Colunga and Osornio (2006) also studied the same phenomenon which is the degree of contribution of orthogonal components in ground motion analysis.

In the study of Mosqueda *et al*. (2004), five ground motions were considered, and only three of them were designated as near-field record. Conversely, Warn and Whittaker (2004) used twelve near-field records. However, the motions used in the RHA were not scaled to represent a particular response spectrum. Furthermore, all of the records have the same soil classification where the average shear wave velocities were in the range of 180 m/sec to 360 m/sec. Hence, authors did not address the effect of soil type on contribution of orthogonal horizontal component. On the other hand, Colunga and Osornia (2006) considered the effect of soil classification by employing numerous records recorded at different soil types. Nevertheless, all of the considered ground motions were limited to a specific region which is Mexican Pacific Coast. Moreover, authors used a scaling procedure where only the "*dominant*" component of a record would match the target spectrum at a target period. Bommer and Acevedo (2004) and Haselton and Baker (2006) implied the importance of scaling records in a range of periods rather than a single period. This observation is especially important for highly non-linear systems such as seismic isolation systems. Another drawback of the scaling used by Colunga and Osornia (2006) was that it is only based on the strong component instead of considering both horizontal components. This is especially important for records with near-field effects to preserve the difference between the components (Stewart *et al*., 2001). Additionally, the scaling factors used in their study were up to 100 which is unacceptably high (Krinitzsky and Chang, 1977; Vanmarcke, 1979; Malhotra, 2003; Bommer and Acevedo, 2004; Hancock *et al*., 2008). Moreover, authors did not consider the effect of near-field records by discarding the records with pulse type behavior.

Considering the previous studies conducted to investigate the effect of orthogonal horizontal components on the response of isolated structures, there is a need for a systematical research compatible with codified procedures. To fill this

need, the study reported herein concentrated on motions with near-field characteristics by considering pulse-type behavior but implemented a selection and a new scaling method proposed for dynamic analysis of isolated structures (see Section 2.4) that is consistent with contemporary practices in the representation of site-specific response spectra by ground motion assemblies.

5.2 ANALYSES CONDUCTED

To shed light on the contribution of orthogonal horizontal component on the response of isolated structures, two isolated case-study buildings were subjected to both uni-directional and bi-directional ground motion excitations. Considered buildings are 3-story and 7-story symmetric RC structures as presented in Chapter 3 (Figures 3.9 and 3.10).

5.2.1 Non-linear Response History Analysis

A total of 792 nonlinear RHA were conducted under uni-directional and bi-directional earthquake excitations in structural analysis program SAP2000 (2008). Evaluation was performed for MCE. Corresponding 5% damped response spectra for stiff and soft soil conditions were given in Figure 4.1 (TEC, 2007). Selection and scaling of original records was done as described in Section 2.4 of Chapter 2.

Considering the isolator properties presented in Table 3.5 of Chapter 3, characteristics of the isolation systems were presented through Tables 3.6-3.9.

The applications of ground motions are illustrated in Figure 5.1. First, both of the case-study buildings were subjected to fault-normal and fault-parallel components of the records separately (Figures 5.1a and 5.1b). Then, both fault-normal and fault-parallel components were applied simultaneously. As a consequence of having completely symmetric systems, maximum displacements of the isolators under bi-directional loading conditions depicted in Figures 5.1(c) and 5.1(d) are exactly the same. This observation yields the reduction of required

number of simulations from 1056 to 792, as only the loadings depicted in Figures 5.1a, 5.1b and 5.1c (or 5.1d) are needed for the analyses.

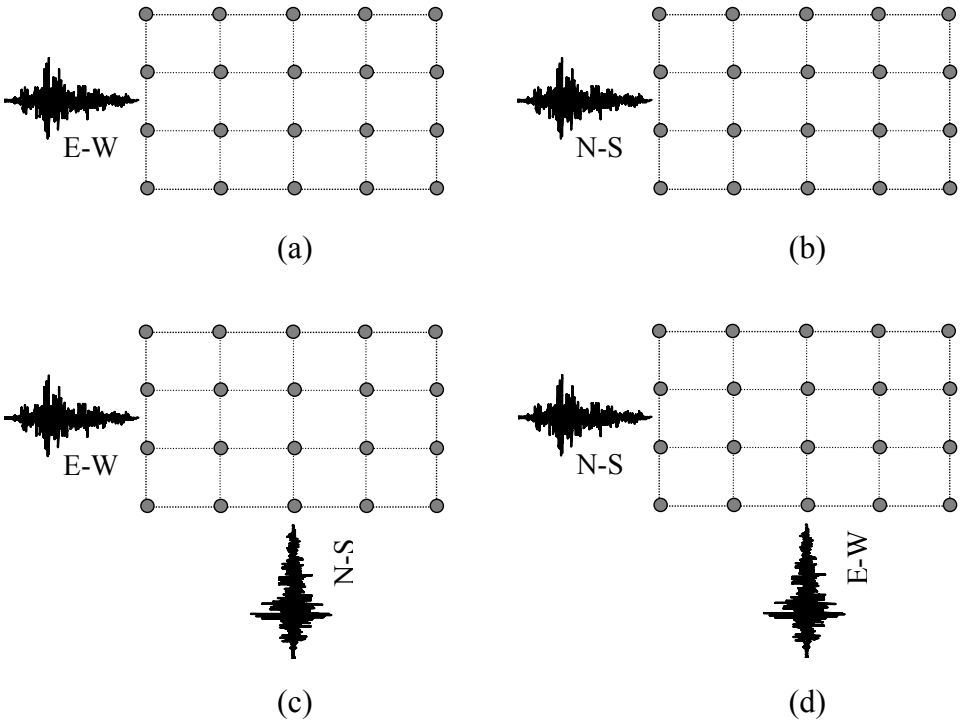

Figure 5.1 Application of uni-directional and bi-directional ground motion excitations.

5.3 ANALYSIS RESULTS

The results are discussed in two parts. First, response of isolation systems is presented in terms of isolator displacements and base shears. Then, response of superstructures is of concern. In this second part, variations in floor accelerations, roof displacements, and drift ratios are studied. In each group, effects of damping (Q/W ratio) and isolation period T are investigated accordingly.

5.3.1 Response of Isolation System

In this section, the variations of maximum isolator displacements and base shears transferred from the isolators to the superstructure are studied in detail. Comparisons are presented in terms of isolation period T and Q/W ratio for both 3- and 7-story RC buildings. Results are also grouped regarding the soil type of the ground motions.

5.3.1.1 Maximum Isolator Displacements

The bi-directional isolator displacements of the isolated structures in nonlinear RHA were calculated by taking the SRSS of displacements in both horizontal orthogonal directions at each time step. Then, by taking the maximum of those values, the maximum isolator displacements were obtained for each ground motion pair. Once the maximum displacements are obtained for all of the eleven analyses in each earthquake bin (Tables 2.1 and 2.2), results are processed to represent the mean values of those eleven analyses. The data presented under the name of D_{RHA} are the mean isolator displacements.

In Figures 5.2 and 5.3, the variations of D_{RHA} are presented as functions of isolation period and damping for stiff and soft soil cases, respectively. As it is seen for both type of soil conditions, variation in superstructure has almost no effect on displacement responses of the isolation systems. Therefore, it can be said that maximum isolator displacements are not sensitive to superstructure's itself. As expected, the isolator displacements decrease with increasing damping (Q/W ratio) regardless of the considered isolation period. However, amount of reduction in isolator displacements is higher at lower Q/W ratios in stiff soil case as a function of isolation period (Figure 5.2) whereas it is almost insensitive to variation of isolation period in soft soil case (Figure 5.3). For stiff soil case, when Q/W ratio is small, maximum isolator displacements may increase upto 50% when isolation period is increased from 3 sec. to 4 sec. However, the amount of increment in isolator displacements due to increase in isolation period decreases with increasing Q/W ratio, and period becomes insignificant on maximum isolator displacements for

Q/W = 0.10. On the other hand, for all of the Q/W ratios considered in soft soil conditions, period is not a significant parameter on the displacements of isolators. This observation is more evident in Figure 5.4. In this figure, the resultant isolator displacements, obtained by applying bi-directional excitations, are normalized with that of smallest Q/W ratio in corresponding bin. For stiff soil bin, results are normalized by the resultant displacements of the system with Q/W = 0.04, whereas resultant displacements of the system with Q/W = 0.08 is used to normalize the displacements in soft soil bin.

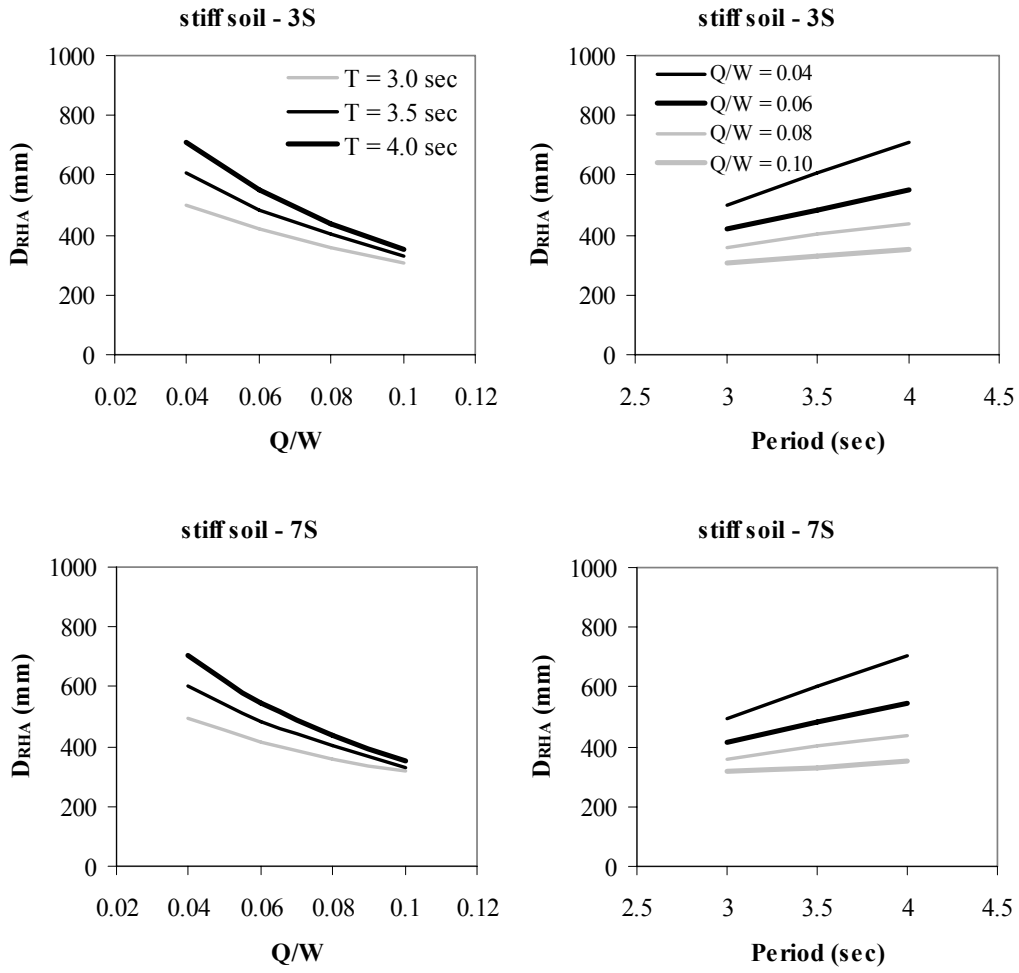

Figure 5.2 Variation of maximum isolator displacements with isolation period and damping for stiff soil condition.

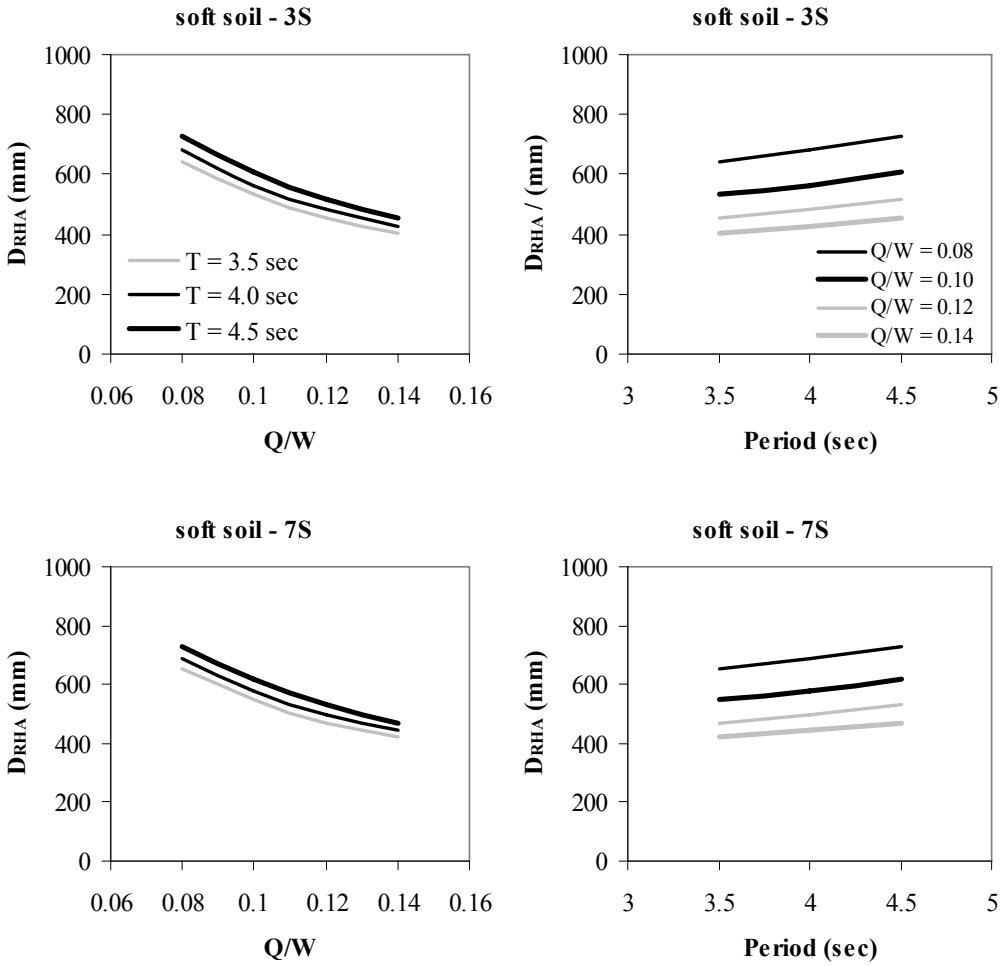

Figure 5.3 Variation of maximum isolator displacements with isolation period and damping for soft soil condition.

One of the most significant differentiation between the results of nonlinear RHA clustered in two bins is presented in Figure 5.4. In this figure, responses of isolation systems, corresponding to stiff and soft soil conditions, under increasing *Q*/*W* ratio differentiate as a function of isolation period. It is shown that normalized isolator displacements are on top of each other, implying that the amount of reductions in isolator displacements due to change in *Q*/*W* ratio at various isolation periods are the same. On the other hand, effectiveness of increasing *Q*/*W* ratio in reducing the isolator displacements increases as isolation period increases for stiff soil

conditions. For the considered Q/W ratios, the maximum amount of reduction in maximum isolator displacements is about 40% compared to smallest Q/W ratio in soft soil case. However, this amount may vary up to 50% depending on the isolation period T in stiff soil case.

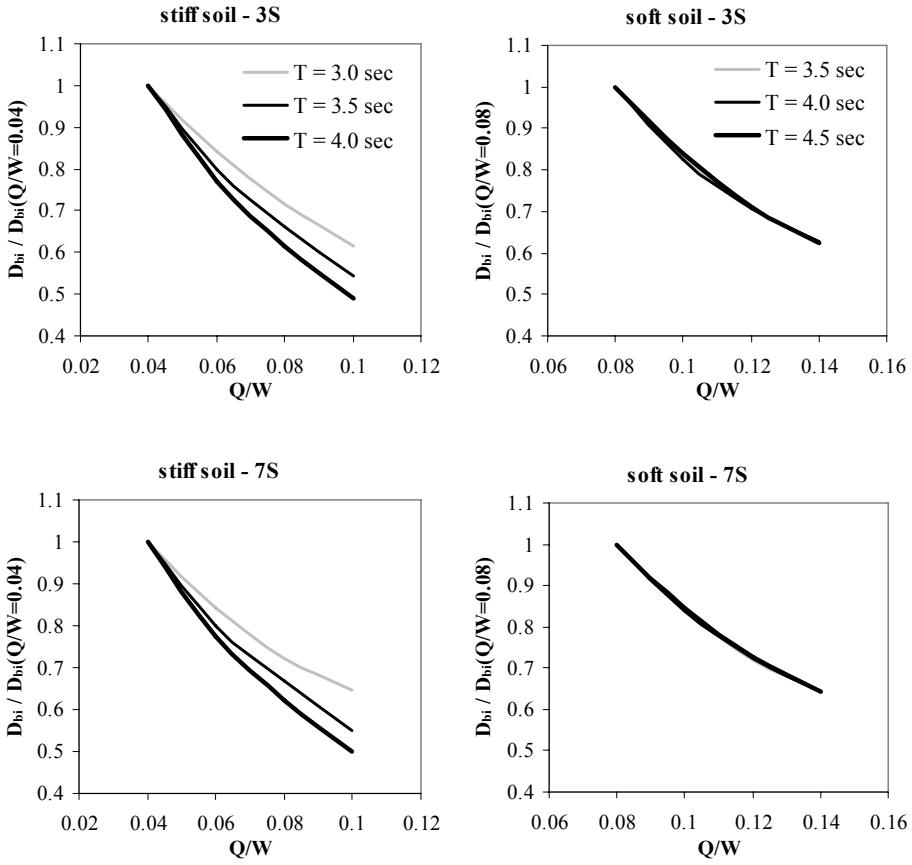

Figure 5.4 Normalized isolator displacements obtained from bi-directional excitations for 3- and 7-story buildings and stiff and soft soil conditions.

To indicate the effect of orthogonal horizontal component on isolator displacements, displacements obtained from bi-directional analyses (D_{bi}) were normalized by that of uni-directional analyses (D_{uni}) and plotted against Q/W ratio for considered isolation periods in Figure 5.5. D_{uni} of each ground motion pair is referred as the maximum displacement obtained by application of both horizontal

components individually. The solid lines in Figure 5.5 represent the value suggested by Jangid and Kelly (2001) to incorporate the effect of orthogonal component.

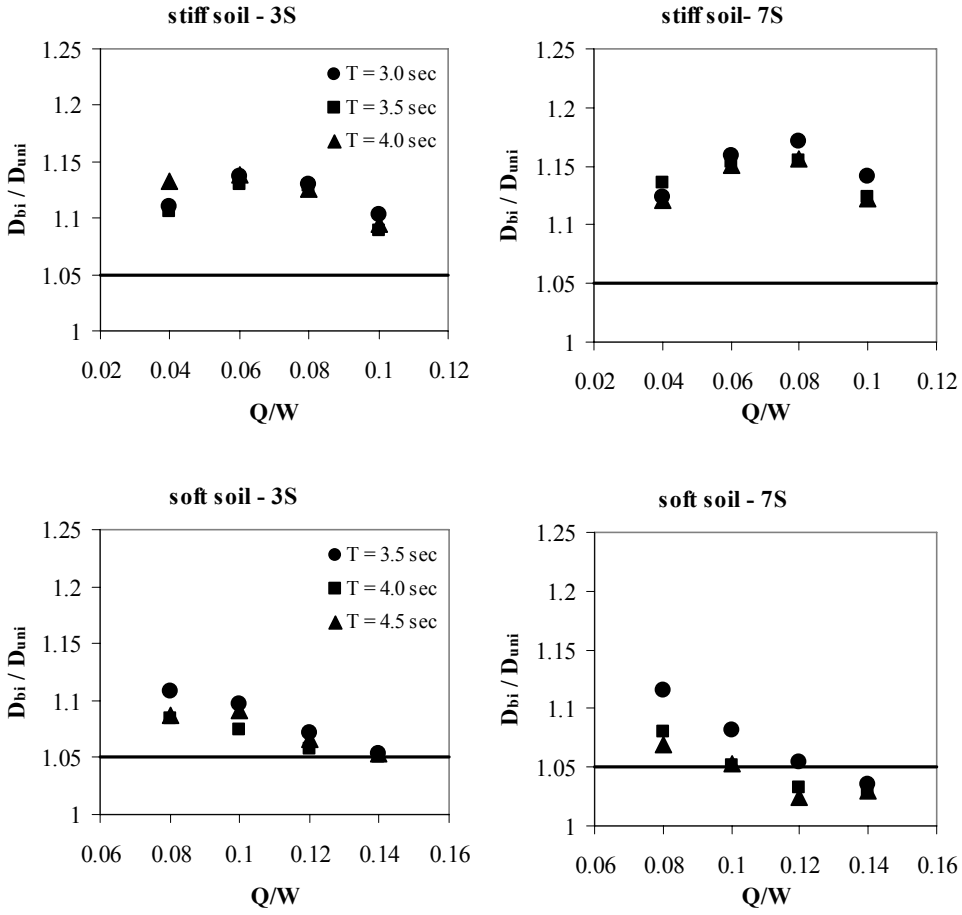

Figure 5.5 Variation of D_{bi}/D_{uni} ratio versus Q/W ratio as a function of isolation period T for stiff (top) and soft (bottom) soil conditions.

It is clear that, there is a considerable distinction between results of two soil conditions. For soft soil, D_{bi}/D_{uni} ratio decreases gradually with increasing Q/W ratio regardless of isolation period. D_{bi}/D_{uni} ratios are roughly in between 1.03 - 1.10 for soft soil case. Although the 5% increment seems conservative in some cases, it should not be forgotten that those limited number of cases have high equivalent damping values ranging between 33 - 37%. Thus, for an isolation system

whose effective damping value is around 15~20%, as in most of the applications, 5% increase for incorporating the orthogonality effect would not be enough and it would underestimate the real response.

For stiff soil, D_{bi}/D_{uni} ratio first increases but then slightly decreases with increasing Q/W ratio. D_{bi}/D_{uni} ratios vary from 1.10 to 1.17 depending on the Q/W ratio. Hence, 5% increment is not enough to incorporate the effect of orthogonal component for any of the considered isolation systems in stiff soil conditions.

5.3.1.2 Maximum Base Shear

The analyses results regarding the obtained base shears are given in Figures 5.6 and 5.7 for stiff and soft soil conditions in the same order. In those figures, V_{RHA} represents the maximum base shear observed in any of the horizontal direction under bi-directional excitations of ground motions. They are normalized with the weight of the structure so that it becomes unitless. Those figures also depict how sensitive is the variation of base shear to story height of the superstructure.

Variation of V_{RHA} is very similar in both of the soil conditions. It decreases with increasing isolation period. Moreover, alteration of Q/W ratio has almost no consequence on V_{RHA} and its effects can be negligible. An additional parameter that can be neglected considering the base shear variations presented is the variation in superstructure. Maximum normalized base shears of 3- and 7-story structures are almost identical. This observation eradicates the effect of superstructure on base shear of isolated structures.

Similar to D_{bi}/D_{uni}, the relation between V_{bi} and V_{uni} is illustrated in Figure 5.8. The solid line in Figure 5.8 stands for the case where V_{bi} and V_{uni} are equal to each other. Apart from V_{bi}, V_{uni} is the maximum base shear obtained by applying the two horizontal components individually. Figure 5.8 indicates that consideration of uni-directional response in determining the base shears under bi-directional excitations is almost convenient for all of the cases covered in this study. In general, the prediction of base shears by using uni-directional results is more conservative in

soft soil conditions compared to that of stiff soil conditions. And, degree of conservatism increases as *Q*/*W* ratio increases regardless of the soil condition. When different superstructures are considered, there are only minor differences in V_{bi}/V_{uni} ratios for stiff soil cases which can be ignored. Hence, effect of the superstructure can be assigned as an ineffective parameter for base shear variation.

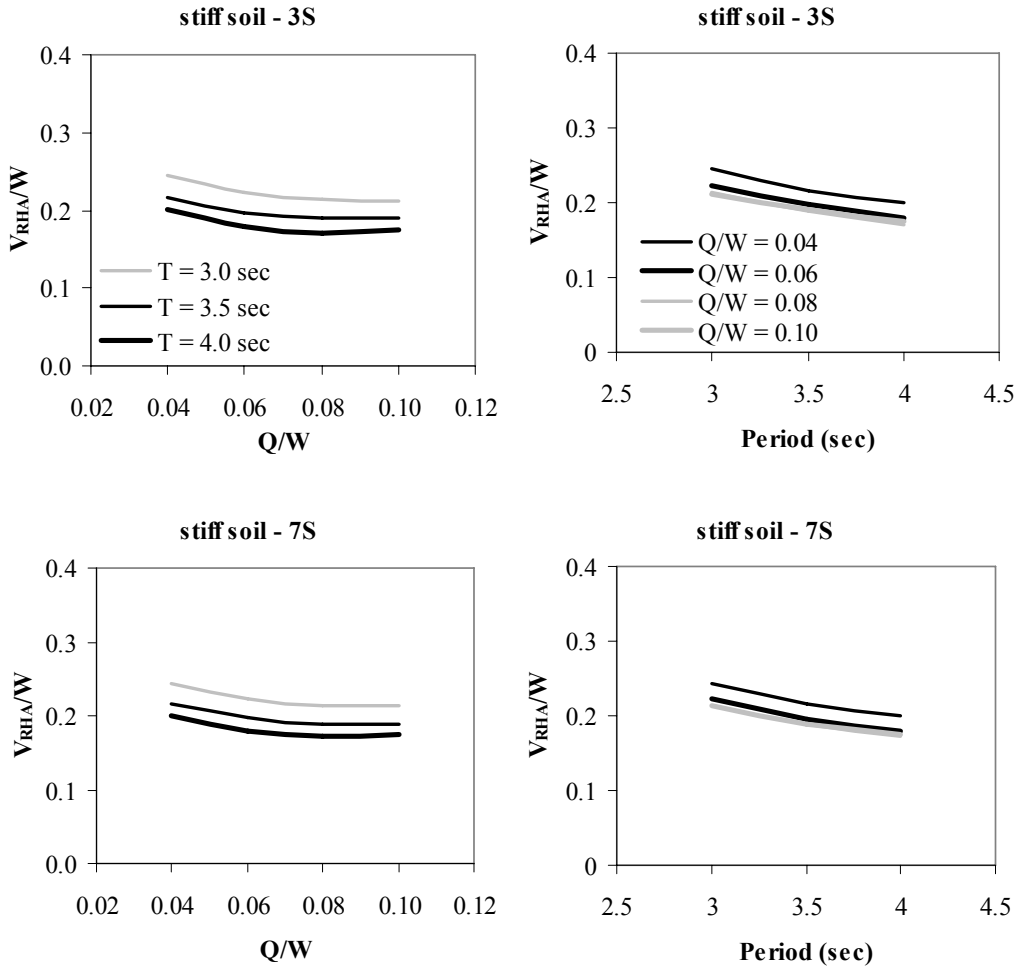

Figure 5.6 Variation of maximum base shears with isolation period and damping for stiff soil condition.

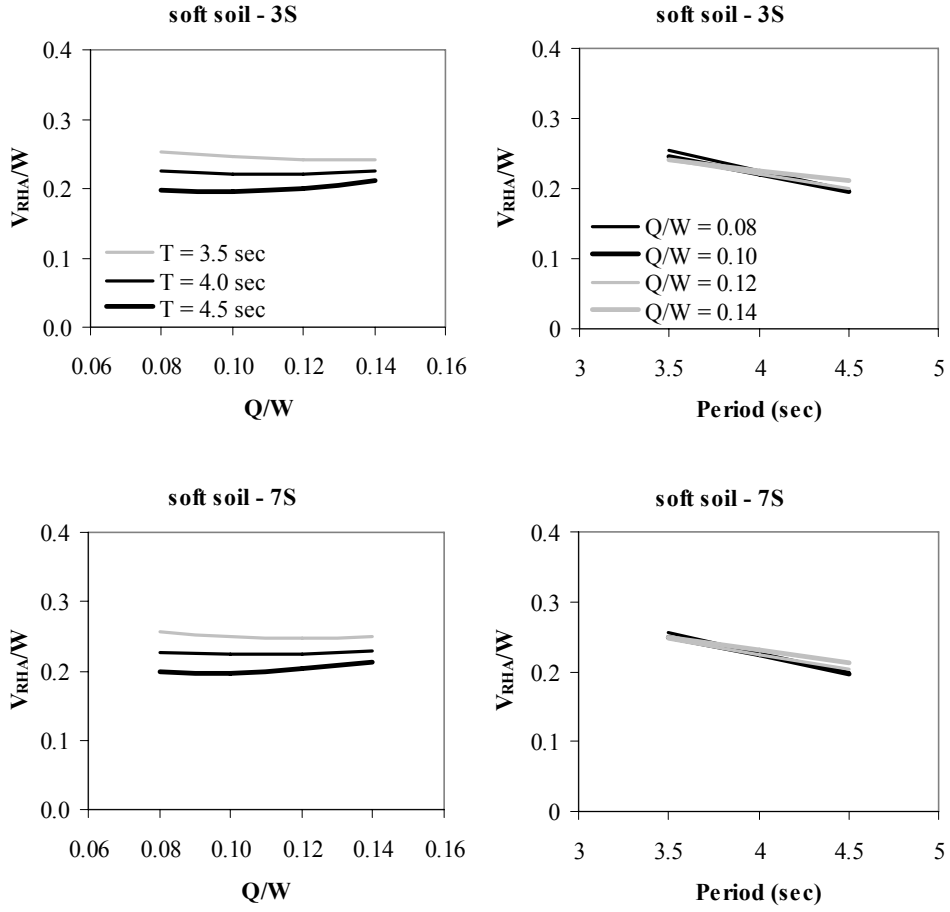

Figure 5.7 Variation of maximum base shears with isolation period and damping for soft soil condition.

5.3.2 Response of Superstructure

The basic problem with the design approach of seismically isolated structures in the current codes is that isolation systems are used mainly for buildings that house sensitive and expensive internal equipment. Thus, typical examples of base isolated buildings are emergency service centers, hospitals, and similar structures where the internal equipment is much more important than the structure's itself. The damping systems that are available to control the large displacements have the characteristic that the damping is strongly displacement dependent. To achieve the level of damping to reduce the code-mandated displacements at the MCE hazard level

means that the isolation system will have higher damping and stiffness (since the displacement of the isolator decreases), and therefore the behavior of the building may no longer be dominated by the fundamental isolated response. In this case, there may be serious damage to the sensitive internal equipment. It is worth noting that although the code permits the use of high damping in the isolation system to reduce the design displacement, only the elastic force is included in the calculation of the base shear. This provides the incentive for the use of highly damped systems, but damping amplifies response in the higher modes of the isolated structure that in turn produces higher floor accelerations which can cause damage in the equipment.

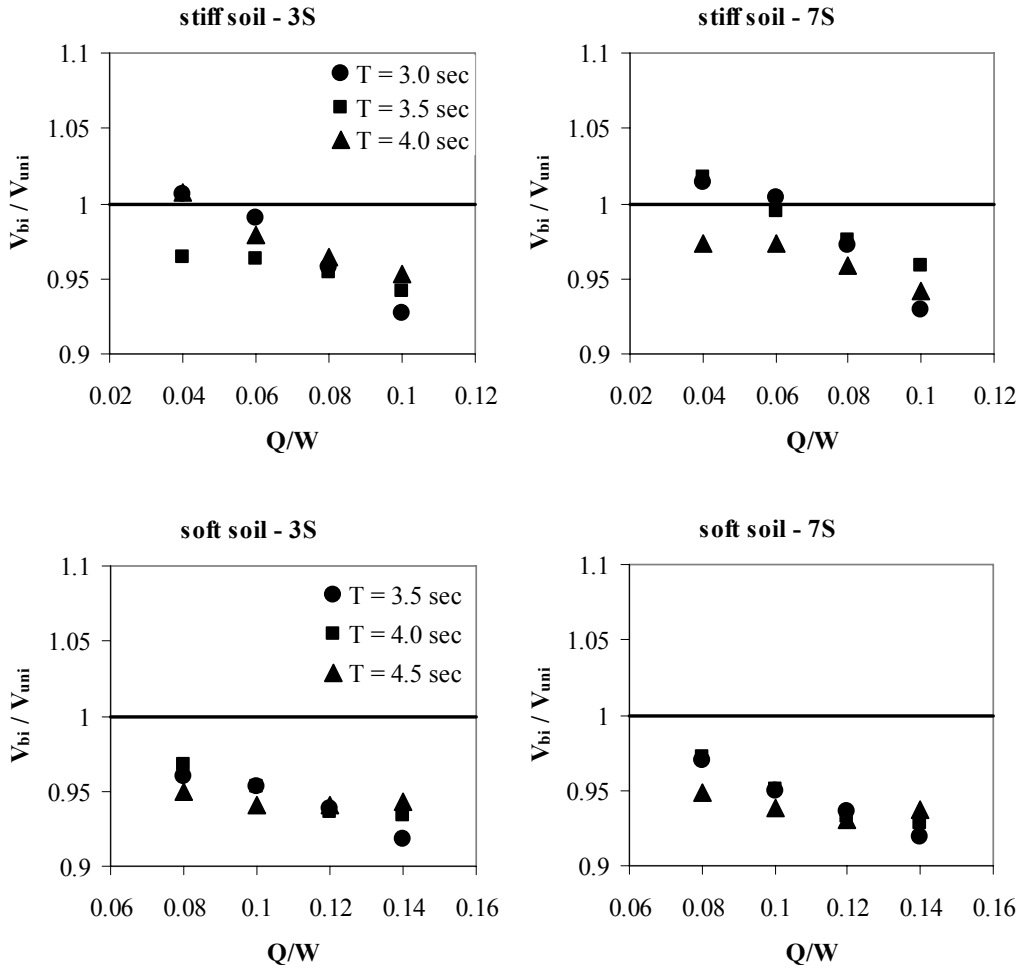

Figure 5.8 Variation of V_{bi}/V_{uni} ratio versus Q/W ratio as a function of isolation period T for stiff (top) and soft (bottom) soil conditions.

It should be realized that the higher modes in an isolated structure are orthogonal to base shears. Thus, reduction in base shear and isolator displacement will not necessarily end up with reduced floor accelerations. Response of isolated structures in terms of floor accelerations has been of concern by several researchers. Kelly (1999), Hall (1999), Hall and Ryan (2000), Matsagar and Jangid (2004), and Alhan and Gavin (2004) are among those studies. The study conducted by Alhan and Gavin (2004) somehow differentiates from the others by applying the ground motions bi-directionally. However, authors did not consider any scaling for the considered ground motions which is mandatory to use in nonlinear dynamic analysis of isolated structures as described in codes. On the other hand, Carballo and Cornell (2000) and Huang *et al*. (2006) stated that distribution of acceleration and displacements through the height of the structure depends highly on the scaling of the ground motions. Moreover, Huang *et al*. (2006) strongly recommended the use of amplitude scaling method rather than the methods where spectral matching is used.

The purpose of this section is to show how highly damped isolation systems are counterproductive to the main purpose of isolation. In this sense, effects of isolation period T and Q/W ratio on responses of both 3- and 7-story RC buildings are examined by employing the new proposed scaling method, which is also shown to be appropriate for dynamic analysis of isolated structures in Chapter 4, to shed light on the variations of floor accelerations, interstory drifts and roof displacements of the superstructures under consideration. Comparisons are conducted for two different soil conditions.

5.3.2.1 Floor Accelerations

Through Figures 5.9 – 5.14, floor accelerations obtained by applying bi-directional excitations are depicted to show how they change by increasing both isolation period T and Q/W ratio. In those figures, bi-directional accelerations are represented by Acc_{bi} and are computed by taking the SRSS of accelerations in both orthogonal horizontal directions. This process was performed at each time step of

the analyses and the maximum values were considered only. The data presented in the related graphs are the mean values of eleven analyses for both of the soil conditions.

5.3.2.1.1 Effect of Isolation Period

In Figures 5.9 and 5.10, variations in Acc_{bi} as a function of isolation period are given for 3-story RC building at stiff and soft soil conditions, respectively. Those figures reveal the effect of isolation period on variation of floor accelerations through the height of the structure.

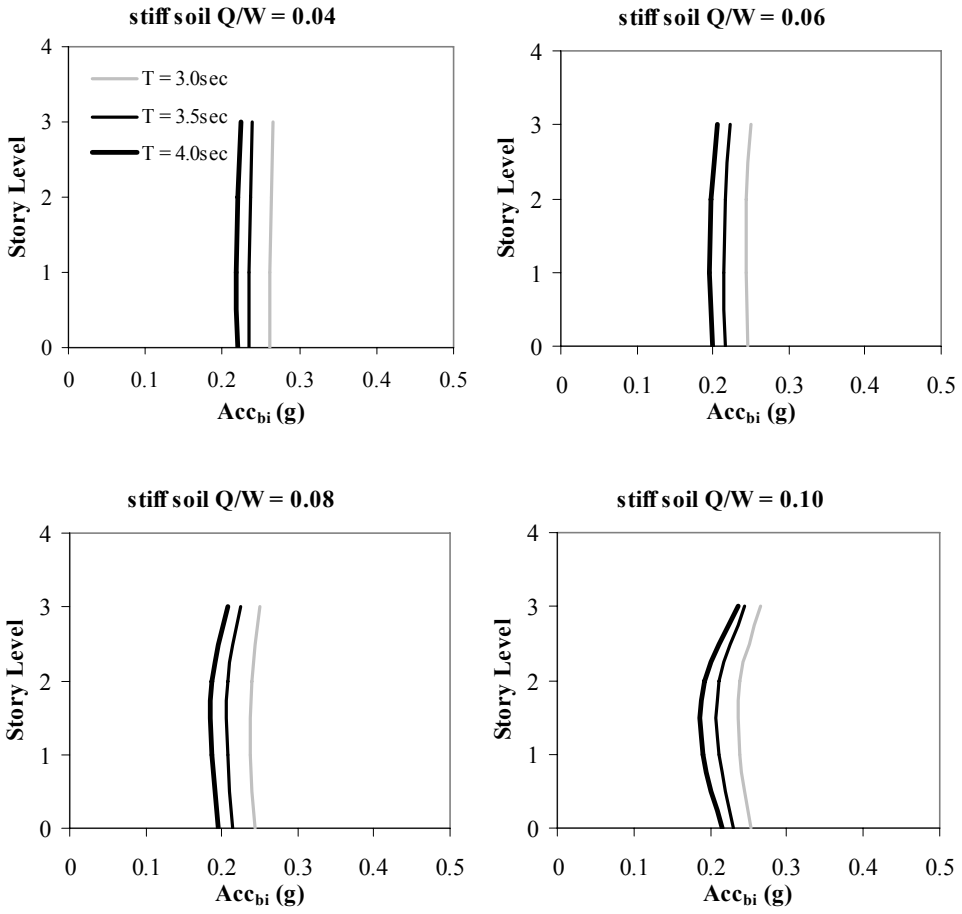

Figure 5.9 Variations in Acc_{bi} of 3-story RC building as a function of isolation period T for various Q/W ratios under stiff soil condition.

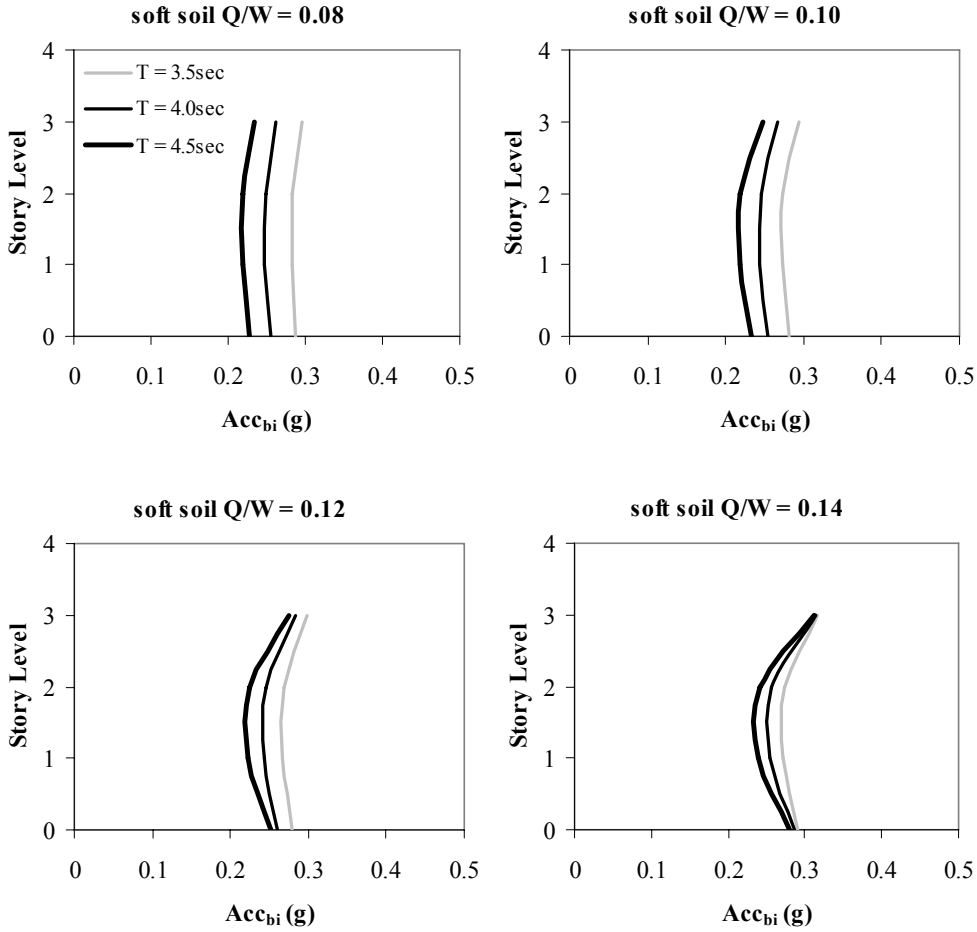

Figure 5.10 Variations in Acc_{bi} of 3-story RC building as a function of isolation period *T* for various *Q*/*W* ratios under soft soil condition.

As it is seen, floor accelerations decrease when isolation period increases. Amount of reduction in Acc_{bi} is almost the same for all *Q*/*W* ratios considered in both soil conditions. On the other hand, increasing the isolation period to reduce the Acc_{bi} through the height of the structure becomes less effective at higher Q/W ratios compared to lower ones. This observation is especially valid for *Q*/*W* ratio equals to 0.12 and 0.14 (Figure 5.10) in soft soil condition. For these two cases, Acc_{bi} also tends to be equal at ground and top story levels as *Q*/*W* ratio increases.

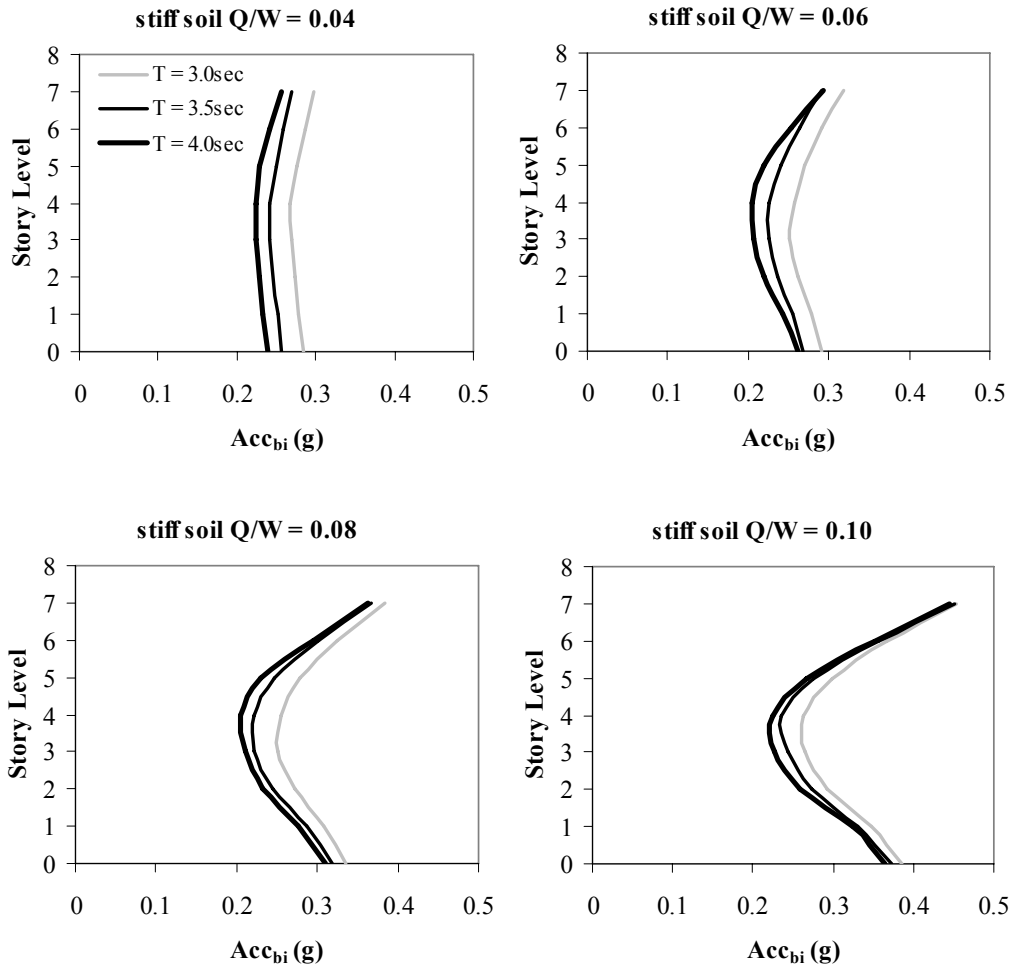

Figure 5.11 Variations in Acc_{bi} of 7-story RC building as a function of isolation period *T* for various *Q*/*W* ratios under stiff soil condition.

Similar graphs are presented in Figures 5.11 and 5.12 for 7-story isolated RC building. Apart from 3-story isolated building, variation of Acc_{bi} through the height of the structure in 7-story building is less prone to change in isolation period. This is especially valid for soft soil condition (Fig. 5.12). For almost all of the *Q*/*W* ratios under consideration, the maximum Acc_{bi} values observed in the superstructure are the same (with the exception of *Q*/*W* = 0.08). Moreover, the distributions of the floor accelerations become identical at higher *Q*/*W* ratios regardless of the isolation period. Under stiff soil conditions, increasing isolation period seems to be a way to

reduce the floor accelerations at lower Q/W ratios such as 0.04 and 0.06 (Figure 5.11). However, as Q/W ratio increases to 0.08 and 0.10, effectiveness of isolation period decreases and similar observations as in soft soil conditions are made.

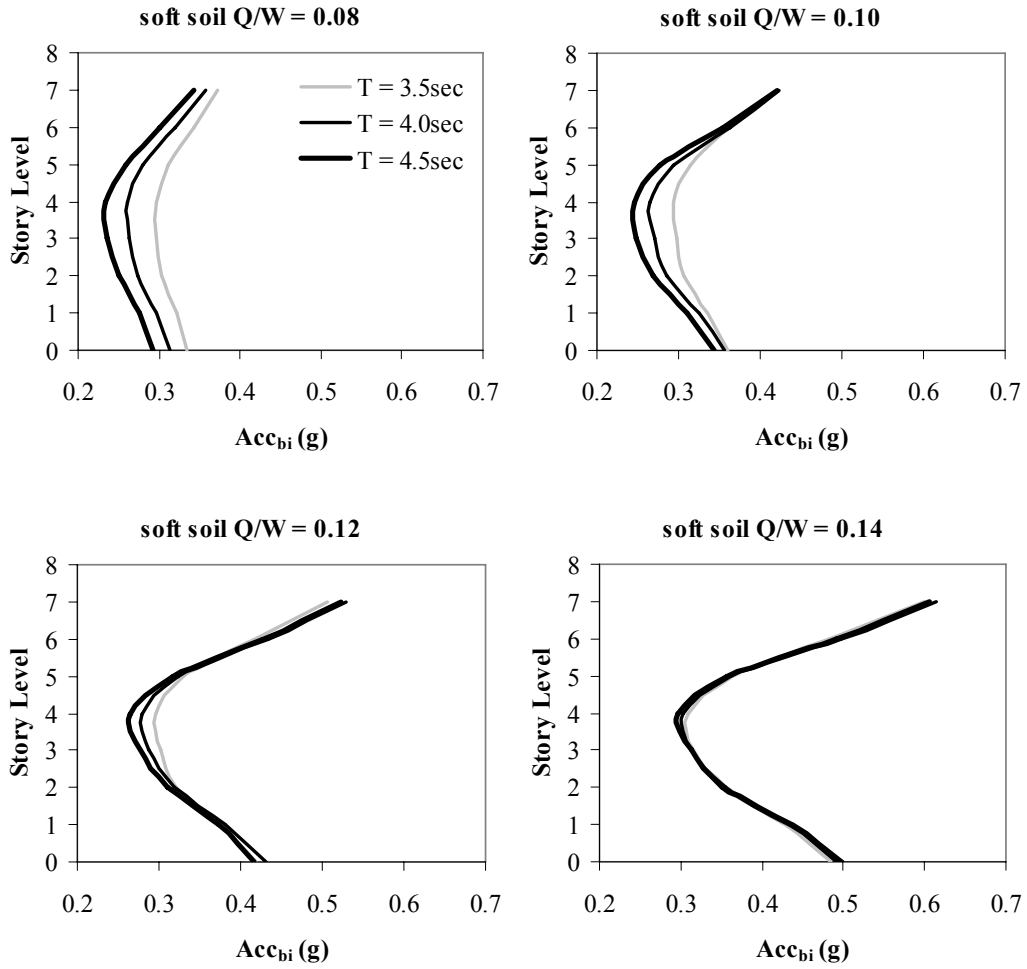

Figure 5.12 Variations in Acc_{bi} of 7-story RC building as a function of isolation period T for various Q/W ratios under soft soil condition.

5.3.2.1.2 Effect of Damping (Q/W Ratio)

To indicate how sensitive the floor accelerations are to the change in effective damping ratio, Figures 5.13 and 5.14 are depicted. In Figure 5.13, comparisons are

done for 3-story building in terms of soil conditions. It is obvious that, there is a significant increase in floor accelerations due to increasing Q/W ratios in soft soil condition. Moreover, amount of increment in Acc_{bi} becomes higher as isolation period increases. The amount of increments in maximum floor accelerations is 35% for T = 4.5 sec., and followed by 19% and 10% for T = 4.0 and 3.5 sec. when Q/W ratio is increased from 0.08 to 0.14. On the other hand, Acc_{bi} first reduces with an increase in Q/W ratio (from 0.04 to 0.08) but for further increase of Q/W ratio (from 0.08 to 0.10) maximum amount of Acc_{bi} through the height also increases in stiff soil condition. However, that increment is not significant when compared to Acc_{bi} values of the system where Q/W = 0.04.

Evaluation of change in Acc_{bi} due to increased Q/W ratios at 7-story building is performed in the light of Figure 5.14. In contrast to 3-story building, the maximum Acc_{bi} increases substantially at both of the soil conditions. When the maximum floor accelerations corresponding to case with highest Q/W ratios are normalized with that of the lowest Q/W ratio, the amount of increments are obtained as 50%, 65% and 69% in stiff soil for T = 3.0, 3.5 and 4.0 sec., respectively. When the same comparison is conducted for soft soil cases, increments will be 62%, 69% and 76% for T = 3.5, 4.0 and 4.5 sec., in the same order. Variation of Acc_{bi} through the height of the structure shows the counterproductive effect of increasing damping. The building did not act as an isolated one when Q/W ratios are high.

Figures 5.13 and 5.14 indicate that floor accelerations of isolated structures in soft soil conditions are more sensitive to increase in Q/W ratio than that of stiff soil conditions. Increments in the floor accelerations with increasing damping are due to contribution of higher modes. Transfer of energy to higher modes associated with a small reduction in first mode accelerations is able to produce relatively large higher mode accelerations, because higher modes require much smaller energies to achieve a given maximum acceleration (Skinner, 1993). This ensures that although higher mode responses may be severe, which is important for the distribution of floor accelerations, first mode response that governs the base shear is little affected by the interaction with higher modes as shown in Figures 5.6 and 5.7.

To evaluate the success of uni-directional analyses in predicting the floor accelerations, accelerations obtained from bi-directional analyses (Acc_{bi}) were normalized by that of uni-directional analyses (Acc_{uni}) and plotted against Q/W ratio for considered isolation periods in Figure 5.15 and 5.16. Acc_{uni} of each ground motion pair is referred as the maximum acceleration obtained by application of both horizontal components individually.

In Figure 5.15, Acc_{bi}/Acc_{uni} ratios of 3-story building are given for both of the soil classifications. In stiff soil cases, having the values higher than 1.0 in almost all of the cases, accelerations obtained by uni-directional analyses are not appropriate to predict bi-directional ones. The only exception is the case with T = 4.0 sec. and Q/W = 0.10. On the other hand, prediction of bi-directional accelerations by uni-directional analyses is on the conservative side in soft soil conditions. However, this generalization is not valid in isolation systems with low Q/W ratio (0.08) for all of the considered isolation periods. Degree of conservatism is up to 10% depending on the story level and damping ratio.

In Figure 5.16, comparisons of Acc_{bi} and Acc_{uni} are presented for 7-story building at both of the soil classifications. In contrast, using uni-directional accelerations to predict the bi-directional ones may be conservative in stiff soil case for 7-story building. This observation does not depend on the isolation period but on Q/W ratio. For Q/W ratios higher than 0.06, accelerations by uni-directional analyses give safe results. The amount of safety is up to 10%. Highest safety is observed for isolation system with T = 4.0 sec. and Q/W = 0.10. On the other hand, comparisons for soft soil cases show that uni-directional analyses give safe predictions for almost all of the cases under consideration. The maximum degree of safety is around 15% for soft soil conditions. Variation of Acc_{bi}/Acc_{uni} ratio is more uniform for stiff soil conditions compared to soft soil cases.

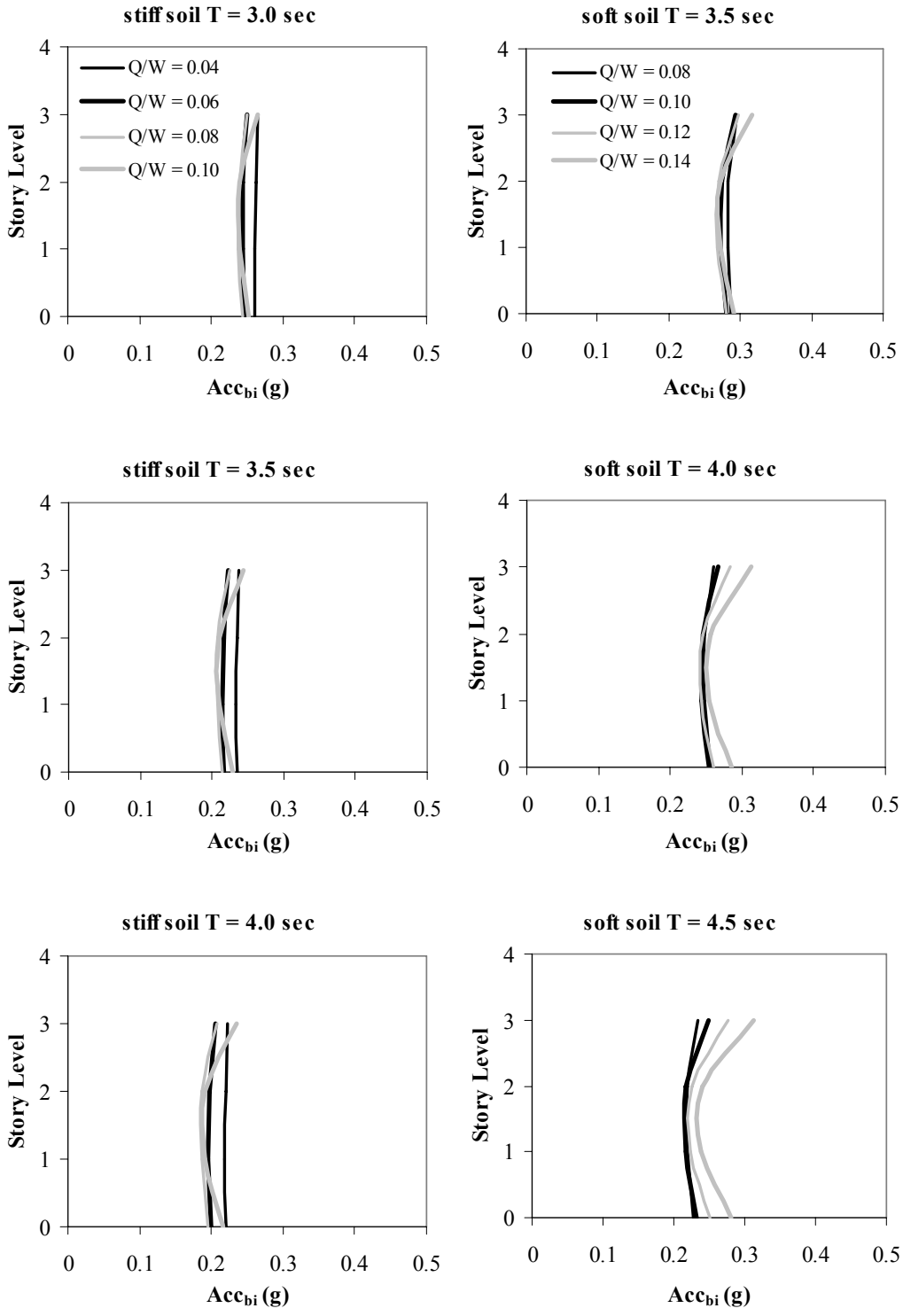

Figure 5.13 Variations in Acc_{bi} of 3-story RC building as a function of Q/W ratios for various isolation periods T under stiff (left) and soft (right) soil conditions.

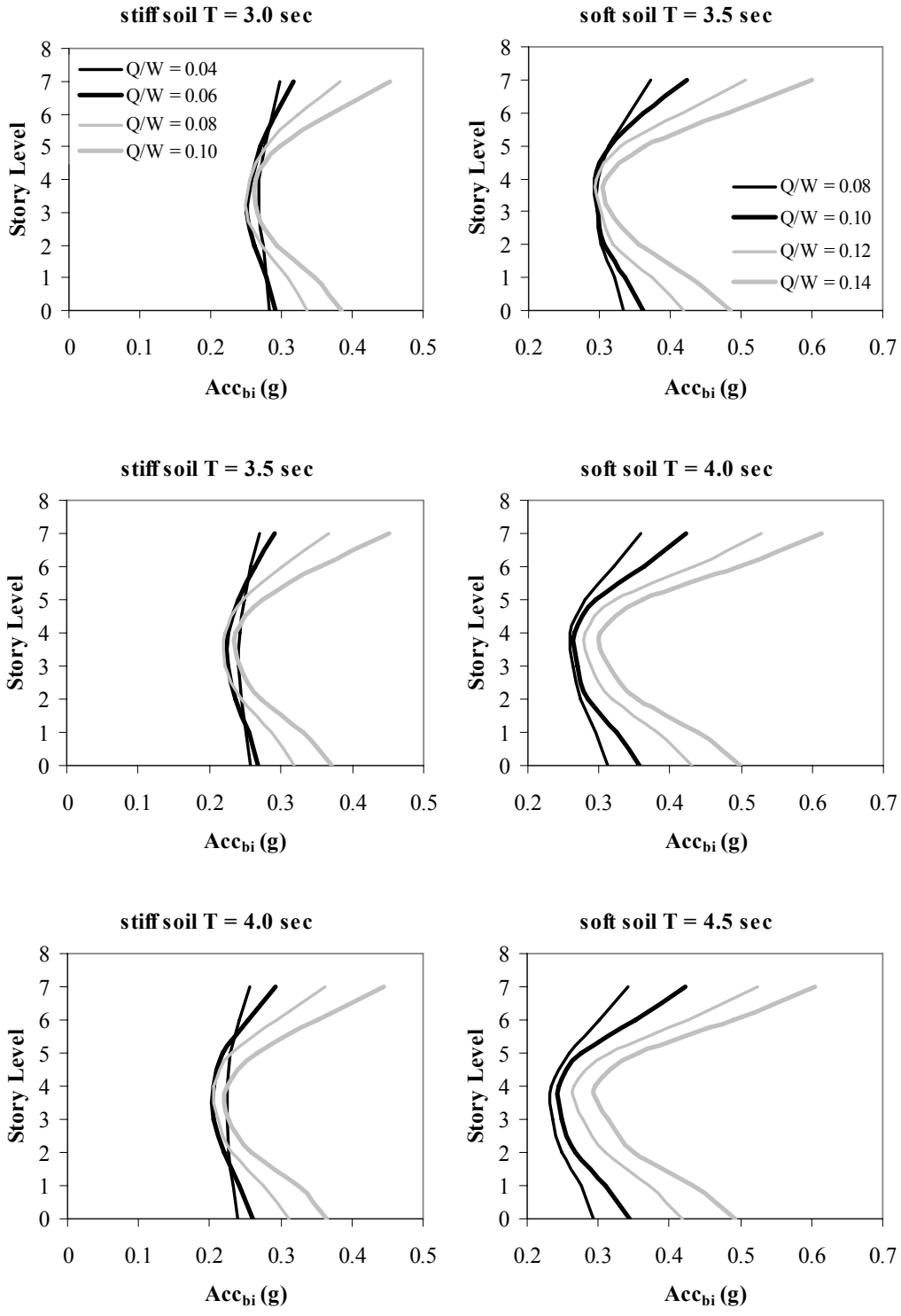

Figure 5.14 Variations in Acc_{bi} of 7-story RC building as a function of Q/W ratios for various isolation periods T under stiff (left) and soft (right) soil conditions.

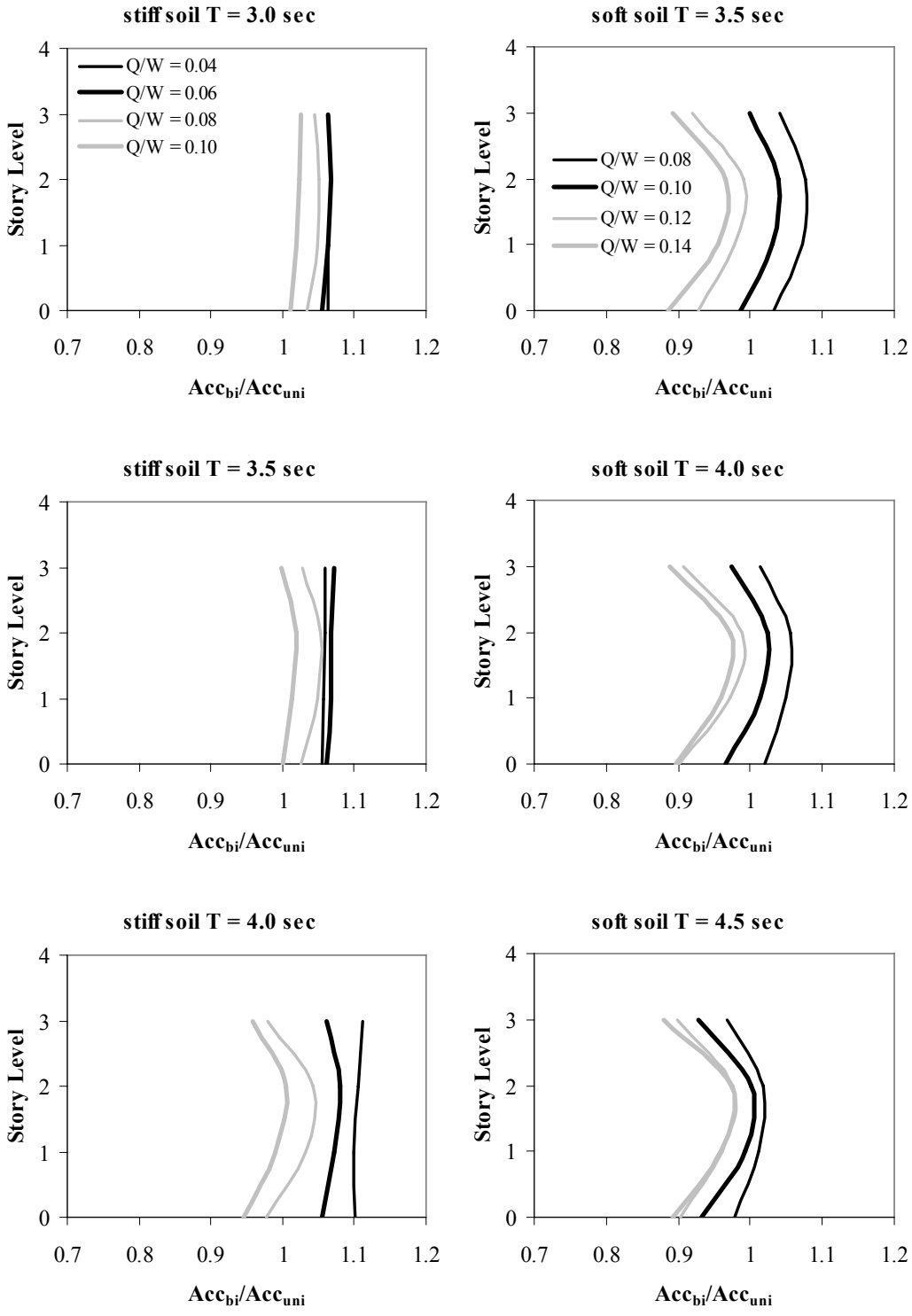

Figure 5.15 Comparison of bi-directional and uni-directional accelerations of 3-story RC building for stiff (left) and soft (right) soil conditions.

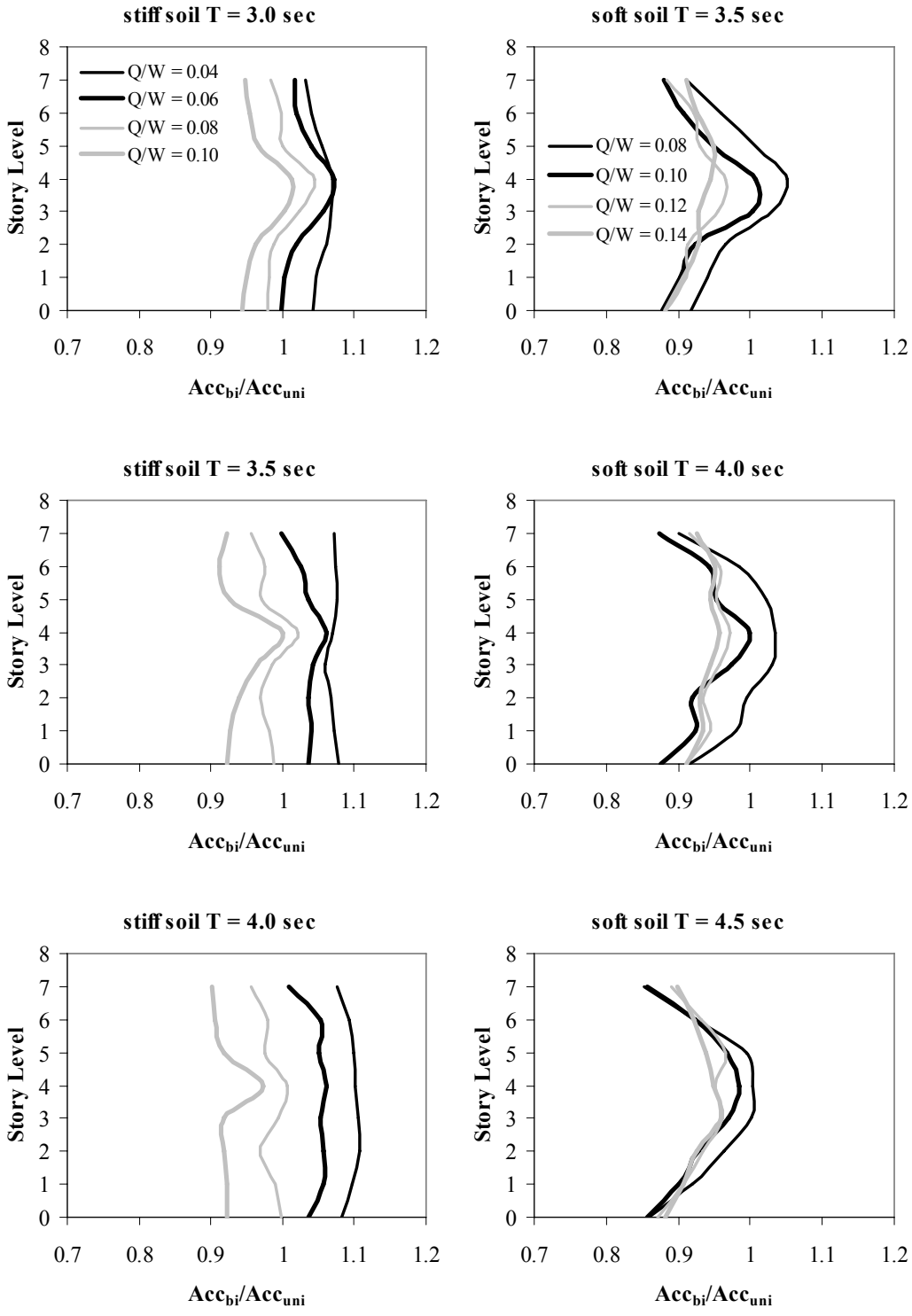

Figure 5.16 Comparison of bi-directional and uni-directional accelerations of 7-story RC building for stiff (left) and soft (right) soil conditions.

5.3.2.2 Roof Displacements

Since only the superstructure is of concern, the maximum roof displacements of the 3- and 7-story RC buildings are presented relative to isolation level. Maximum difference between the roof and isolator displacements is calculated at each time increment through the nonlinear RHA. Maximum displacements at both isolation and roof levels are calculated by taking the SRSS of displacements in both orthogonal horizontal directions. Results are presented in Figures 5.17 and 5.18 for 3- and 7-story RC buildings, respectively. The data given in the related graphs are the mean values of the analyses performed.

In Figure 5.17, variation of a 3-story RC building is depicted for stiff and soft soil conditions. It is obvious that both Q/W ratio and isolation period T have no effect on the variation of roof displacements. Although increasing the isolation period T seems to reduce the roof displacements, the amount of reduction is less than a milimetre which is negligible. The same observation is also valid when Q/W ratio increases.

Similar to Figure 5.17, Figure 5.18 shows the variation of roof displacements in a 7-story RC building for stiff and soft soil conditions. In stiff soil cases, increasing Q/W ratio decreases the roof displacements up to a point. Further increase in Q/W ratio causes an increase in roof displacements. On the other hand, increasing Q/W ratio increases roof displacements for all of the cases considered under soft soil conditions. Figure 5.18 also shows that increasing isolation period T decreases the roof displacements regardless of the soil condition.

5.3.2.3 Interstory Drifts

To indicate the influence of damping, where damping effects are created by non-linear mechanisms such as yielding, on superstructure, the maximum interstory drift ratios are presented in Figures 5.19 and 5.20. Drift ratios are calculated as the ratio of the maximum relative displacement between two consecutive story levels to the story height. Maximum relative displacement is defined as the maximum

difference between resultant displacements at each story level. Resultant displacements are obtained by taking the SRSS of displacements in horizontal orthogonal directions.

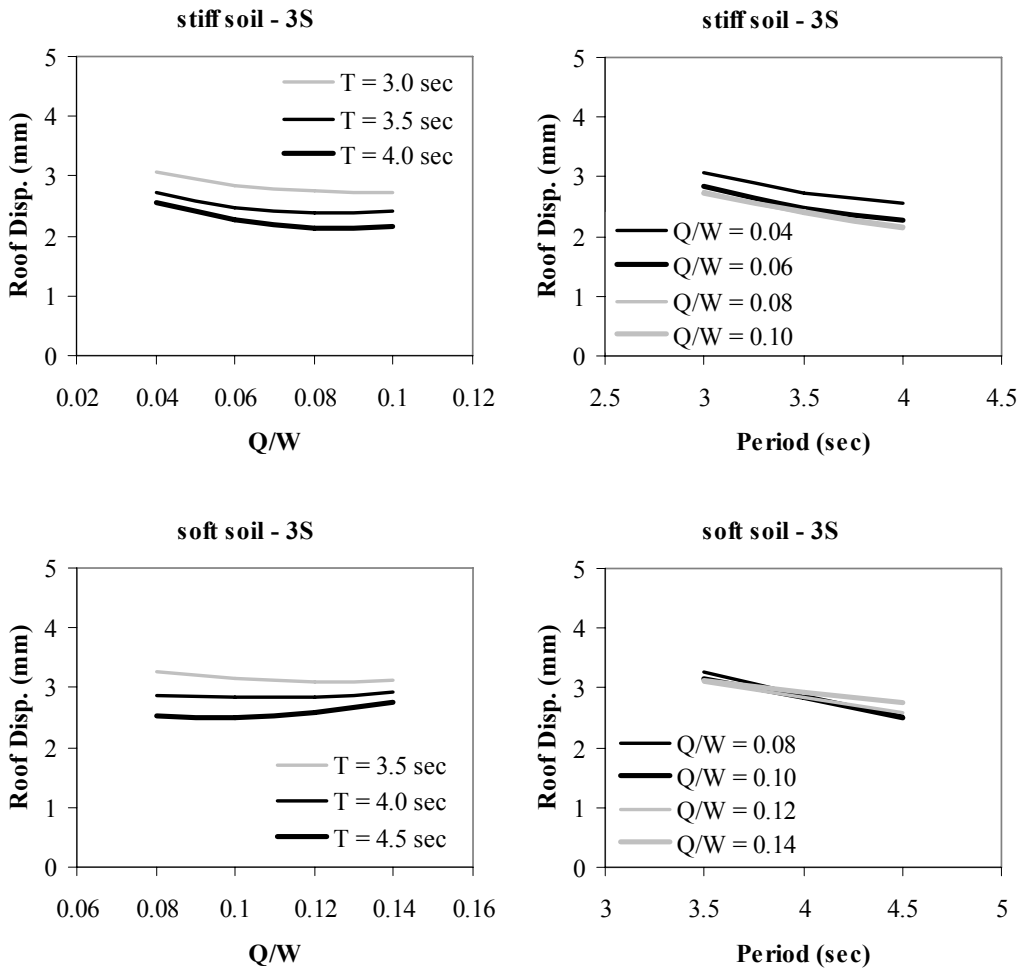

Figure 5.17 Variation of roof displacements in isolated 3-story building for stiff (top) and soft (bottom) soil conditions.

Variation of drift ratios with various *Q*/*W* ratios for each isolation period is given in Figure 5.19 for 3-story RC building. Change in *Q*/*W* ratio has almost no effect on drift ratios regardless of the soil condition and increasing isolation period

decreases interstroy drifts slightly. On the other hand, in Figure 5.20, where variation of drift ratios is given for 7-story RC building, it is clear that drift ratios at upper story levels increase as *Q*/*W* ratio increases. The amount of increment is observed to be dependent on soil condition in 7-story building. It is more significant in soft soil conditions. Moreover, in both of the soil conditions, increment in drift ratios due to variation in *Q*/*W* ratio increases as isolation period increases. In the mean time, a slight reduction in drift ratios of very first floor is observed with an increase in isolation period.

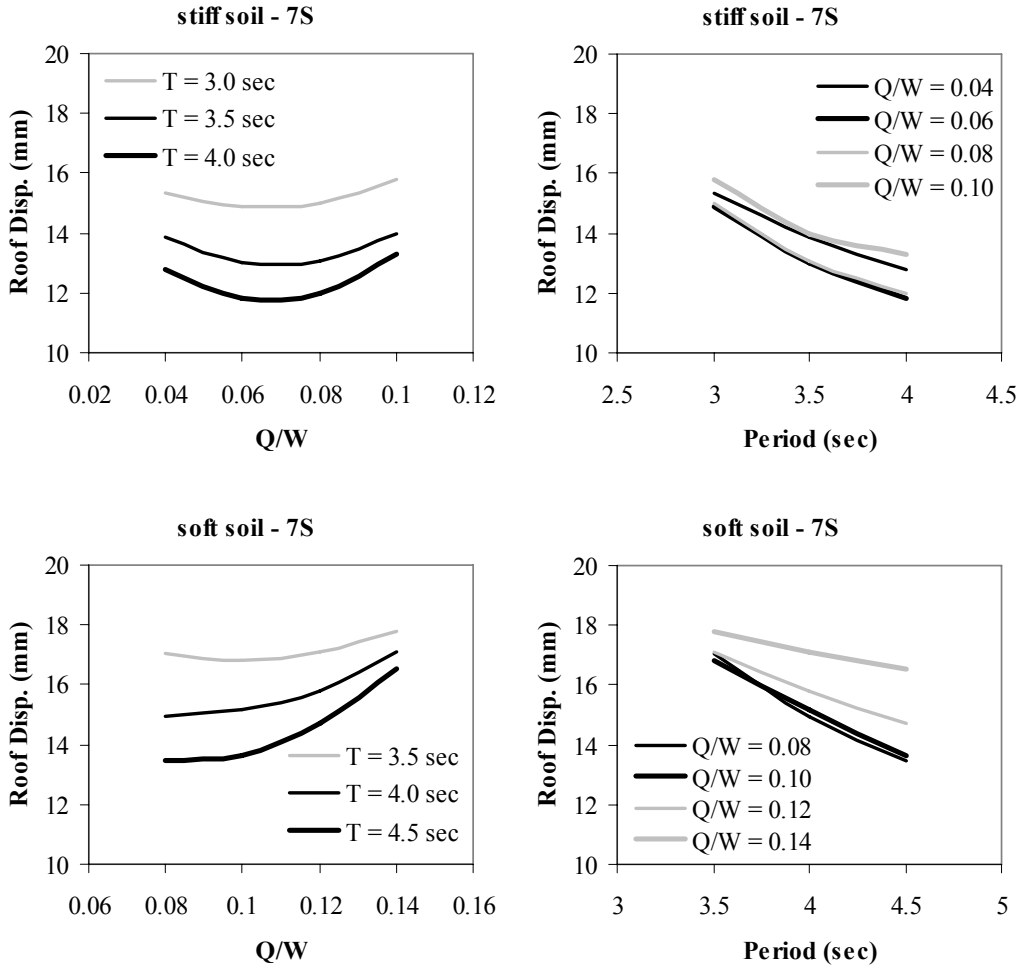

Figure 5.18 Variation of roof displacements in isolated 7-story building for stiff (top) and soft (bottom) soil conditions.

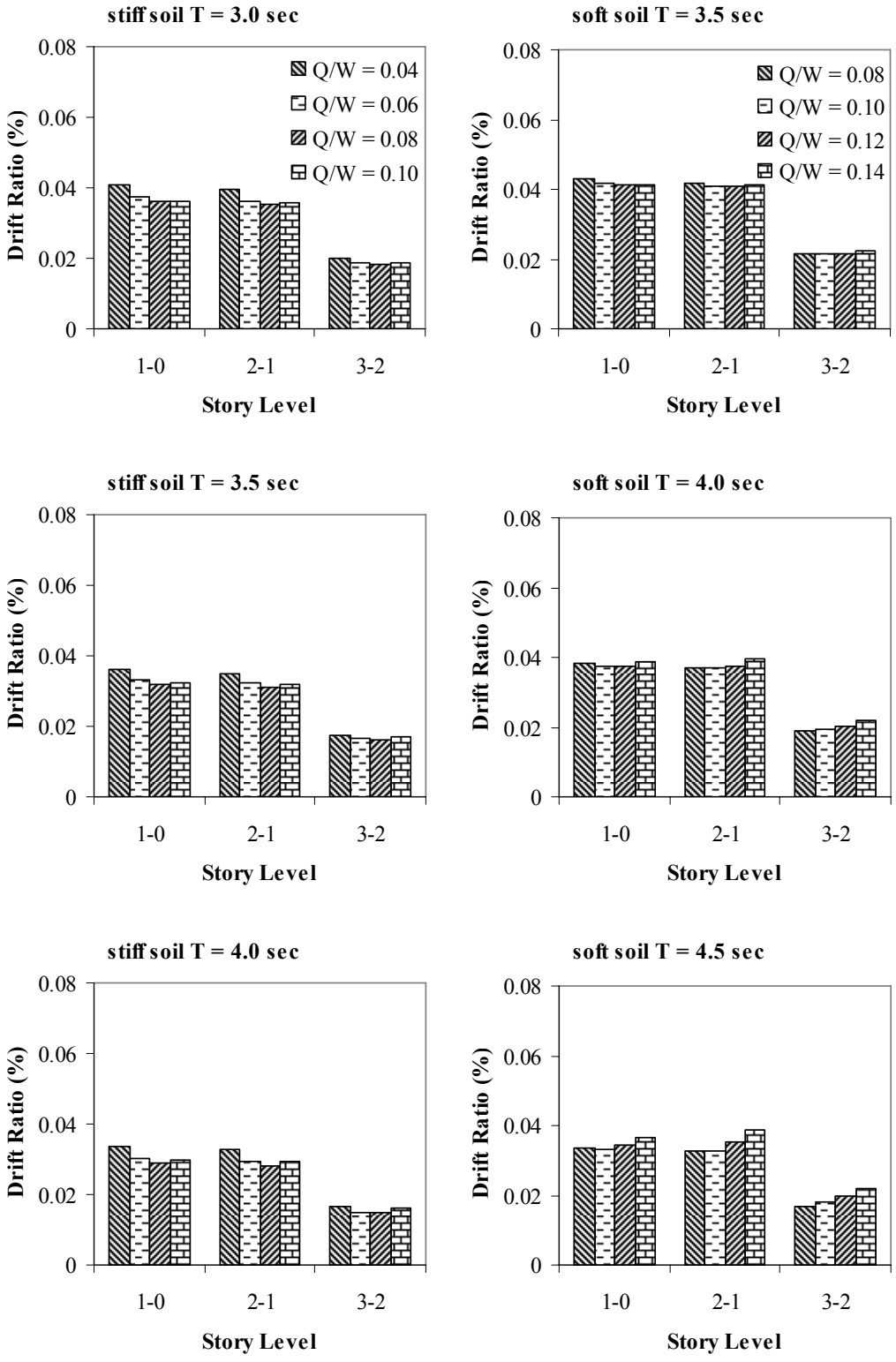

Figure 5.19 Variation of interstory drift ratios with increasing *Q*/*W* ratio in 3-story RC building.

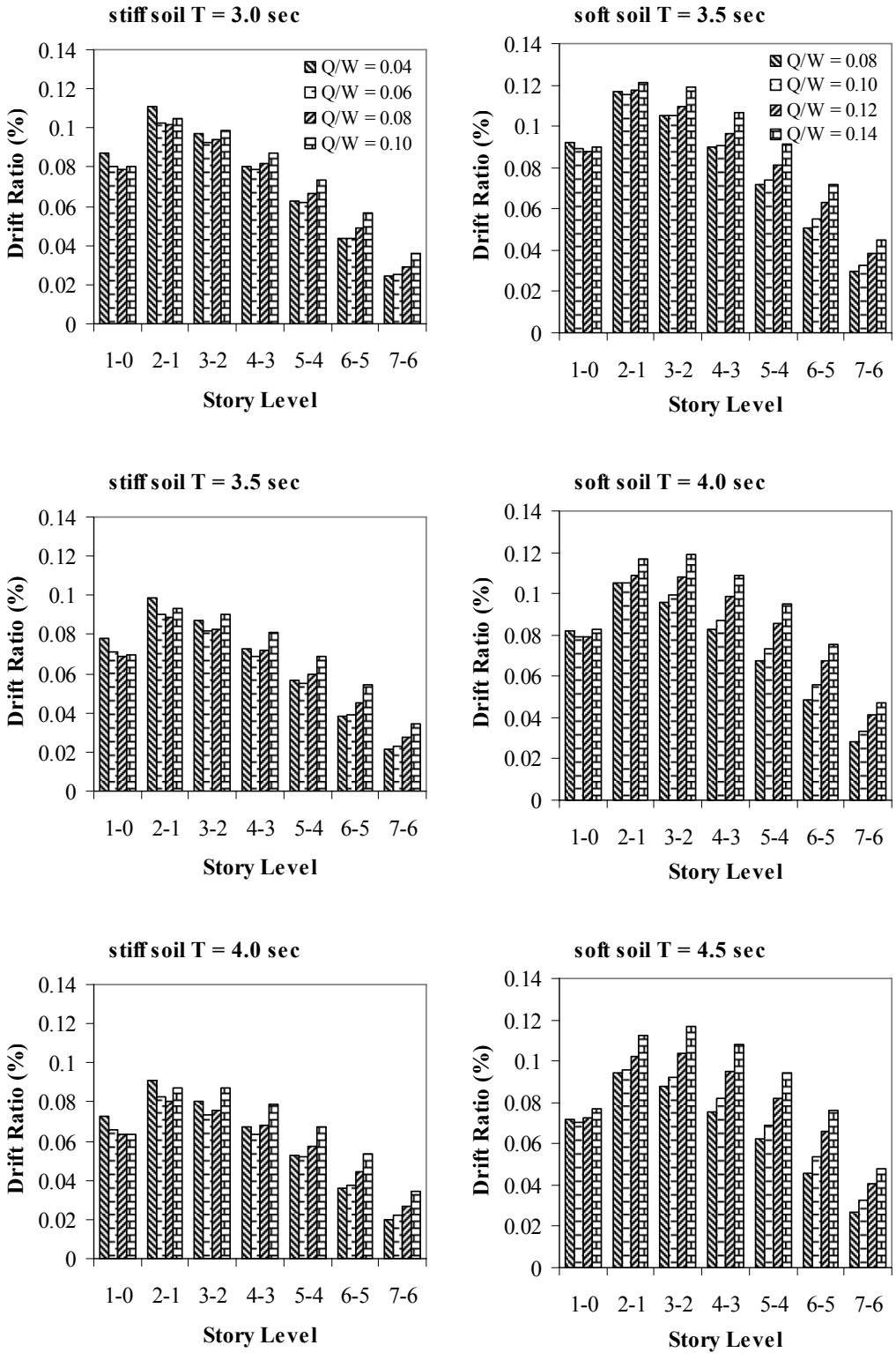

Figure 5.20 Variation of interstory drift ratios with increasing *Q*/*W* ratio in 7-story RC building.

CHAPTER 6

TORSIONAL AMPLIFICATIONS IN ISOLATOR DISPLACEMENTS DUE TO ASYMMETRY IN THE SUPERSTRUCTURE

6.1 INTRODUCTION

Torsional response of isolated structures due to asymmetry in the superstructure has received less attention among the aspects already considered so far. There are only a few studies in the literature where the torsional response of isolated structures is of concern (Lee, 1980; Eisenberger and Rutenberg, 1986; Nagarajaiah *et al*., 1993a-b; Jangid and Datta, 1994a-b; Tena-Colunga *et al*., 1997; Tena-Colunga and Gomez-Soberon, 2002; Tena-Colunga and Escamilla-Cruz, 2007).

Lee (1980) studied response of a single story isolated structure. Isolation system was comprised of bilinear hysteretic force-deformation relation. Lee (1980) applied the ground motion bi-directionally. However, the only considered ground motion was 1940 El Centro record. The author concluded that the effect of superstructure eccentricity on isolator displacements is negligible. Similar conclusion was derived by Jangid and Datta (1994a-b) where they investigated the non-linear response of torsionally coupled isolated systems under random ground motions. They revealed that "*eccentricity of superstructure does not have a significant influence on isolator displacements*". However, conclusions indicating the futility of eccentric superstructures regarding isolator displacements were contradicted by study of Nagarajaiah *et al*. (1993a). Authors focused on torsion in multi-story isolated structures where isolation system consists of inelastic elastomeric isolation systems. For this purpose, Nagarajaiah *et al*. (1993a) employed two records namely, 1940 El

Centro and 1952 Taft. Torsional response of isolated structures was studied under bi-directional excitations of the selected records. Nagarajaiah *et al*. (1993a) reported that although the major cause of torsional response in isolated structures is the existence of eccentricity in isolation system, asymmetry in superstructure is also of vital importance as that of the isolation system. Nagarajaiah *et al*. (1993b) also studied torsion in isolated structures where isolation is provided by sliding systems. Authors indicated that the major cause of torsion in isolated structures with sliding systems is the superstructure stiffness eccentricity. Parallel to previous studies, Tena-Colunga *et al*. (1997) revised the effect of eccentricities in both isolation system and superstructure on isolator displacements. In their study, isolation system consisted of lead rubber bearings. Authors stated that isolator displacements are highly affected by the torsional response of the superstructure. This issue was also addressed in study of Tena-Colunga and Gomez-Soberon (2002). Conclusion of that study revealed that asymmetry in the superstructure reduces the effectiveness of the isolation system. Authors also investigated the influence of degree of eccentricity on isolation system by considering various eccentricities. In a more recent study, Tena-Colunga and Escamilla-Cruz (2007) concentrated on effect of type of eccentricities in superstructure. Hence, authors studied the influences of both mass and stiffness eccentricities in superstructure regarding torsional response of isolated systems. Tena-Colunga and Escamilla-Cruz (2007) reported that mass eccentricity gives more severe amplifications in isolator displacements than stiffness eccentricity.

Most of the previous studies investigated response of single-story structures or considered limited number of ground motion records with a fixed value for effective isolation period (Nagarajaiah, 1993a). In addition, previous studies did not address the bi-directional excitations and bi-directional eccentricities. In this sense, studies of Tena-Colunga and Gomez-Soberon (2002) and Tena-Colunga and Escamilla-Cruz (2007) differed from the other aforementioned studies by considering a series of isolation periods, bi-directional eccentricities and multi-story structures. However, all of the considered ground motions in those recent studies were limited

to a specific region which is Mexican Pacific Coast. Moreover, authors used a scaling procedure where only the "*dominant*" component of a record matches the target spectrum at a target period. That scaling method is questionable especially when bi-directional response is of concern (Bommer and Acevedo, 2004). In addition, none of the earlier studies considered the amplification in isolator displacements due to torsional response of superstructure under near-field conditions.

The study presented herein focused on the amplification of isolator displacements due to mass eccentricity in the superstructure under bi-directional excitations. For this purpose, a scaling procedure that can preserve the difference between the two horizontal components of a record is employed. This is especially of utmost importance for bi-directional analyses considering records with near-field effects (Stewart *et al*., 2001). Results obtained from nonlinear RHA are also compared with the amount of amplification in isolator displacements suggested by the codified procedures.

6.2 ANALYSES CONDUCTED

A series of nonlinear RHA were conducted to determine torsional response of isolated structures under bi-directional excitations. Considered buildings are 3-story and 7-story RC structures as presented in Chapter 3 (Figures 3.9 and 3.10). The asymmetry in superstructure was included by considering 5% mass eccentricity in both of the horizontal directions to satisfy bi-directional eccentricity. Torsional response of isolated structures was investigated in two different soil classes namely, stiff and soft soil conditions. Hence, two sets of ground motions were selected to be representative of those soil classes. Detailed information about selected records was given in Tables 2.1 and 2.2 for stiff and soft soil conditions, respectively.

6.2.1 Non-linear Response History Analyses

Considered 3- and 7-story isolated buildings were subjected to bi-directional excitations by means of structural analysis program SAP2000 (2008). Response of

isolation system to mass eccentricity in the superstructure was studied for MCE. Corresponding 5% damped response spectra for stiff and soft soil conditions were selected in accordance with TEC (2007) to be compatible with the code provisions. Figure 4.1 presents the related spectra.

Analyses were conducted with carefully selected and scaled records. The scaling procedure employed can preserve the difference between the two horizontal components of a record and is compatible with the codified spectra. This is especially of utmost importance for bi-directional analyses considering records with near-field effects. Details of selection and scaling of recorded ground motions were discussed in Chapter 2 and Figure 5.1c illustrates how ground motions were applied bi-directionally.

Before evaluation of amplifications in isolator displacements due to asymmetry in superstructure and comparison of results obtained from nonlinear RHA with that of code provisions, a set of sensitivity analyses were conducted. Those sensitivity analyses were used to identify the effects of isolation period in the isolated buildings when eccentricity is of concern. Characteristics of the isolation systems were presented through Tables 3.6-3.9.

6.2.2 Sensitivity Analyses

To understand the dependency of analyses results to isolation period, nonlinear RHA were performed. Sensitivity analyses were conducted only for 3-story isolated RC building. Data given in the related graphs are the mean values of eleven cases performed in accordance with the clustered ground motion bins.

In order to determine the amplifications in maximum displacements experienced by isolators, displacements of the isolators at four outer most corners of the isolation system were recorded (see Figure 6.1) when there are eccentricities in superstructure and were divided by that of the symmetric systems. Although there are four different combinations for the location of mass eccentricity in the superstructure as shown in Figure 6.1, cases 1 and 2 are identical with cases 3 and

4. Hence, comparisons are done considering only the results obtained from cases 1 and 2.

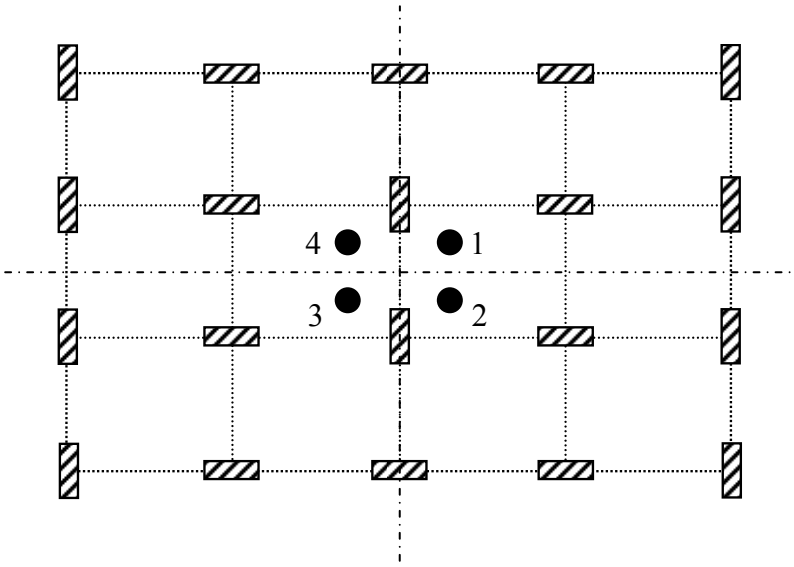

Figure 6.1 Locations of eccentricity in superstructure.

Since, it may differentiate according to soil condition of the records, analyses were conducted for both of the soil conditions. Figure 6.2 shows the variation of D_{RHA}^{ECC}/D_{RHA} ratio for various Q/W ratios as a function of isolation period. For both of the ground motion bins, D_{RHA}^{ECC}/D_{RHA} ratio is not affected by the alteration of isolation period. Although, D_{RHA}^{ECC}/D_{RHA} ratio increases slightly with increasing isolation period, those increments are not significant and can be neglected.

In Figures 6.3 and 6.4, individual D_{RHA}^{ECC}/D_{RHA} ratios are presented for all of the eleven records in each ground motion bin. These figures show that the distributions of D_{RHA}^{ECC}/D_{RHA} ratios are very uniform for all of the individual records. However, in studies of Almazan and De la Llera (2000) and Tena-Colunga and Gomez-Soberon (2002), the distribution was not uniform throughout the considered isolation systems. D_{RHA}^{ECC}/D_{RHA} ratios presented at those two studies were in the range of 1.2 and 2.2 even for an individual record. This means that almost 100% increase occurs in D_{RHA}^{ECC}/D_{RHA} ratio due to increasing isolation period which is totally contradicts with the observations presented here. This is an

indicative of the importance of selection and scaling of records together with selection of realistic isolation systems.

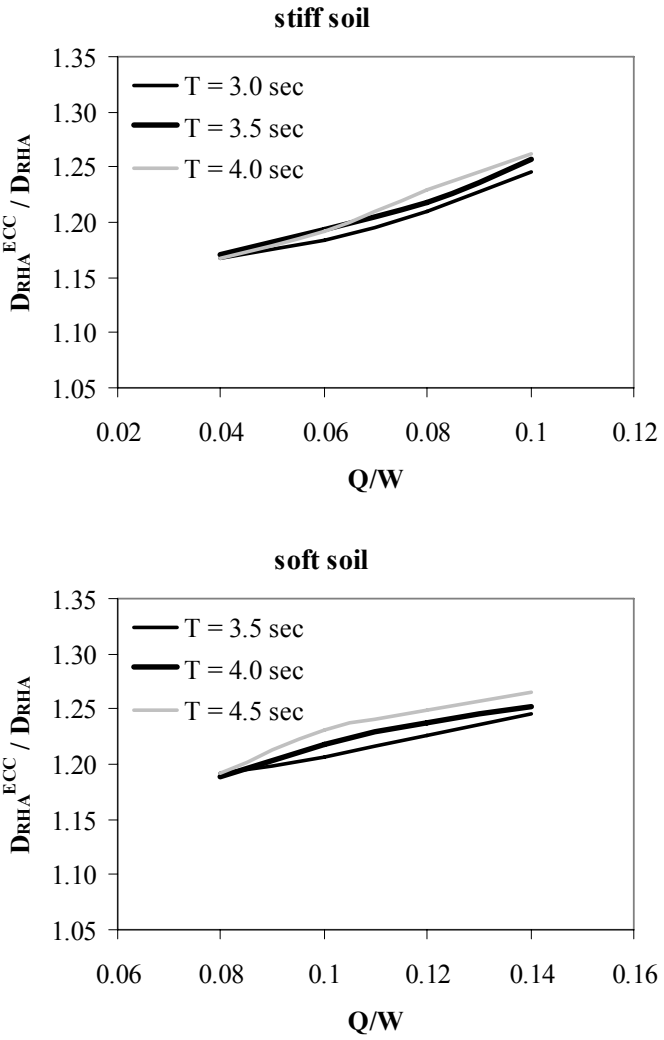

Figure 6.2 Amplifications in isolator displacements due to isolation period under increasing *Q*/*W* ratios in 3-story superstructure.

Figures 6.3 and 6.4 also reveal that above mentioned uniformity does not depend on the *Q*/*W* ratio. Regardless of the soil condition, similar observations are clear for all of the considered *Q*/*W* ratios.

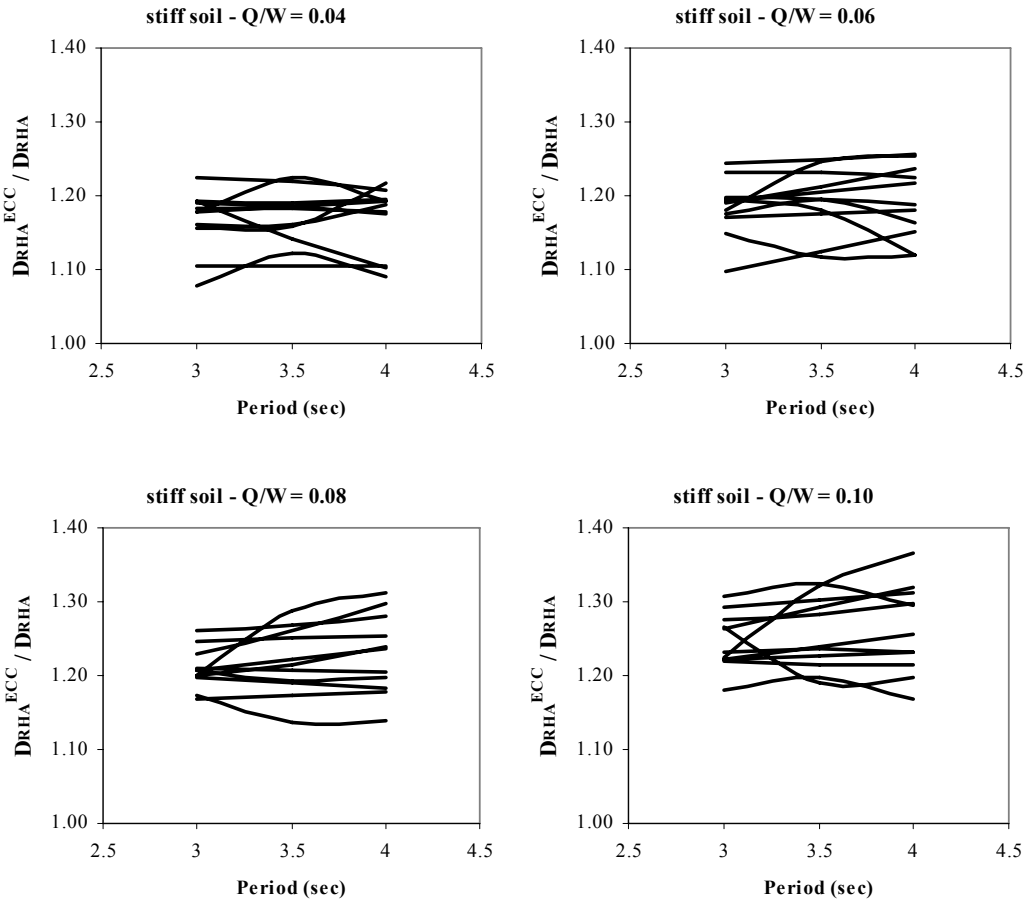

Figure 6.3 Distribution of amplification in isolator displacements due to asymmetry in superstructure for each individual case of stiff soil conditions.

6.2.3 Effects of *Q*/*W* ratio and soil condition

In the light of the sensitivity analyses, once the effect of isolation period on the variation of response of isolated structures with eccentric superstructures is found to be insignificant, alterations in $D_{RHA}{}^{ECC}/D_{RHA}$ ratios are investigated for isolation systems only with lowest isolation periods to emphasize the effect of superstructure eccentricities with the isolation periods 3 sec. and 3.5 sec. for stiff and soft soil conditions, respectively. The maximum of the resultant isolator displacement obtained both from cases 1 and 2 are designated as the maximum isolator displacement for isolation system with eccentric superstructure, $D_{RHA}{}^{ECC}$.

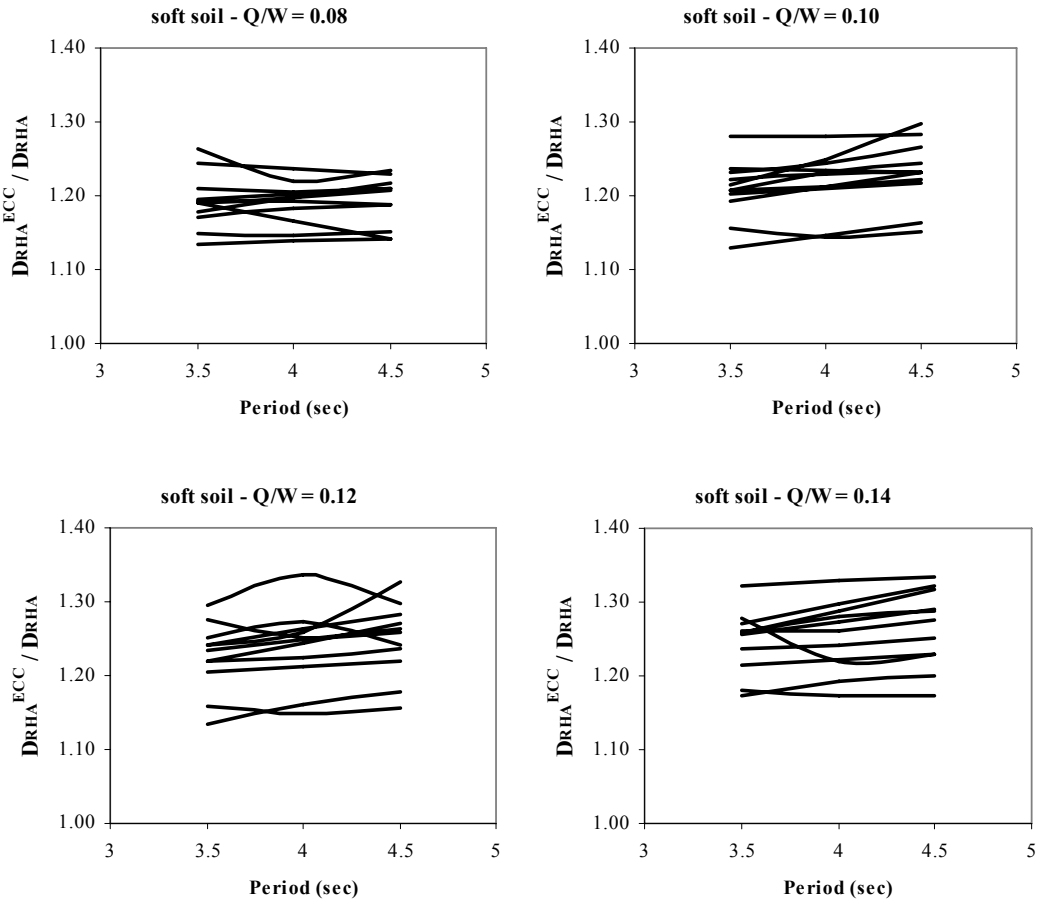

Figure 6.4 Distribution of amplification in isolator displacements due to asymmetry in superstructure for each individual case of soft soil conditions.

Results for 3- and 7-story isolated RC buildings are given through Figures 6.5 and 6.6, respectively. Solid lines in those figures represent the mean values for each *Q*/*W* ratio. It is clear that for 3-story isolated structure, amount of amplifications in isolator displacements increase as *Q*/*W* ratio increases. When the average of eleven analyses is considered, D_{RHA}^{ECC}/D_{RHA} ratios are in between 1.15 – 1.25 depending on the *Q*/*W* ratio. On the other hand, when the same comparison is done for 7-story isolated RC building, *Q*/*W* ratio is observed to be an ineffective parameter for amplification of maximum isolator displacement due to eccentricity in

superstructure. The average line is almost constant and equal to 1.15 for both of the ground motion bins, regardless of the *Q*/*W* ratios.

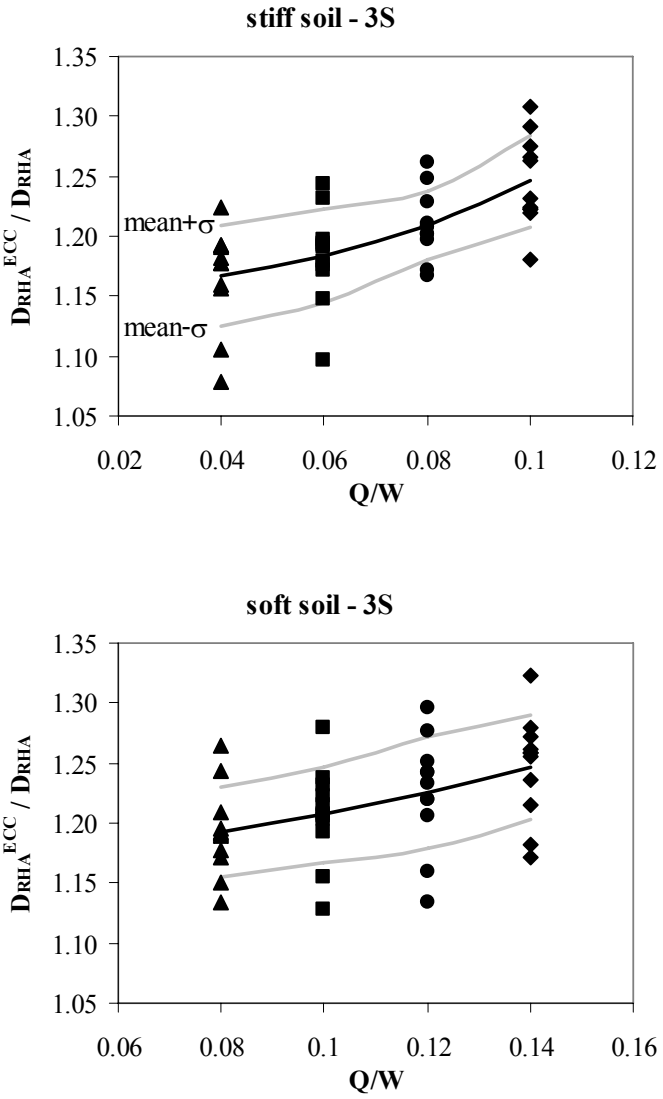

Figure 6.5 Variation of D_{RHA}^{ECC}/D_{RHA} ratios due to increase in *Q*/*W* ratio for 3-story isolated structure for stiff (top) (T = 3.0 sec.) and soft (bottom) (T = 3.5 sec.) soil conditions.

When Figures 6.5 and 6.6 are revisited for the effect of soil condition on the amplification of isolator displacements due to eccentricity in superstructure, it is observed that amplifications are not affected by variation in soil condition. In both stiff and soft soil cases, the amplifications are almost identical, regardless of the variation in superstructure.

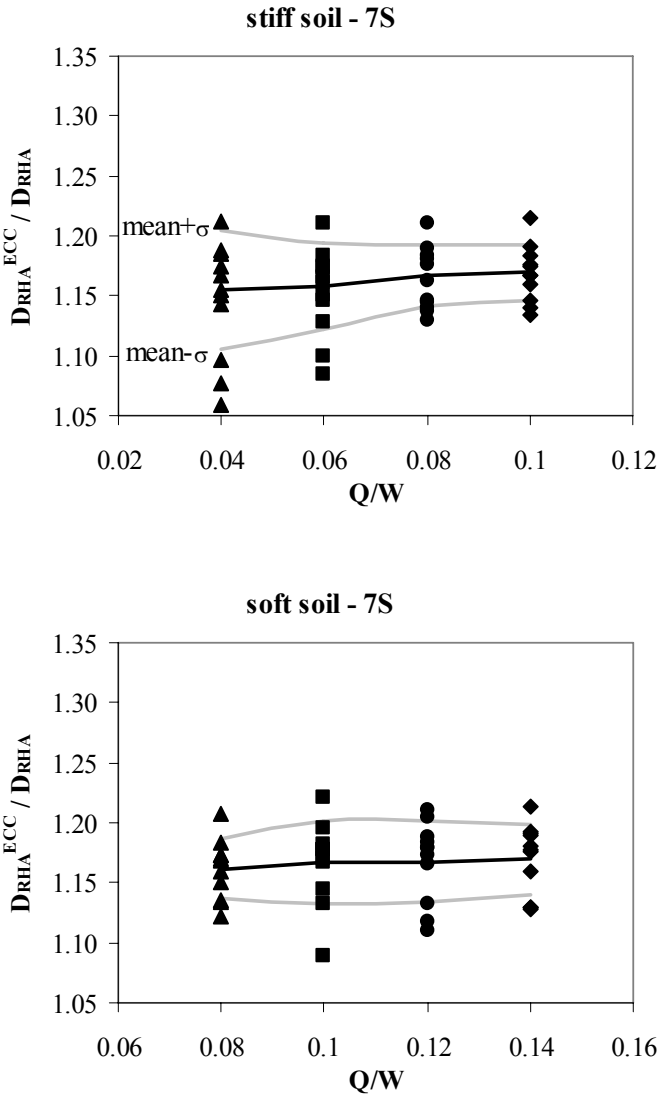

Figure 6.6 Variation of D_{RHA}^{ECC}/D_{RHA} ratios due to increase in Q/W ratio for 7-story isolated structure for stiff (top) (T = 3.0 sec.) and soft (bottom) (T = 3.5 sec.) soil conditions.

6.2.4 Evaluation of Simplified Method

Simplified methods of analysis described in codes and specifications for seismically isolated structures (i.e., ASCE (2005)) ensures an increment in the isolator displacements due to actual or accidental torsion calculated from the most disadvantageous location of eccentric mass. That amplification should be in accordance with the following equation.

$$D_{TM} = D_M\left(1 + y\frac{12e}{b^2 + d^2}\right) > 1.1D_M \qquad (6.1)$$

In Equation (6.1), D_{TM} is the total maximum isolator displacement, D_M is the maximum displacement at the center of rigidity of isolation system calculated by the iterative method discussed in Chapter 3, e is the actual plus accidental eccentricity taken as five percent of the longest plan dimension of the structure, y is the distance between centers of rigidity of the isolation system and the element of interest measured perpendicular to the direction of seismic loading, b and d are the shortest and longest plan dimensions of the structure, respectively (Figure 6.7). Limitation for Equation (6.1) is that it should not be less than $1.1D_M$.

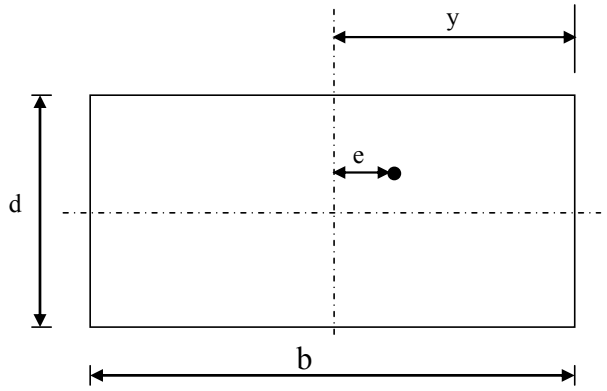

Figure 6.7 Schematic view of parameters affecting torsional response of isolated structures.

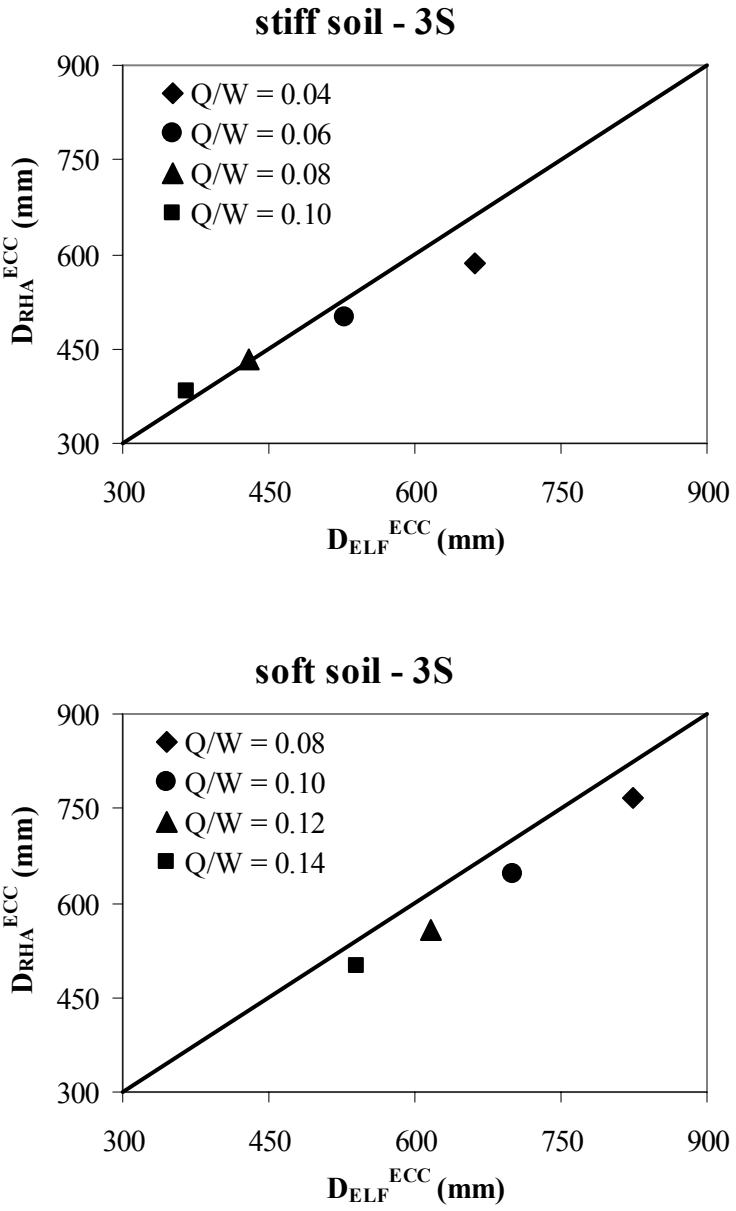

Figure 6.8 D_{RHA}^{ECC} versus D_{ELF}^{ECC} for 3-story superstructure in stiff (top) (T = 3.0 sec.) and soft (bottom) (T = 3.5 sec.) soil conditions.

To assess the accuracy of suggested amplification by simplified method of analysis described in codes, D_{RHA}^{ECC} obtained from analyses results of 3-story

building is plotted against D_{ELF}^{ECC} in Figure 6.8 for stiff and soft soil conditions. D_{ELF}^{ECC} is the amplified values of displacements calculated by multiplication of displacements obtained by ELF procedure with the constants obtained by Equation (6.1).

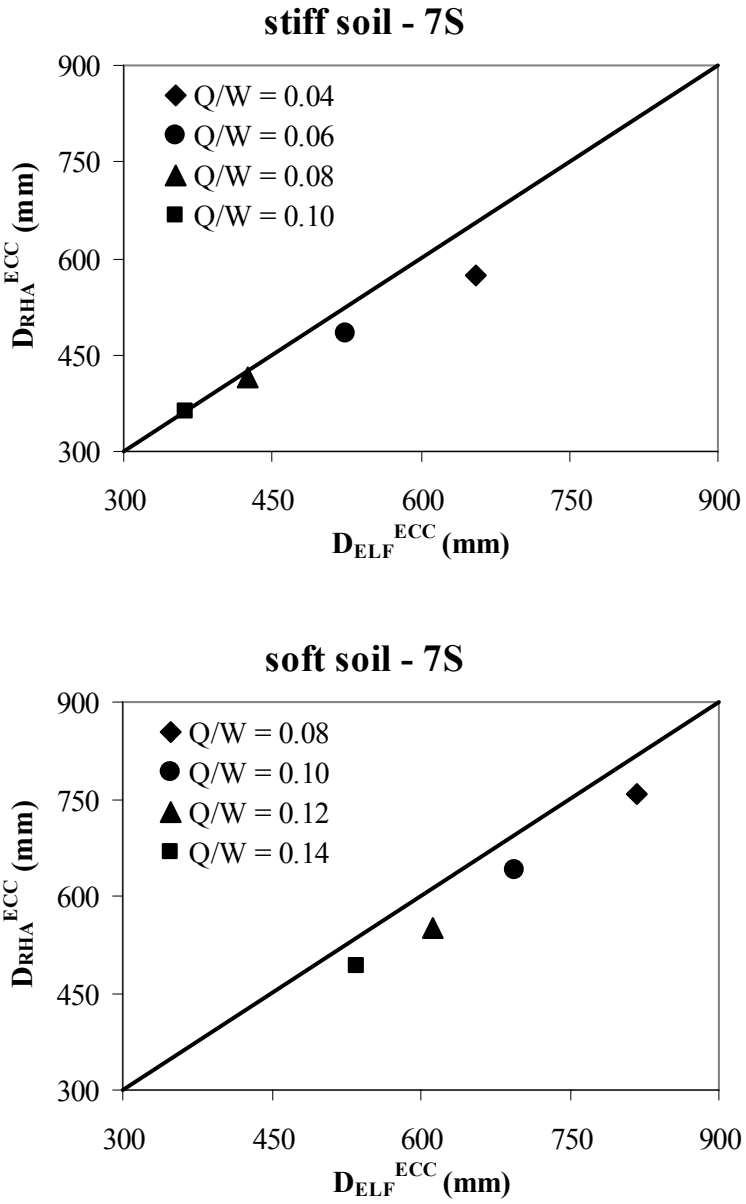

Figure 6.9 D_{RHA}^{ECC} versus D_{ELF}^{ECC} for 7-story superstructure in stiff (top) (T = 3.0 sec.) and soft (bottom) (T = 3.5 sec.) soil conditions.

In Figure 6.8, solid lines have a slope of 45^{o} and stand for the case where results of both nonlinear RHA and simplified analyses are equal. The amount of amplification factor estimated by Equation (6.1) for the considered 3-story structure is 1.21. Figure 6.8 shows that the simplified method is also quite accurate in estimation of maximum isolator displacements with due consideration of asymmetry in superstructure, regardless of the soil condition.

The same comparison is presented in Figure 6.9 for 7-story building and amplification factor estimated by Equation (6.1) for the considered 7-story structure is 1.20. Results are almost the same with that of 3-story isolated RC building. Figures 6.8 and 6.9 show that the simplified method is also quite accurate in estimating the maximum isolator displacements with due consideration of asymmetry in superstructure, regardless of the soil condition.

CHAPTER 7

IMPLEMENTATION OF BIAXIAL INTERACTION OF HYSTERETIC FORCE-DEFORMATION RELATION OF ISOLATORS IN OPENSEES

7.1 INTRODUCTION

Previous researches have demonstrated that isolation bearings exhibit a coupling between the responses in each orthogonal direction (Mokha *et al*., 1993; Huang *et al*., 2000; Mosqueda *et al*., 2004; Warn and Whittker, 2004; Tena-Colunga and Perez-Osornia, 2006). Analyses done without considering the effects of that coupling in determining the isolator displacements underestimate the maximum resultant displacements (Mokha *et al*., 1993). From the simulations done in the previous studies, the amount of underestimation can be as much as 15%. Hence, to capture the behavior of seismic isolators under dynamic loading, the coupled behavior must be considered.

In this Chapter, the implementation of nonlinear force-deformation relation in a freeware Finite Element Analysis (FEM) program, namely Open System for Earthquake Engineering Simulation (OpenSees), by considering the coupled behavior between two horizontal orthogonal directions is described. Then, verification of implemented model is done by comparing the maximum isolator displacements obtained from nonlinear RHA performed by OpenSees and SAP2000. Verifications are conducted for both individual isolators and isolators mounted under a superstructure. Finally, the significance of coupled behavior is

marked by comparing the maximum isolator displacements obtained from coupled and uncoupled analyses of the considered systems.

7.2 OPENSEES

Object-oriented programming is being revealed as an option for simulations of structural and geotechnical systems. Object-oriented framework is flexible and modular, and it is open to contributions of new developers by means of new classes added to source code. Use of object-oriented techniques requires a compatible language that supports the related concepts. Two of the most common object-oriented programming languages are C++ and Java.

The object-oriented program used to implement the new coupled material model in this study is OpenSees. OpenSees is an open source structural analysis program and implemented in C++. It is developed at the Pasific Earthquake Engineering Research (PEER) center (McKenna, 2009). Being an open source program, OpenSees has the advantage of having components such as materials, elements, and solvers, which are already tested and validated. This key feature simplifies and provides a basis for testing of integrated new components (Fenves, 2005).

Implementation of new components (i.e. materials) into OpenSees is seamlessly performed owing to modular architecture of the software. One can use a new material model with an available element model. Moreover, researchers do not have to make any modifications to those available element models.

There are three readily available materials in OpenSees: (i) UniaxialMaterial, (ii) NDMaterial, (iii) SectionForceDeformation. In OpenSees, "*Each material abstraction is a subclass of class Material, and Material class is a subclass of both the TaggedObject and MovableObject*" (Bian, 2002) as illustrated in Figure 7.1. Tagged object class adds tagging capability while MovableObject class provides parallel processing capabilities. Those abstract classes are responsible for force-deformation relationship of an element.

7.3 *COUPLEDMATERIAL* CLASS

Coupled hysteretic force-deformation relation is implemented in OpenSees with the name of *CoupledMaterial*. Although, *CoupledMaterial* is a subclass of *UniaxialMaterial* class (Figure 7.1), it also represents the two-dimensional generalization of *UniaxialMaterial* by considering coupling between two horizontal directions.

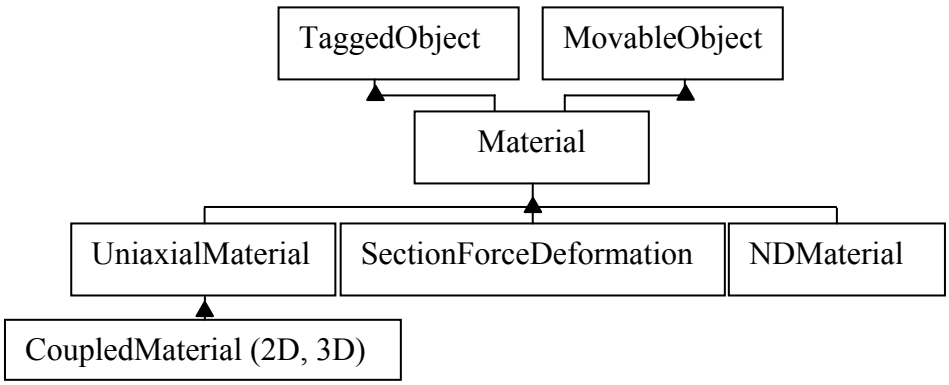

Figure 7.1 Material class hierarchy in OpenSees.

CoupledMaterial class is a modified version of Steel01 class, which is currently available in OpenSees. Steel01 is used to define a bi-linear force-deformation relation (Figure 3.1) and does not consider any coupling between the force-deformation relations defined in two orthogonal horizontal directions (Mazzoni *et al*., 2009). Definition of Steel01 is based on deformation of individual springs and is appropriate only for uni-directional analysis where there are no coupling effects. Details of Steel01 class are available at http://opensees.berkeley.edu/cgi-bin/cvsweb2.cgi/OpenSees/SRC/.

The *CoupledMaterial* class makes it possible to include the coupled behavior of bi-linear hysteretic representation of LRBs and by means of a key feature included in *CoupledMaterial*, during the class construction user can indicate whether the solution will be uncoupled (for uni-directional excitations) or coupled (bi-

directional excitations). If it is uncoupled, Equations (7.1) and (7.2) are used to obtain the corresponding force on LRB. If coupling effects are considered, Equations (7.3), (7.4), and (7.5) are employed to get the force carried by LRB. In those equations, Z or Z_x and Z_y are the hysteretic dimensionless quantities that account for the direction and the biaxial interaction of hysteretic forces (Park *et al*., 1986). *A* and *B* in Equation (7.4) are set to 1 and 0.5, respectively to satisfy the relation of *A*=2*B* (Constantinou and Adnane, 1987). This assumption is crucial because it assures that Z or Z_x and Z_y to be bounded between +1 and -1 when yielding occurs (Nagarajaiah *et al*., 1989).

$$F = k_d D + F_y Z \tag{7.1}$$

$$D_y \cdot \dot{Z} = \left(A - |Z|^2 B \cdot \left(1 + sgn\left(\dot{D} Z \right) \right) \right) \cdot \dot{D} \tag{7.2}$$

$$\begin{Bmatrix} F_X \\ F_Y \end{Bmatrix} = r \cdot \begin{bmatrix} \dfrac{F_y}{D_y} & 0 \\ 0 & \dfrac{F_y}{D_y} \end{bmatrix} \cdot \begin{Bmatrix} D_X \\ D_Y \end{Bmatrix} + (1-r) \cdot \begin{bmatrix} F_y & 0 \\ 0 & F_y \end{bmatrix} \cdot \begin{Bmatrix} Z_x \\ Z_y \end{Bmatrix} \tag{7.3}$$

$$D_y \cdot \begin{Bmatrix} \dot{Z}_x \\ \dot{Z}_y \end{Bmatrix} = \left(A \cdot [I] - B \cdot [\Omega] \right) \cdot \begin{Bmatrix} \dot{D}_X \\ \dot{D}_Y \end{Bmatrix} \tag{7.4}$$

$$[\Omega] = \begin{Bmatrix} Z_x^2 \cdot \left[sgn\left(\dot{D}_X Z_x \right) + 1 \right] & Z_x Z_y \left[sgn\left(\dot{D}_Y Z_y \right) + 1 \right] \\ Z_x Z_y \left[sgn\left(\dot{D}_X Z_x \right) + 1 \right] & Z_y^2 \left[sgn\left(\dot{D}_Y Z_y \right) + 1 \right] \end{Bmatrix} \tag{7.5}$$

where *r* is post-yield to elastic stiffness ratio; *D* or D_X and D_Y are displacements of isolator in orthogonal horizontal directions for uncoupled and coupled cases, respectively; $\dot{D}$ or $\dot{D}_X$ and $\dot{D}_Y$ are the relative velocities in orthogonal horizontal

directions experienced by the isolator for uncoupled and coupled cases, respectively. F or F_X and F_Y are the hysteretic forces carried by the bearings depending on the solution type (coupled or uncoupled) considered. [I] is the identity matrix where diagonal members are equal to one.

The coupling of the two horizontal deformations is considered in *CoupledMaterial* class by adding *pairMaterial* variable. The choice of defining the *pairMaterial* is left to the user for considering coupling effects. Once the *pairMaterial* variable is initiated, the solution considers one master and one slave material assigned to a single *zeroLengthElement* in both horizontal directions. Procedure starts with getting the tag number of master-slave materials. Initiation of *pairMaterial* varible is set by writing the material tag of slave material at the end of the input line of master material definition. *CoupledMaterial* is uncoupled by default.

During coupled computations, master material combines the deformation information from both master and slave materials. Master material is also responsible for iterating the algorithm to calculate the deformations. The results of this computation is used to compute the force in both master and slave material.

In order to solve for the nonlinear forces, Equations (7.2) and (7.4) are solved via fourth order Runge–Kutta (Butcher, 1987) method to obtain the hysteretic quantities Z or Z_x and Z_y at each time step. When h is the step size, this method allows h^5 error per step of iteration. Z or Z_x and Z_y values are updated using the result of this numerical solution, instantaneously.

Since calculation of Z or Z_x and Z_y depends on the displacement history of LRB, solution of *CoupledMaterial* starts with a trial deformation. That trial deformation leads to calculation of Z for uncoupled or Z_x and Z_y for coupled solution. Class then calls the necessary methods to obtain the force carried by LRB, which is defined by a bi-linear force-deformation relation initially. The calculated force value is used to calculate corresponding deformation. This process is repeated until the difference between trial and converged deformations is small enough to be neglected. Steps

followed during the procedure can be summarized in the pseudo-code given below. The complete software code is given in Appendix A.

```
If (trial deformation – current deformation) > error term
{
  //Calculate Z (uni-directional) or Zx and Zy (bi-directional)
  ...
  //Determine the forces F or FX and FY carried by isolator
  ...
  //Obtain corresponding deformation
  ...
}
  //Assign the current deformation as converged deformation
  ...
  //Consider the converged deformation to finalize the computations
at any instant
  ...
```

7.4 VERIFICATION OF IMPLEMENTED MATERIAL MODEL

Two sets of cases are considered to verify the implemented *CoupledMaterial* model, one for individual isolators and one for isolators mounted under a superstructure. For verification purpose, a series of nonlinear RHA were conducted in both OpenSees and SAP2000. Analyses were performed under bi-directional excitation of the selected ground motion records where the system under consideration is subjected to two horizontal orthogonal components of the record, simultaneously.

7.4.1 Verification for Individual LRBs

Two different LRBs, representing one large and one relatively small size bearing, are selected to verify the implemented model. Those isolators are taken from Constantinou *et al*. (2007). Properties of those bearings are given in Tables 7.1 and 7.2. LRBs of which schematic views are given in Figures 7.2 and 7.3 are referred as LRB1 and LRB2, respectively. Selected LRBs are subjected to bi-directional excitation of a motion recorded during 1992 Erzincan, Turkey earthquake. The considered record station is Erzincan and scaled as described in

Chapter 2. Its M_w is 6.7 and closest distance to fault-rupture is 4.4 km. The 5% damped acceleration spectra of the orthogonal components are presented in Figure 7.4 and Table 7.3 shows the characteristics of the selected records.

Table 7.1 Data used in analysis of LRB1

Weight on bearing	10266 kN
Total thickness of shims	125 mm
Radius of lead core	153 mm
Bonded rubber radius	559 mm
Height of lead core	333 mm
Yield force	1302.9 kN
Yield displacement	30 mm
Post-yield stiffness	2000 N/mm
Post-yield to elastic stiffness ratio	0.046

Table 7.2 Data used in analysis of LRB2

Weight on bearing	1441 kN
Total thickness of shims	71 mm
Radius of lead core	70 mm
Bonded rubber radius	241 mm
Height of lead core	224 mm
Yield force	207.7 kN
Yield displacement	7 mm
Post-yield stiffness	1080 N/mm
Post-yield to elastic stiffness ratio	0.0364

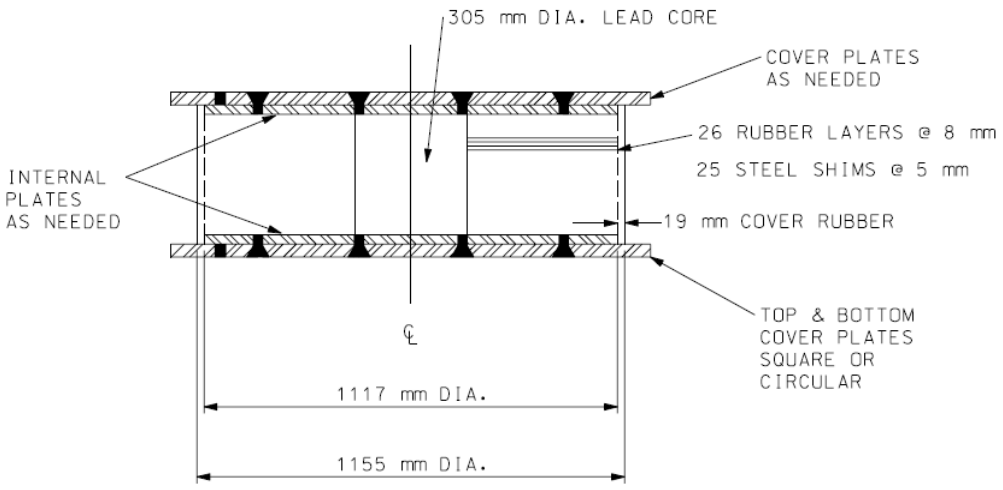

Figure 7.2 Analyzed isolator LRB1 (taken from Constantinou *et al*., 2007)

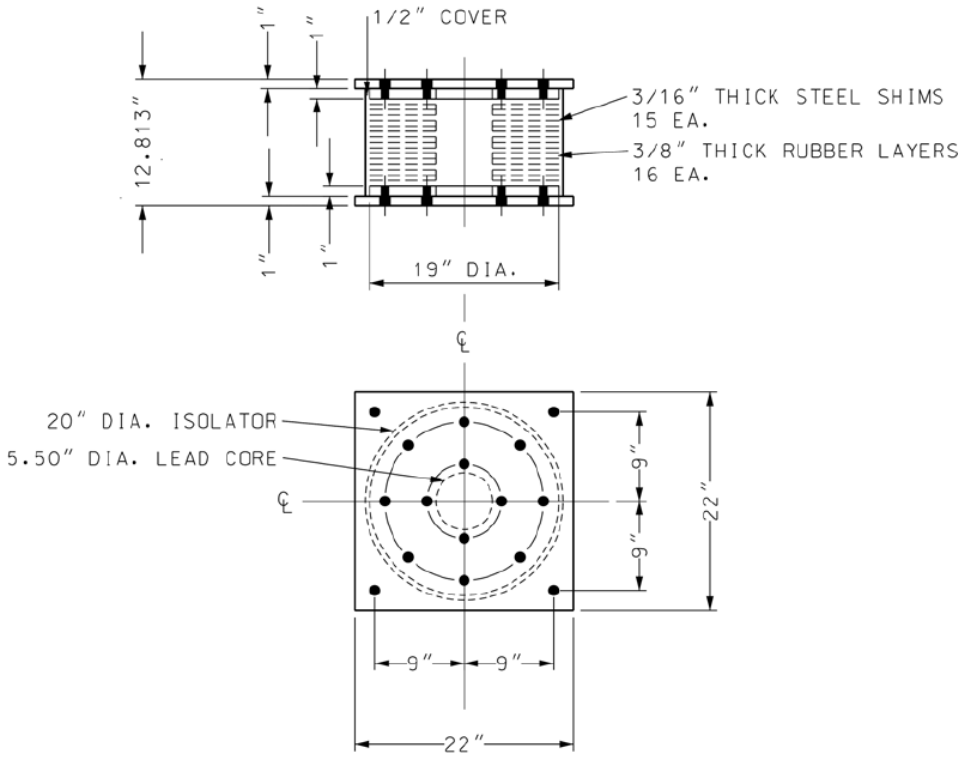

Figure 7.3 Analyzed isolator LRB2 (1 inch = 25.4 mm) (taken from Constantinou *et al*., 2007)

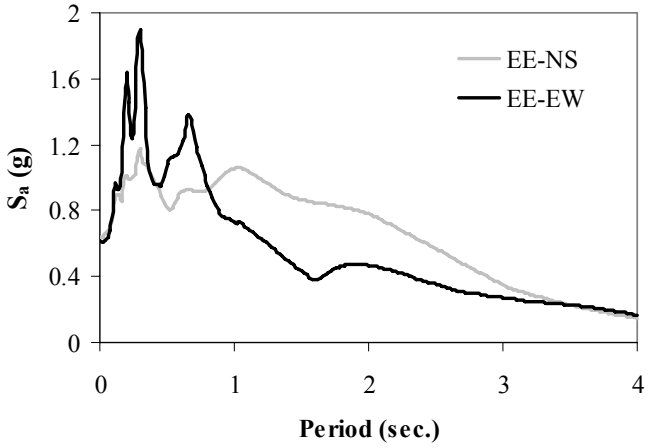

Figure 7.4 Acceleration spectra of EE record.

Table 7.3 Characteristics of EE record.

Earthquake	Station	Magnitude (M_w)	d (km)	Component	PGA (g)	PGV (cm/sec)	PGD (cm)
Erzincan (EE)	Erzincan	6.7	4.4	NS	0.52	83.9	27.4
				EW	0.50	64.3	22.8

The considered LRBs were modeled in SAP2000 by means of nonlinear link elements. One end of that element is connected to ground and restrained to be fixed. The other end is assigned a mass to represent the weight on the isolator. The parameters needed to conduct nonlinear RHA in SAP2000 with isolators are initial elastic stiffness, k_e, yield force, F_y and post-yield to elastic stiffness ratio (Figure 3.1) of the LRB.

The definition of LRBs in OpenSees is very similar to that of SAP2000. The bilinear force-deformation relation of isolators are defined by *CoupledMaterial* model where above mentioned parameters are defined. The connection of the defined material is assigned to a *ZeroLengthElement*. That element's length is zero and defined between two joints having exactly the same coordinates.

Comparisons of nonlinear RHA results are given through Figures 7.5 and 7.6 for LRB1 and LRB2, respectively. Results obtained from OpenSees are represented by dark solid lines whereas light solid lines stand for results obtained from SAP2000. These figures demonstrate that the implemented coupled material model is capable of capturing the behavior of isolators under bi-directional excitations. Force-displacement loops of both structural programs are identical.

To further emphasize the success of implemented coupled material model, the variations of Z_x and Z_y versus analysis time are depicted in Figures 7.7 and 7.8. It is clear that the obtained Z_x and Z_y values are in good agreement with the statement of Nagarajaiah *et al*. (1989) as being altered between +1 and -1. Figures 7.7 and 7.8 also present the relation between Z_x and Z_y. These results are parallel to the study of Park *et al*. (1986) where the hysteretic behavior prescribed by Equation (7.4) was indicated to be represented by a simple circular path.

7.4.2 Verification for LRBs Mounted Under Superstructure

Once the implemented new coupled material model is verified for individual LRBs, the behavior of an isolation system mounted under a superstructure is tested in this section. The 3-story isolated RC building with the corresponding isolator characteristics investigated so far is chosen as the case study building. The isolated structure is also subjected to Erzincan record.

The superstructure is modeled as elastic in both of the structural analysis programs where the modulus of elasticity and poissons ratios are 30 GPa and 0.2, respectively. Rigid diaphrams are assigned at each floor to provide equal displacements of joints at the same story level.

Q/W ratio of the considered LRBs is 0.08 and corresponding yield force is 14240 N. The elastic stiffness k_e is equal to 1424 N/mm with the assumption that the yield displacement D_y is 10 mm. Post-yield to elastic stiffness ratio is 0.04 which result in isolation period T = 3.5 sec.

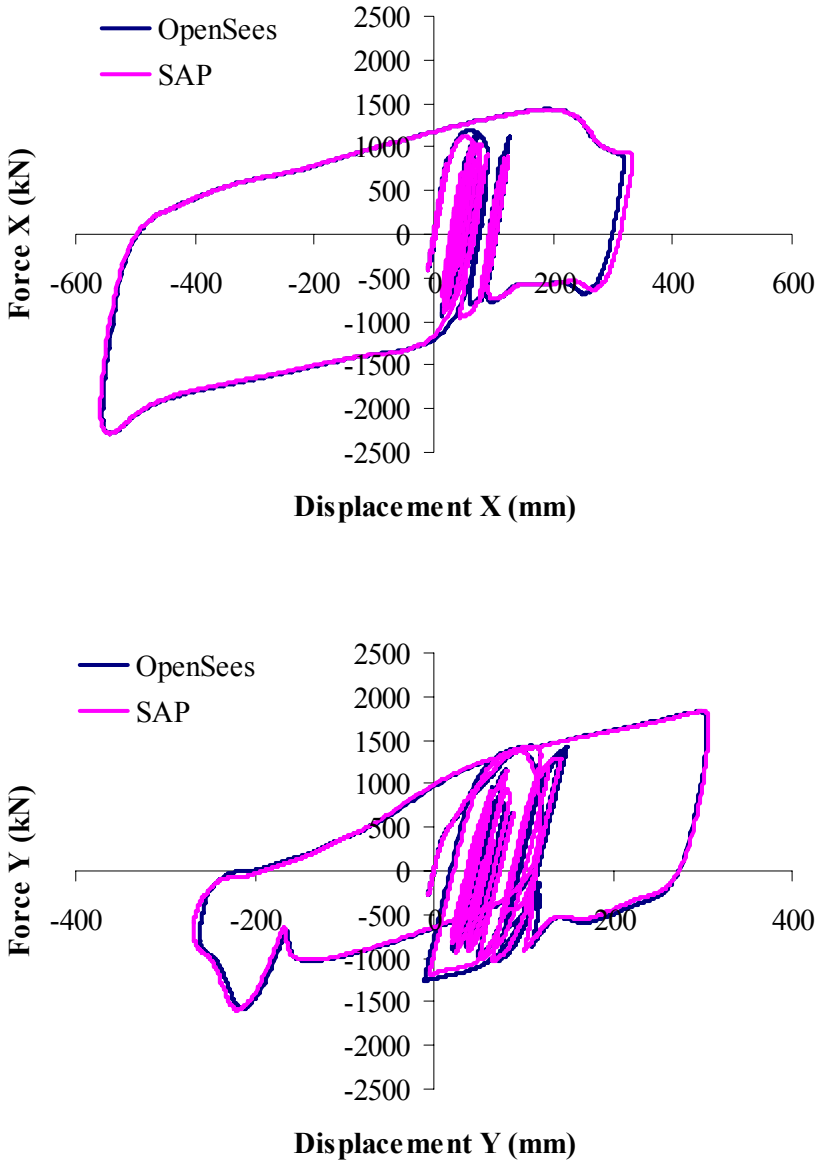

Figure 7.5 Force-displacement loops of isolator LRB1

Analyses results obtained from SAP2000 are presented in Figure 7.9 together with that of OpenSees, where the coupled material model is implemented, to show the accuracy of the *CoupledMaterial* class to capture the behavior of LRBs. It is clear that there is almost a perfect match for the force-deformation curves in the two orthogonal horizontal directions, as in the case of individual LRBs.

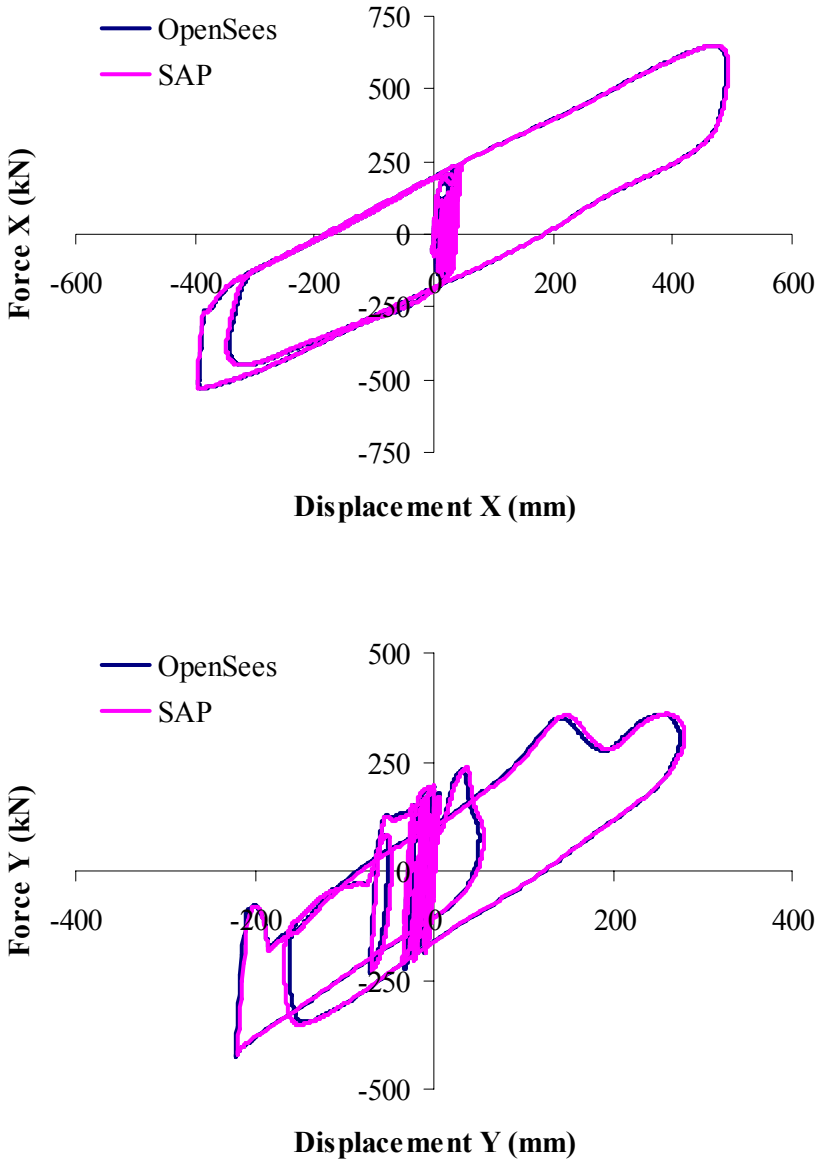

Figure 7.6 Force-displacement loops of isolator LRB2

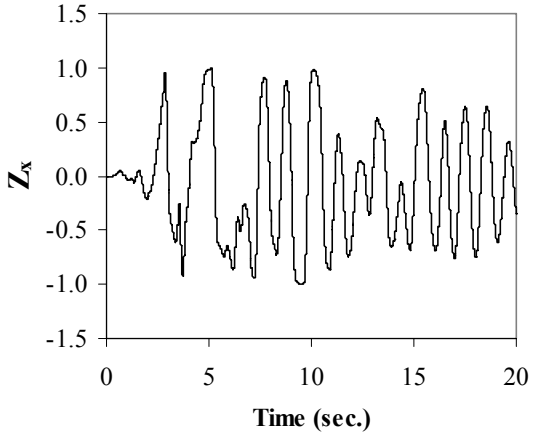

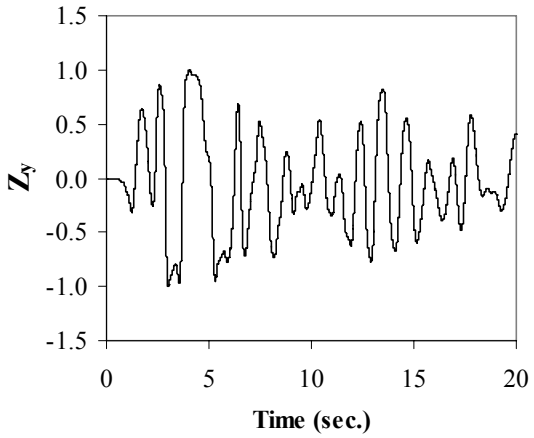

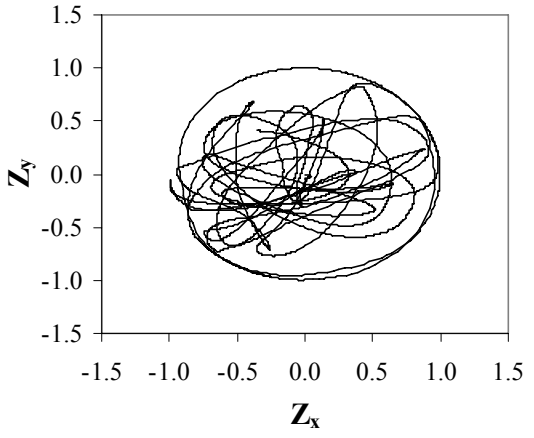

Figure 7.7 Variation of hysteretic components Z_x and Z_y with time for LRB1.

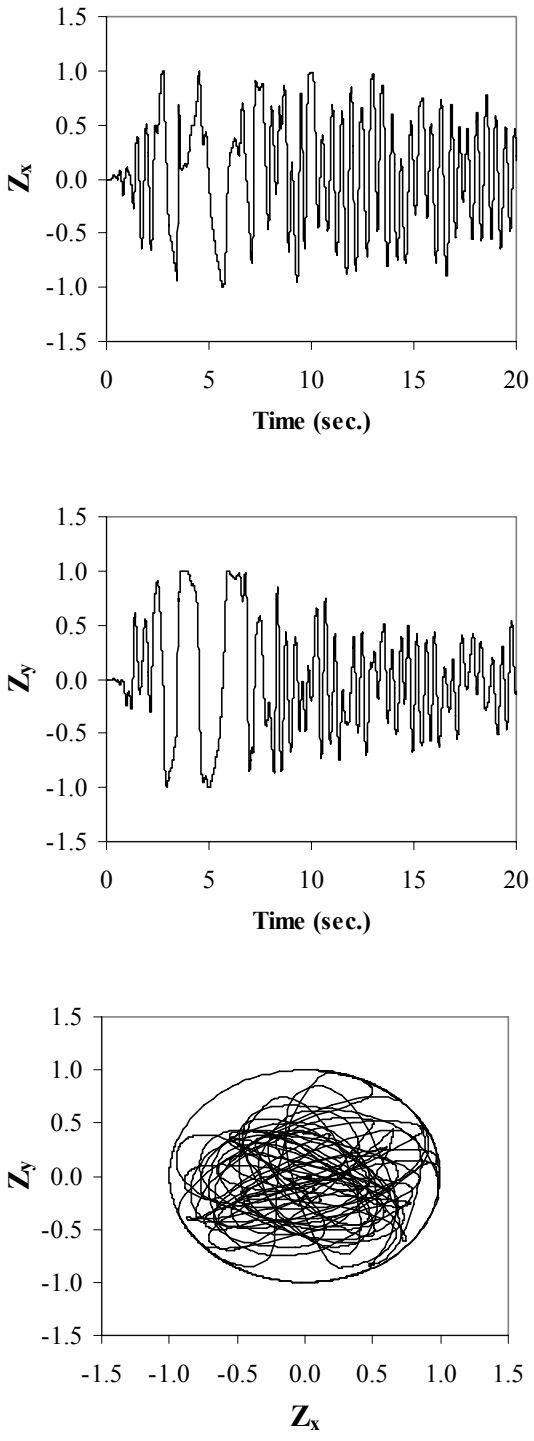

Figure 7.8 Variation of hysteretic components Z_x and Z_y with time for LRB2.

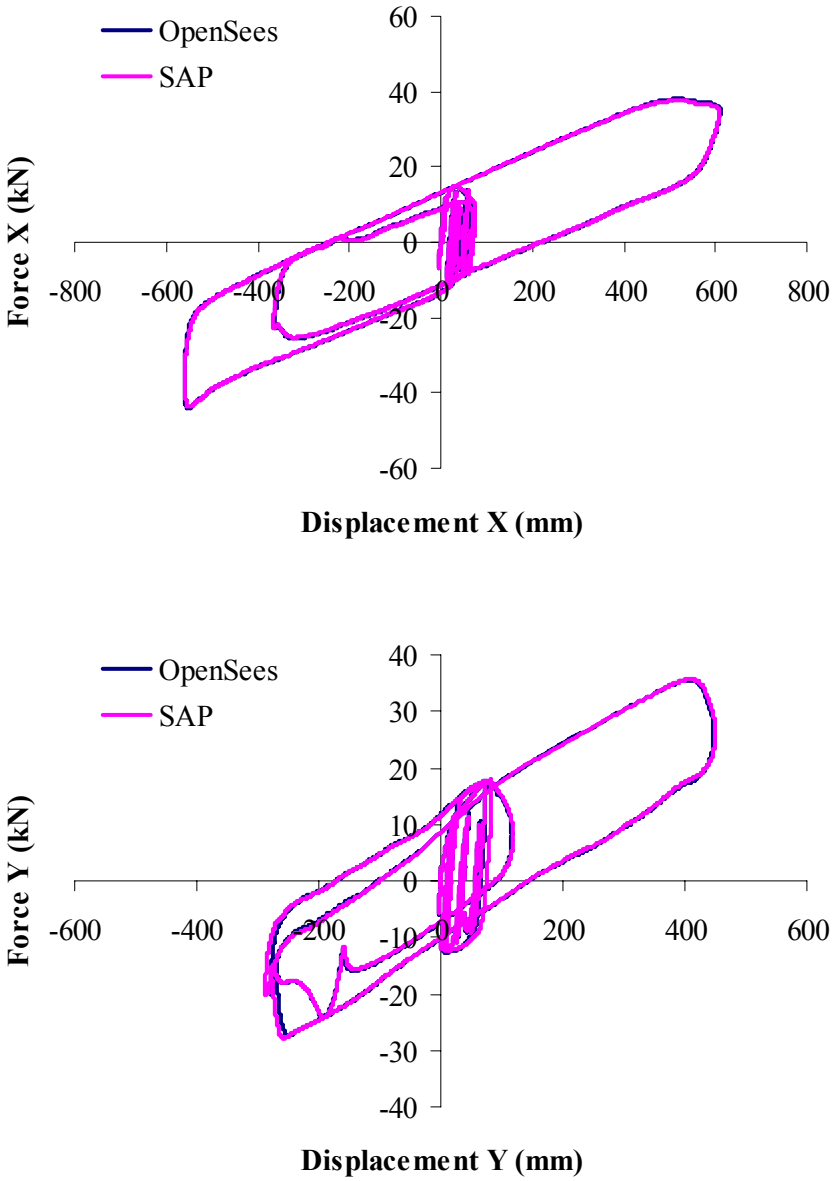

Figure 7.9 Symmetric 3S isolated RC building.

7.5 SIGNIFICANCE OF COUPLED MATERIAL MODEL

To show the difference between coupled and uncoupled hysteretic behavior under bi-directional excitation, considered two LRBs and isolated 3-story RC building were analyzed in OpenSees for both of the coupled and uncoupled cases.

Comparisons are done in terms of maximum resultant isolator displacements defined as the maximum value obtained by taking the SRSS of displacements in both of the horizontal directions at each time step.

In the uncoupled material model, the nonlinear forces carried by isolators are calculated by means of Equations (7.1) and (7.2) whereas, Equations (7.3)-(7.5) are used in coupled material model.

Comparison of maximum displacements of LRB1 and LRB2 are presented through Figures 7.10 and 7.11, respectively. Presented force-deformation loops of LRB1 and LRB2 in both horizontal directions show that there are significant differences between coupled and uncoupled solutions when the maximum isolator displacements are of concern. For the specific cases considered here, the maximum displacements of LRB1 and LRB2 are 642 mm and 459 mm with due consideration of uncoupled model. On the other hand, maximum displacements of LRB1 and LRB2 are 586 mm and 508 mm when coupled model is employed. The differences between two solution methods are 10% for both LRB1 and LRB2.

Similarly, coupled and uncoupled hysteretic force-deformation idealization of LRBs mounted under a superstructure results also in significant differences for maximum isolator displacements as shown in Figure 7.12. The amount of error in maximum isolator displacements is 5% where the displacements for coupled and uncoupled cases are 725 mm and 695 mm, respectively.

Comparisons indicate that use of the coupled material model for design of any isolation system is very crucial to estimate the probable maximum isolator displacements appropriately as it is stated in most of the previous studies.

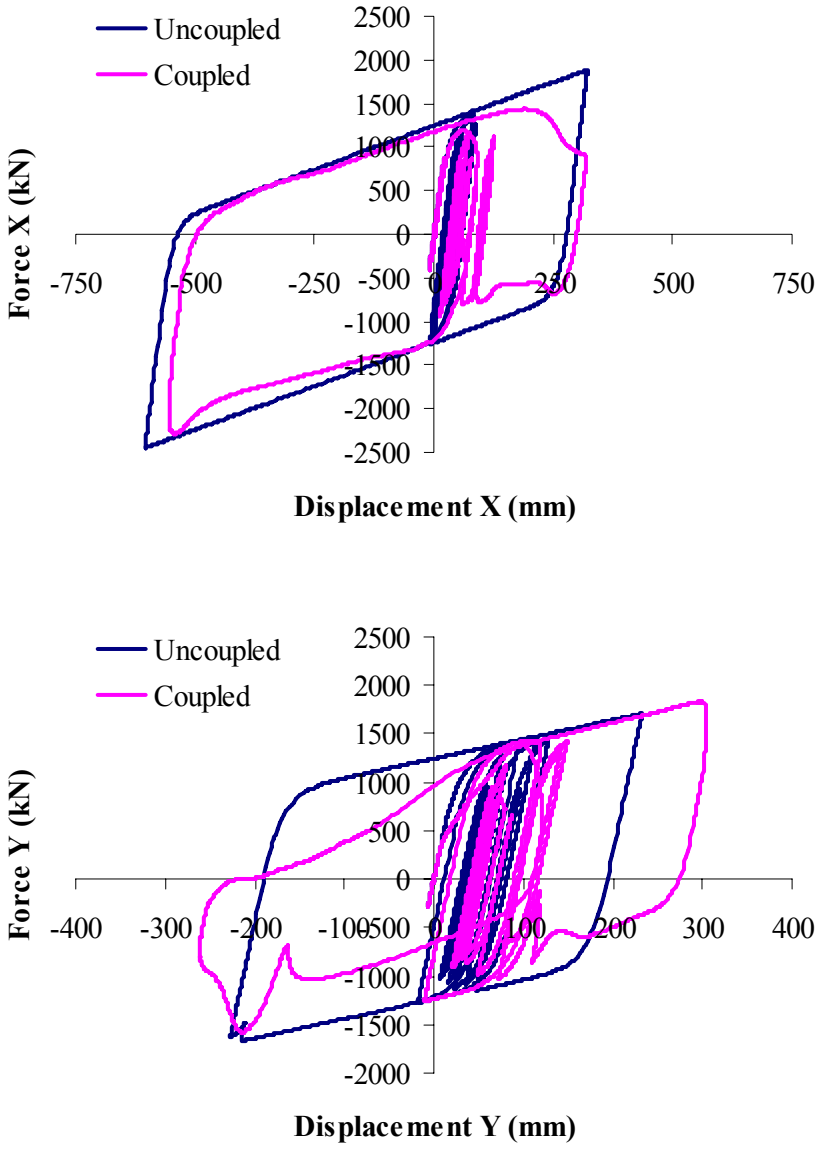

Figure 7.10 Comparison of coupled and uncoupled behavior of LRB1.

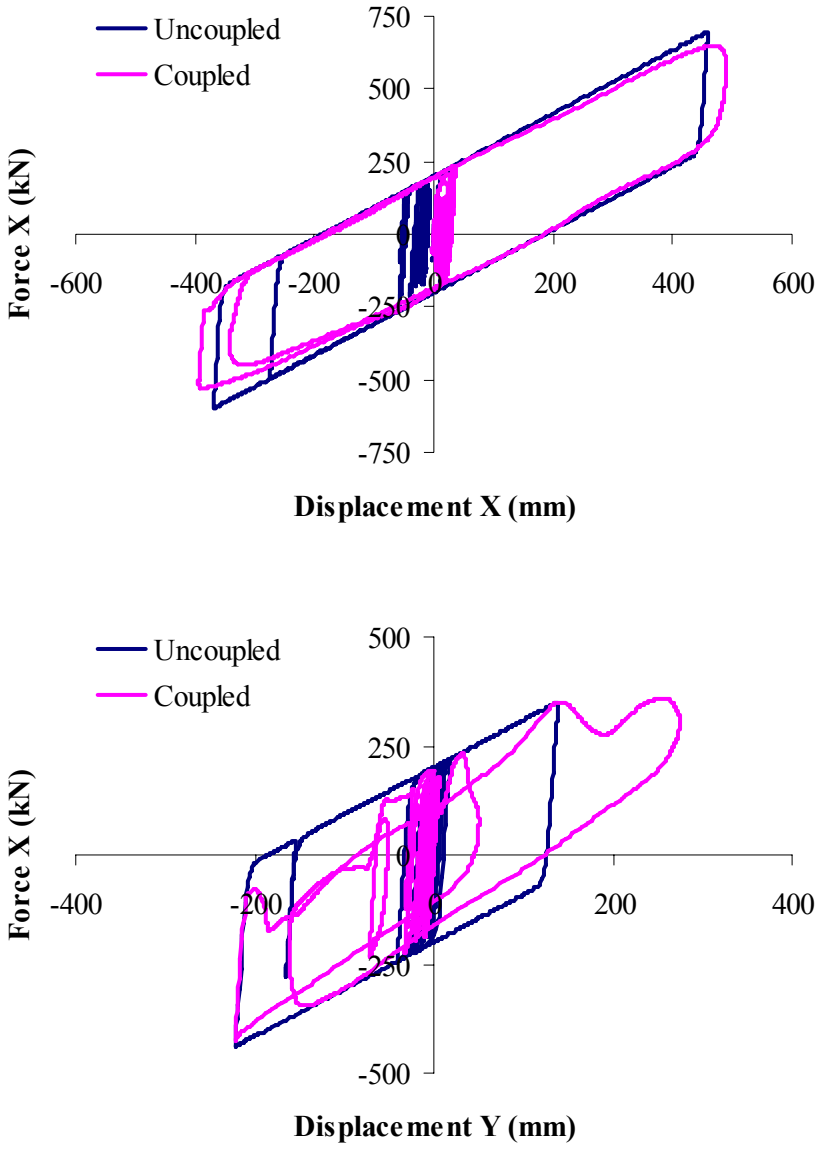

Figure 7.11 Comparison of coupled and uncoupled behavior of LRB2.

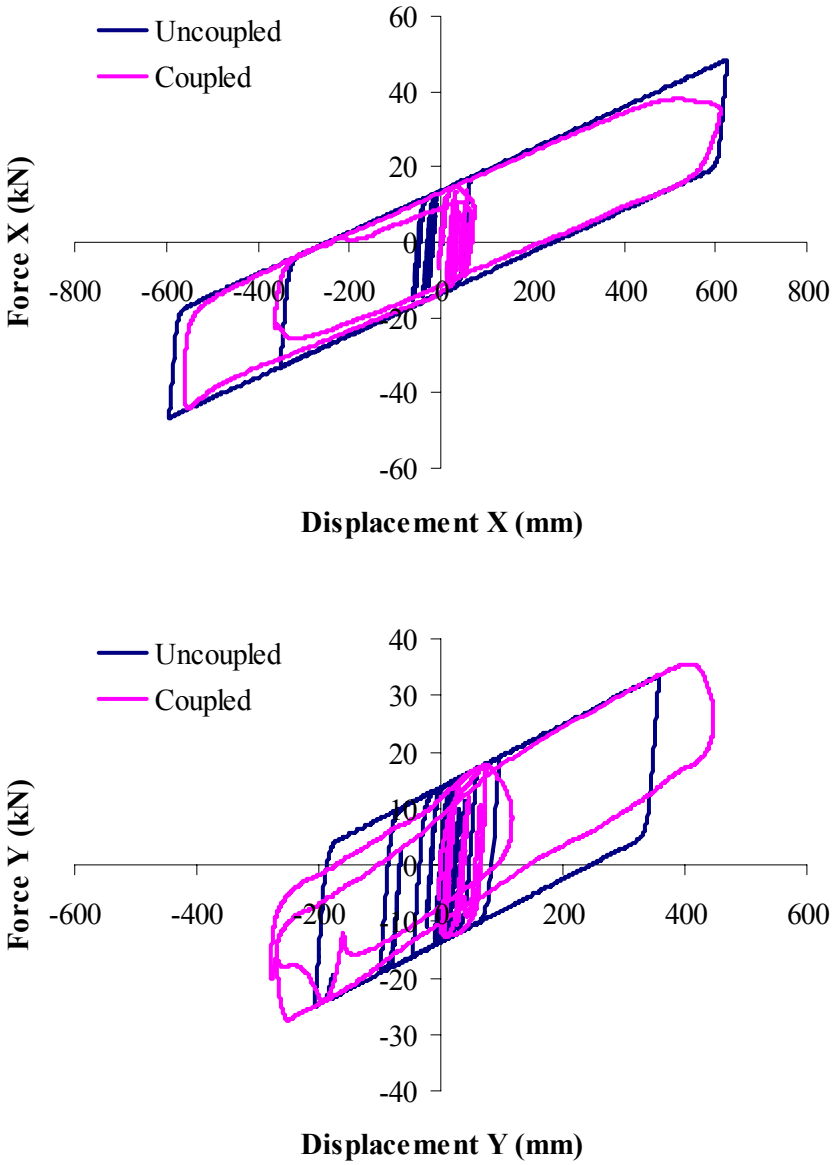

Figure 7.12 Comparison of coupled and uncoupled behavior of 3S isolated RC building.

CHAPTER 8

CONCLUSIONS AND RECOMMENDATIONS

8.1 SUMMARY

In this dissertation, nonlinear response history analyses (RHA) of isolated reinforced concrete (RC) buildings are investigated under bi-directional earthquake excitations. All of the ground motions are selected so that they contain a distinct pulse-type behavior, which is the characteristic of near-fiel records, in their velocity traces. Hence, two sets of near-field ground motion records are used, and each set have eleven records. These two sets of ground motions are classified according to site classes they were recorded (stiff and soft soil). Selected near-field ground motions are used to investigate the difference in responses of both isolation system and superstructure when ground motions are applied bi-directionally rather than uni-directionally. Nonlinear RHA are conducted by structural analysis program SAP2000 where the isolation system is modeled by non-linear link elements and the superstructure is modeled as elastic.

The questions answered in this dissertation regarding bi-directional excitations for the design of isolation systems are:

- Is it suitable to use the simplified method of analyses to determine maximum isolator displacements under near-field conditions?
- Does the soil condition have an effect on the accuracy of predictions of the simplified method of analysis?

- What is the contribution of horizontal orthogonal components of ground motions to the response of both isolation system and superstructure?
- Does the contribution of horizontal orthogonal components depend on the ground motion characteristics?
- How does the response of superstructures change due to variations in the isolation systems?

To answer the above questions, a parametric study has been conducted for bilinear isolation systems. The parametric study is rigorous with the selection criteria and scaling of the ground motions and design of both isolation systems and superstructures. As being representative of realistic isolation systems, the period range of isolation period T is selected so that the base shear of the superstructure is not more than a specific value, i.e. 30% of the weight of the superstructure in MCE. This criterion ensures that the isolation period T are in the ranges of $3\text{sec} \leq T \leq 4\text{sec}$ and $3.5\text{sec} \leq T \leq 4.5\text{sec}$ for stiff and soft soil conditions, respectively. Similarly, designs of superstructures are done to be representative of the real RC structures in Turkey and based on a statistical research that presents the average plan area, column orientation through the plan, number of bays in both long and short directions of the plan, and story heights for numerous RC buildings.

Final part of the dissertation is devoted to the implementation of a material model in OpenSees where the coupled behavior of isolators under bi-directional excitations can be captured. The accuracy of the implemented model is also verified by comparing the results with that of SAP2000, accordingly. Finally, significance of coupled behavior is examined throughly by comparing the maximum isolator displacements obtained from both coupled and uncoupled analyses results.

8.2 CONCLUSIONS

Conclusions presented here are based on the proposed new scaling procedure developed for nonlinear RHA of isolated structures. The scaling procedure followed

is rational and systematic and, moreover, results in predictions that are consistent with the equivalent lateral force (ELF) procedure.

Assessing results of the parametric study described in this dissertation, the following conclusions can be revealed:

- The most significant contribution of this study is the description of a proper methodology for scaling of the ground motion records, that is compatible with the design spectra, to be used for dynamic analysis of isolated structures. The power of the proposed scaling procedure is that it can also preserve the effect of the orthogonal "weak" component, which is especially crucial in near-field records. Employing the proposed scaling procedure, the simplified method of analysis is shown to be accurate enough to predict the maximum isolator displacements even under bi-directional excitations of near-field records. This is important because the use of simplified methodology in calculation of maximum isolator displacements in near-field conditions (d<10 km) is restricted by the codes. For reliable nonlinear RHA, it is believed that the proposed scaling procedure should be used, especially for near-field regions where the fault-parallel component may also be as strong as the fault-normal component.

- Accuracy of the simplified method of analysis depends on the soil characteristics of the ground motions. For stiff soil records, the simplified method slightly underestimates the maximum isolator displacements obtained by RHA analysis. The amount of underestimation is not more than 5%. For soft soil records, ELF procedure overestimates the displacement demands by 10 %.

- The effect of orthogonal horizontal components on maximum isolator displacements depends highly on the soil characteristics of the records. Variation in D_{bi}/D_{uni} ratios may be up to 17%. D_{bi}/D_{uni} ratios are in the range of 10% - 17% for stiff soil conditions whereas it is in between 5%

- 10% for soft soil conditions. It is clear that increasing the maximum isolator displacements by 5%, which is suggested by Jangid and Kelly (2001), is not enough to incorporate the effect of orthogonal horizontal component in near-field conditions.

- There is no need to use 100%+30% rule for ground motions with soft soil characteristics. Only 100% estimation is observed to be enough for soft soil cases. On the other hand, 100%+30% rule is obtained to be necessary for stiff soil cases.

- The effectiveness of increasing damping to reduce the maximum isolator displacements at different isolation periods is different for each soil class. The rate of reduction in isolator displacements due to increase in effective damping for soft soil conditions are identical for all of the considered isolation periods. On the other hand, efficiency of increasing effective damping in stiff soil conditions increases with increasing isolation period.

- Simplified method of analysis also gives reasonable predictions for base shears of the isolated structures. For both of the soil conditions, calculated base shears are very close to obtained base shears from nonlinear RHA. Predictions of simplified method for base shears are observed to be not sensitive to changes in both considered isolation periods and effective damping values.

- Regardless of the soil characteristics, V_{bi}/V_{uni} ratios are less than 1.0 and decrease with increasing effective damping values for all isolation periods. This indicates that shear forces obtained from uni-directional analyses can be used for design purposes. Similar to D_{bi}/D_{uni} ratios, V_{bi}/V_{uni} ratios obtained under stiff soil conditions are higher than that of soft soil conditions as an indicative of the higher contribution of orthogonal component.

- Based on the characteristics of the selected superstructures (3- and 7-story RC structures), variation in superstructure has almost no effect on both maximum isolator displacements and maximum base shears. Results obtained from nonlinear RHA are almost identical.

- Variation in superstructure is obtained to be an important parameter when floor accelerations are of concern. At higher damping ratios, increasing isolation period does not yield to decrease in maximum floor accelerations in 7-story isolated building. In contrast, the distribution of floor accelerations through the height becomes identical. However, in 3-story isolated building, increasing isolation period decreases floor accelerations.

- Contribution of horizontal component of records may not be considered when floor accelerations are of concern under soft soil conditions where Acc_{bi}/Acc_{uni} ratios are less than 1.0. However, Acc_{bi}/Acc_{uni} ratios are greater than 1.0 for stiff soil condition indicating that uni-directional analyses are not enough for detemination of floor accelerations.

- Comparisons of asymmetric results with that of the symmetric ones (based on D_{RHA}^{ECC}/D_{RHA} ratios) revealed that degree of amplification is almost independent of both isolation period and soil condition. On the other hand, effect of damping ratio is different depending on the variation of superstructure. The variations in D_{RHA}^{ECC}/D_{RHA} ratios are observed to be a function of effective damping ratio at the isolation level for 3-story isolated RC building and may be up to 25% in average. However, it is not sensitive to variation in effective damping ratio for 7-story isolated RC building and equals to 15% regardless of the damping ratio.

- It is also found that the code requirements for simplified method of analysis to incorporate the effect of eccentricity in superstructure are accurate enough to estimate the maximum isolator displacements.

Moreover, variation in superstructure has almost no effect on the accuracy of estimations.

- The developed and implemented biaxial interaction of hysteretic force-deformation relation of isolators in OpenSees is verified by comparison with the results obtained from SAP2000. Force-deformation relations in both of the orthogonal horizontal directions obtained from OpenSees and SAP2000 are identical. Superiority of OpenSees is that results can be obtained almost 50 times faster than SAP2000 and leads to a great amount of time saving.

8.3 RECOMMENDATIONS FOR FUTURE STUDIES

In the light of the studies conducted in this dissertation, the following recommendations can be made for further research on the subject.

- Asymmetry in the superstructure should be studied in detail by considering different plan dimensions to sustain various aspect ratios which are defined as the ratios of long dimension to the short one in the plan. The research area should also be widened by considering different amounts of eccentricity in the superstructure.
- All of the previous studies including this one considered a non-deteriorating force-deformation relation for LRB. However, two pioneer papers (Kalpakidis and Constantinou, 2009a, b) present that yield force of the lead in a LRB changes gradually with deformation due to heating in the lead core. Maximum isolator displacement in an isolation system should be investigated by employing the temperature dependent force-deformation relation. Hence, future efforts should be directed to developing a material model that can model the temperature dependent behavior of LRBs under cyclic motions.
- Knowing that temperature increase in the lead core of an LRB is a function of deformation, the relation between uni- and bi-directional

responses regarding isolator displacements should be studied. Since, the temperature increase in the lead core for bi-directional excitations may be higher than uni-directional one.

- Accuracy of simplified method of analysis should be questioned when temperature dependent hysteretic behavior of LRB is of concern. Since, simplified method is based on a constant force-deformation relation which will not be adequate for temperature dependent behavior, it may need to be modified accordingly.
- Vertical component of ground motion records should be taken into consideration to assess the effect of uplift force on the response of superstructure. Vertical components may be critical especially for near-field records.

REFERENCES

AASHTO, 1999, American Association of State Highway and Transportation Officials. Guide Specification for Seismic Isolation Design, Washington, DC.

Abrahamson N.A., 2000, "Effects of Rupture Directivity on Probabilistic Seismic Hazard Analysis", Proceedings of the Sixth International Conference on Seismic Zonation, EERI, Palm Springs, CA, pp. 151-156.

Akkar S. and Gulkan P., 2002, "A Critical Examination of Near-Field Accelerograms from the Sea of Marmara Region Earthquakes", Bulletin of the Seismological Society of America, 92(1), pp. 428-447.

Akkar S., Yazgan U. and Gulkan P., 2005, "Drift Estimates in Frame Buildings subjected to near-Fault Ground Motions", Journal of Structural Engineering, ASCE, 131(7), pp. 1014-1024.

Alavi B. and Krawinkler H., 2004, "Behavior of Moment-Resisting Frame Structures Subjected to Near-Fault Ground Motions", Earthquake Engineering and Structural Dynamics, 33, pp. 687-706.

Alhan C. and Gavin H., 2004, "A Parametric Study of Linear and Non-linear Passively Damped Seismic Isolation Systems for Buildings", Engineering Structures, 26, pp. 485-497.

Almazan J.L. and De la Llera J.C., 2000, "Lateral Torsional Coupling in Structures Isolated with the Frictional Pendulum System", Proceedings 12 WCEE, Auckland, New Zealand, paper 1536.

Applied Technology Council, 2005, "Improvement of Nonlinear Static Seismic Analysis Procedures", Report Federal Emergency Management Agency-FEMA 440, Washington, DC.

ASCE, 2005, American Society of Civil Engineers. Minimum Design Loads for Buildings and Other Structures. Standard ASCE/SEI 7-05, Reston, VA.

Asher J.W., Hoskere S.N., Ewing R.D., Mayes R.L., Button M.R. and Van Volkinburg D.R., 1997, "Performance of Seismically Isolated Structures in the 1994 Northridge and 1995 Kobe Earthquakes", Proceedings, Structures Congress XV. Vol. 2, American Society of Civil Engineers, New York.

Baker J.W. and Cornell C.A., 2005, "A Vector-Valued Ground Motion Intensity Measure Consisting of Spectral Acceleration and Epsilon", Earthquake Engineering and Structural Dynamics, 34(10), pp. 1193-1217.

Bazzurro P. and Cornell C.A., 1994a, “Seismic Hazard Analysis of Nonlinear Structures. I:Methodology”, Journal of Structural Engineering, ASCE, 120(11), pp. 3320-3344.

Bazzurro P. and Cornell C.A., 1994b, “Seismic Hazard Analysis of Nonlinear Structures. II:Applications” , Journal of Structural Engineering, ASCE, 120(11), pp. 3345-3365.

Beresnev I.A. and Atkinson G.M., 1998, “FINSIM – A FORTRAN Program for Simulating Stochastic Acceleration Time Histories from Finite Faults”, Seismological Research Letters, 69(1), pp. 27-32.

Bian Y., 2002, “Adding Anisotropic Elastic Material Model into OpenSees”, Available at http://sokocalo.engr.ucdavis.edu/~jeremic/CG/TermProjects/2002/YiBianTermReport.pdf, 13/03/2010.

Bommer J.J. and Acevedo A.B., 2004, “The Use of Real Earthquake Accelerograms as Input to Dynamic Analysis”, Journal of Earthquake Engineering, Volume 8, Special Issue 1, pp. 43-92.

Bommer J.J., Douglas J. and Strasser F.O., 2003, “Style-of-Faulting in Ground-Motion Prediction Equations”, Bulletin of Earthquake Engineering, 1(2), pp.171-203.

Bommer J.J., Scott S.G. and Sarma S.K., 1990, “Hazard-Consistent Earthquake Scenarios”, Soil Dynamics and Earthquake Engineering, 19, pp. 219-231.

Bondonet G. and Filiatrault A., 1997, “Frictional Response of PTFE Sliding Bearings at High Frequencies”, Journal of Bridge Engineering (ASCE), 2, pp. 139-148.

Boore D.M, 2004, “Can Site Response be Predicted”, Journal of Earthquake Engineering, Volume 8, Special Issue 1, pp. 1-41.

Boore D.M. and Zoback M.D., 1974, “Two-Dimensional Kinematic Fault Modeling of the Pacoima Dam Strong-Motion Recordings of the February 9, 1971, San Fernando Earthquake”, Bulletin of the Seismological Society of America, 64(3), pp. 555-570.

Boore D.M., 2003, “Simulation of Ground Motion Using the Stochastic Method”, Pure and Applied Geophysics, 160, pp. 635-676.

Buckle I.G. and Mayes R.L., 1990, “Seismic Isolation: History, Application and Performance – a World Review”, Earthquake Spectra, 6, pp. 161-202.

Building Seismic Safety Council (BSSC), 2003, “NEHRP Recommended Provisions for Seismic Regulations for New Buildings and Other Structures”, 2003 Edition, Report Nos. FEMA 450, Federal Emergency Management Agency, Washington, DC.

Butcher J.C., 1987, “The numerical analysis of ordinary differential equations: Runge-Kutta and general linear methods”, ISBN 0-471-91046-5 Wiley-Interscience New York, NY, USA.

Carballo J.E., 2000, “Probabilistic Seismic Demand Analysis: Spectrum Matching and Design”, Department of Civil and Environmental Engineering, Stanford University, 259p. http://www.stanford.edu/group/rms/, 13/03/2010.

Chopra A.K. and Goel R.K., 1999, “Evaluation of NSP to Estimate Seismic Deformation: SDF Systems”, Journal of Structural Engineering, ASCE, 126(4), pp. 482–490.

Chung W.J., Yun C.B., Kim N.S. and Seo J.W., 1999, “Shaking Table and Pseudodynamic Tests for the Evaluation of the Seismic Performance of Base-Isolated Structures”, Engineering Structures, 21, pp 365-379.

Computers and Structures, Inc., 2008. SAP 2000 Nonlinear, Version 12.0.0, Structural Analysis Program, Berkeley, CA.

Constantinou M.C. and Adnane M.A., 1987, “Dynamics of Soil-Base-Isolated Structure Systems: Evaluation of Two Models for Yielding Systems”, Report to NSF, Department of Civil Engineering, Drexel University, Philadelphia.

Constantinou M.C., 2009, Lecture notes of Aseismic Base Isolation at State University of New York at Buffalo.

Constantinou M.C., 2009, Private Communication.

Constantinou M.C., Tsopelas P., Kasalanati A. and Wolf E.D., 1999, “Property Modification Factors for Seismic Isolation”, Report No. MCEER-99-0012, Multidisciplinary Center for Earthquake Engineering Research, State University of New York at Buffalo.

Constantinou M.C., Whittaker A.S., Fenz D.M. and Apostolakis G., 2007, “Seismic Isolation of Bridges”, Department of Civil, Structural and Environmental Engineering, State University of New York at Buffalo.

Cuesta I., Aschheim M.A. and Fajfar P., 2003, “Simplified R-Factor Relationships for Strong Ground Motions”, Earthquake Spectra, 19(1), pp. 25-45.

Dicleli M. and Buddaram S., 2006, “Effect of Isolator and Ground Motion Characteristics on the Performance of Seismic-Isolated Bridges”, Earthquake Engineering and Structural Dynamics, 35, pp. 233-250.

Dicleli M. and Buddaram S., 2007, “Equivalent Linear Analysis of Seismic-Isolated Bridges Subjected to Near-Fault Ground Motions with Forward Rupture Directivity Effect”, Engineering Structures, 29, pp. 21-32.

Douglas J., 2003, “Earthquake Ground Motion Estimation Using Strong Motion Records: A Review of Equations for the Estimation of Peak Ground Acceleration and Response Spectral Ordinates”, Earth Science Reviews, 61, pp. 43-104.

Eisenberger M. and Rutenberg A., 1986, “Seismic Base Isolation of Asymmetric Shear Buildings”, Engineering Structures, 8 (1), pp. 2-9.

EN 8, 2005, Eurocode 8: Design of Structures for Earthquake Resistance Part 2: Bridges. EN 1998-2.

Fadi F. and Constantinou M.C., 2009, "Evaluation of Simplified Methods of Analysis for Structures with Triple Friction Pendulum Isolators", Earthqauke Engineering and Structural Dynamics, published online in Wiley InterScience (www.interscience.wiley.com).DOI: 10.1002/eqe.930.

Fenves G.L., 2005, "Brief Notes on Object-Oriented Software Design and Programming with C++", Available at http://opensees.berkeley.edu/workshop/OpenSeesDays2005_presentations/BB1 OOPNotes1 GLF.pdf, 13/03/2010.

Franchin P., Monti G. and Pinto P.E., 2001, "On the Accuracy of Simplified Methods for the Analysis of Isolated Bridges", Earthquake Engineering and Structural Dynamics, 30, pp. 363-382.

Guyader A.C. and Iwan W.D., 2006, "Determining Equivalent Linear Parameters for Use in a Capacity Spectrum Method of Analysis", Journal of Structural Engineering, ASCE, 132(1), pp. 59–67.

Hall J.F., Heaton T.H., Halling M.W. and Wald D.J., 1995, "Near-Source Ground Motion and its Effects on Flexible Buildings", Earthquake Spectra, 11, pp. 569-605.

Hancock J., Bommer J.J. and Stafford P.J., 2008, "Numbers of Scaled and Matched Accelerograms Required for Inelastic Dynamic Analyses", Earthquake Engineering and Structural Dynamics, 37, pp. 1585-1607.

Haselton C.B. and Baker J.W., 2006, "Ground Motion Intensity Measures for Collapse Capacity Prediction: Choice of Optimal Spectral Period and Effect of Spectral Shape", Proceedings of the Eighth US National Conference on Earthquake Engineering, San Francisco, California.

Heaton T.H., Hall J.F., Wald D.J. and Halling M.W., 1995, "Response of High-Rise and Base-Isolated Buildings to a Hypothetical Mw 7.0 Blind Trust Earthquake", Science, 267, pp. 206-211.

Housner G.W. and Trifunac M.D., 1967, "Analysis of Accelerograms: Parkfield Earthquake", Bulletin of the Seismological Society of America, 57(6), pp. 1193-1220.

Huang Y.-N., 2008, "Performance Assessment of Conventional and Base-Isolated Nuclear Power Plants for Earthquake and Blast Loadings", PhD Thesis, Department of Civil, Structural and Environmental Engineering, State University of New York at Buffalo.

Huang Y.-N., Whittaker A.S. and Constantinou M.C., 2006, "Seismic Demands on Secondary Systems in Conventional and Isolated Nuclear Power Plants", Proceedings, Eighth US National Conference on Earthquake Engineering, Earthquake Engineering Research Institute, San Francisco, California.

Huang Y.-N., Whittaker A.S. and Constantinou M.C., 2007, "Seismic Demands on Secondary Systems in Base-Isolated Nuclear Power Plants", Earthquake Engineering and Structural Dynamics, 36, pp. 1741-1761.

Hwang J.S., 1996, "Evaluation of Equivalent Linear Analysis Methods of Bridge Isolation", Journal of Structural Engineering (ASCE), 122(8), pp. 972-976.

Hwang J.S., Chang K.C. and Tsai M.H., 1997, "Composite Damping Ratio of Seismically Isolated Regular Bridges", Engineering Structures, 19(1), pp. 52-62.

Iervolino I. and Cornell C.A., 2005, "Record Selection for Nonlinear Seismic Analysis of Structures", Earthquake Spectra, 21(3), pp. 685-713.

Iwan W.D. and Gates N.C., 1979, "Estimating Earthquake Response of Simple Hysteretic Structures", Journal of the Engineering Mechanics Division, 105(EM3), pp. 391–405.

Iwan W.D., Huang C.-T. and Guyader A.C., 2000, "Important Features of the Response of Inelastic Structures to Near-Field Ground Motion", 12th World Conference on Earthquake Engineering, Auckland, New Zealand, Paper No. 1740.

Jalayer F., 2003, "Direct Probabilistic Seismic Analysis: Implementing Non-Linear Dynamic Assessments", PhD Thesis, Department of Civil and Environmental Engineering, Stanford University. http://www.stanford.edu/group/rms/, 13/03/2010.

Jangid R.S. and Datta T.K., 1994a, "Nonlinear Response of Torsionally Coupled Base Isolated Structure", Journal of Structural Engineering, ASCE, 120 (1), pp. 1-22.

Jangid R.S. and Datta T.K., 1994b, "Seismic Response of Torsionally Coupled Structures with Elastoplastic Base Isolation", Engineering Structures, 16 (4), pp. 256-262.

Jangid R.S. and Datta T.K., 1995, "Seismic Behavior of Base-Isolated Buildings: A State-of-the-Art Review", Structures and Buildings, 110, pp. 186-202.

Jangid R.S. and Kelly J.M., 2001, "Base Isolation for Near-Fault Motions", Earthquake Engineering and Structural Dynamics, 30, pp. 691-707.

Kalpakidis I.V., 2008, "Effects of Heating and Load History on the Behavior of Lead-Rubber Bearings", PhD Thesis, Department of Civil, Structural and Environmental Engineering, State University of New York at Buffalo.

Kalpakidis I.V. and Constantinou M.C., 2009a, "Effects of Heating on the Behavior of Lead-Rubber Bearing. I:Theory", Journal of Structural Engineering (ASCE), 135(12), pp. 1440-1449.

Kalpakidis I.V. and Constantinou M.C., 2009b, "Effects of Heating on the Behavior of Lead-Rubber Bearing. II:Verification of Theory", Journal of Structural Engineering (ASCE), 135(12), pp. 1450-1461.

Kani N., Takayama M. and Wada A., 2006, "Performance of Seismically Isolated Buildings in Japan", Proceedings, 8th National Conference on Earthquake Engineering, Paper 2181, San Francisco, CA.

Kelly J.M., 1986, "Aseismic Base Isolation: A Review and Bibliography", Soil Dynamics and Earthquake Engineering, 5, pp. 202-216.

Kircher C.A. and Lashkari B., 1989, "Statistical Evaluation of Nonlinear Response of Seismic Isolation Systems", Technical Report No. JBA 109-070. Jack R. Benjamin and Associates, Inc., Mountain View, CA.

Krinitzsky E.L. and Chang F.K., 1977, "Specifying Peak Motions for Design Earthquakes", State-of-the-Art for Assessing Earthquake Hazards in the United States, Report 7, Miscellaneous Paper S-73-1. US Army Corps of Engineers, Vicksburg, Mississippi.

Kunde M.C. and Jangid R.S., 2003, "Seismic Behavior of Isolated Bridges: A State-of-the-Art Review", Electronic Journal of Structural Engineering, 3, pp. 140-170.

Lee D.M., 1980, "Base Isolation for Torsion Reduction in Asymmetric Structures under Earthquake Loading", Earthquake Engineering and Structural Dynamics, 8, pp. 349-359.

Lin Y.-Y. and Chang K.-C., 2004, "Effects of Site Classes on Damping Reduction Factors", Journal of Structural Engineering, ASCE, 130(11), pp. 1667-1675.

Lin Y.-Y. and Miranda E., 2009, "Evaluation of Equivalent Linear Methods for Estimating Target Displacements of Existing Structures", Engineering Structures, doi:10,1016/j.engstruct,2009,08,009.

Lin Y.-Y., 2007, "Statistical Study on Damping Modification Factors Adopted in Taiwan's Seismic Isolation Design Code by Using the 21 September 1999 Chi-Chi Earthquake, Taiwan", Engineering Structures, 29, pp. 682-693.

Luco N., 2002, "Probabilistic Seismic Demand Analysis, SMRF Connection Fractures and Near-Source Effect", PhD Thesis, Department of Civil and Environmental Engineering, Stanford University. http://www.stanford.edu/group/rms/, 13/03/2010.

Makris N, 1997, "Rigidity-Plasticity-Viscosity: can Electrorheological Dampers Protect Base-Isolated Structures from Near-Source Ground Motion?", Earthquake Engineering and Structural Dynamics, 26, pp. 571-591.

Makris N. and Chang S.P., 2000, "Effect of Viscous, Viscoplastic, and Friction Damping on the Response of Seismic Isolated Structures", Earthquake Engineering and Structural Dynamics, 29, pp. 85-107.

Malhotra P.K., 2003, "Strong-Motion Records for Site-Specific Analysis", Earthquake Spectra, 19(3), pp. 557-578.

Matsagar V.A. and Jangid R.S., 2004, "Influence of Isolator Characteristics on the Response of Base-Isolated Structures", Engineering Structures, 26, pp. 1735-1749.

Mavroeidis G.P., 2004, "Modeling and Simulation of Near-Fault Strong Ground Motions for Earthquake Engineering Applications", PhD Thesis, Department of Civil, Structural and Environmental Engineering, State University of New York at Buffalo.

Mazzoni S., McKenna F., Scott M.H. and Fenves G.L., 2009, "OpenSees Command Language Manuel", Available at http://opensees.berkeley.edu/OpenSees/manuals/usermanual/index.html, 13/03/2010.

McKenna, Frank, 2009, "OpenSees Dynamic API", Available at http://opensees.berkeley.edu/OpenSees/OpenSeesDynamicAPI.pdf.

Medina R.A., 2002, "Seismic Demands for Nondeteriorating Frame Structures and Their Dependence on Ground Motion", PhD Thesis, Department of Civil and Environmental Engineering, Stanford University.

Menun C. and Der Kiureghian A., 1998, "A Replacement for the 30%, 40% and SRSS Rules for Multicomponent Seismic Analysis", Earthquake Spectra, 14 (1), pp. 153–156.

Metin A., 2006, "Inelastic Deformation Demands on Moment-Resisting Frame Structures", PhD Thesis, Department of Civil Engineering, Middle East Technical University.

Mokha A., Constantinou M.C. and Reinhorn A.M., 1990, "Teflon Bearings in Base Isolation I: Testing", Journal of Structural Engineering (ASCE), 116, pp. 438-454.

Mokha A.S., Constantinou M.C. and Reinhorn A.M., 1993, "Verification of Friction Model of Teflon Bearings under Triaxial Load", Journal of Structural Engineering, ASCE, 119(1), pp. 240-261.

Mosqueda G., Whittaker A.S. and Fenves G.L., 2004, "Characterization and Modeling of Friction Pendulum Bearings Subjected to Multiple Components of Excitation", Journal of Structural Engineering, ASCE, 130(3), pp. 433-442.

Naeim F. and Kelly J.M., 1999, "Design of Seismic Isolated Structures", Wiley: New York.

Naeim F. and Lew M., 1995, "On the use of Design Spectrum Compatible Time Histories", Earthquake Spectra, 11(1), pp. 111-127.

Nagarajaiah S. and Sun X., 2000, "Response of Base Isolated USC Hospital Building in Northridge Earthquake", Journal of Structural Engineering (ASCE), 126, pp. 1177-1186.

Nagarajaiah S., Reinhorn A.M. and Constantinou M.C., 1989, "Nonlinear Dynamic Analysis of Three-Dimensional Base Isolated Structures (3D-BASIS)", Technical Report NCEER-89-0019, National Center for Earthquake Engineering Research, State University of New York at Buffalo, Red Jacket Quadrangle, Buffalo, NY 14261.

Nagarajaiah S., Reinhorn A.M. and Constantinou M.C., 1993a, "Torsion in Base Isolated Structures with Elastomeric Isolation Systems", Journal of Structural Engineering, ASCE, 119 (10), pp. 2932-2951.

Nagarajaiah S., Reinhorn A.M. and Constantinou M.C., 1993b, "Torsional Coupling in Sliding Base-Isolated Structures", Journal of Structural Engineering, ASCE, 119 (1), pp. 130-149.

Ozdemir G. and Constantinou M.C., 2010, "Evaluation of Equivalent Lateral Force Procedure in Estimating Seismic Isolator Displacements", Soil Dynamics and Earthquake Engineering, doi:10.1016/j.soildyn.2010.04.015.

Park Y.J., Wen Y.K. and Ang A.H., 1986, "Random Vibration of Hysteretic Systems under Bi-Directional Ground Motions", Earthquake Engineering and Structural Dynamics, 14, pp. 543-557.

Pavlou E.A. and Constantinou M.C., 2004, "Response of Elastic and Inelastic Structures with Damping Systems to Near-Field and Soft-Soil Ground Motions", Engineering Structures, 26(9), pp. 1217–1230.

Providakis C.P., 2008, "Pushover Analysis of Base-Isolated Steel Concrete Composite Structures Under Near-Fault Excitations", Soil Dynamics and Earthquake Engineering, 28, pp. 293-304.

Ramirez O.M., Constantinou M.C., Whittaker A.S., Kircher C.A. and Chrysostomou C.Z., 2002, "Evaluation of Simplified Methods of Analysis of Yielding Structures with Damping Systems", Earthquake Spectra, 18(3), pp. 531–547.

Reiter L., 1990, "Earthquake Hazard Analysis: Issues and Insights", Colombia University Press.

Rosenblueth E. and Contreras H., 1977, "Approximate Design for Multicomponent Earthquakes", Journal of Engineering Mechanics, 103, pp. 895–911.

Roussis P.C., Constantinou M.C., Erdik M., Durukal E. and Dicleli M., 2003, "Assessment of Performance of Seismic Isolation System of Bolu Viaduct", Journal of Bridge Engineering (ASCE), 8, pp. 182-190.

Ryan K.L. and Chopra A.K., 2004, "Estimation of Seismic Demands on Isolators Based on Nonlinear Analysis", Journal of Structural Engineering, ASCE, 130(3), pp. 392-402.

Sato M., Nishi H., Kawashima K. and Unjoh S., 1994, "Response of On-Netoh Bridge during Kushiro-Oki Earthquake of January 1993", Proceedings, 3rd U.S.-Japan Workshop on Earthquake Protective Systems for Bridges", Report NCEER-94-0009, National Center for Earthquake Engineering Research, Buffalo, NY.

SeismoSoft, 2009, "SeismoSignal v.3.3.0", www.seismosoft.com, 13/03/2010.

Shakal A., Huang M., Darragh R., Cao T., Sherburne R., Malhotra P., Cramer C., Sydnor R., Graizer V., Maldonado G., Peterson C. and Wampole J., 1994, "CSMIP Strong Motion Records from the Northridge, California, Earthquake of 17 January 1994", Report OSMS 94-07, Calif. Div. Mines Geol., Sacremento, California.

Shome N., 1999, “Probabilistic Seismic Demand Analysis of Nonlinear Structures”, Department of Civil and Environmental Engineering, Stanford University, 320p. http://www.stanford.edu/group/rms/, 13/03/2010.

Shome N., Cornell C.A., Bazzurro P. and Carballo J.E., 1998, “Earthquakes, Records and Nonlinear Responses”, Earthquake Spectra, 14(3), pp. 469-500.

Skinner R.I., Robinson W.H. and McVerry G.H., 1993, “An Introduction to Seismic Isolation”, Wiley: New York.

Somerville P.G., Smith N.F., Graves R.W. and Abrahamson N.A., 1997, “Modification of Empirical Strong Ground Motion Attenuation Relations to Include the Amplitude and Duration Effects of Rupture Directivity”, Seismological Research Letters, 68(1), pp. 199-222.

Stewart J.P., Chiou S.-J., Bray J.D., Graves R.W., Somerville P.G. and Abrahamson N.A., 2001, “Ground Motion Evaluation Procedures for Performance-Based Design”, PEER Report 2001/09, Pacific Earthquake Engineering Research Center, University of California, Berkeley.

Stewart J.P., Conte J.P. and Aiken I.D., 1999, “Observed Behavior of Seismically Isolated Buildings”, Journal of Structural Engineering (ASCE), 125, pp. 955-964.

Tena-Colunga A. and Escamilla-Cruz J.L., 2007, “Torsional Amplifications in Asymmetric Base-Isolated Structures”, Engineering Structures, 29, pp. 237-247.

Tena-Colunga A. and Gomez-Soberon L.A., 2002, “Torsional Response of Base-Isolated Structures due to Asymmetries in the Superstructure”, Engineering Structures, 24 (12), pp. 1587-1599.

Tena-Colunga A., Gomez-Soberon C. and Munoz-Loustaunau A., 1997, “Seismic Isolation of Buildings Subjected to Typical Subduction Earthquake Motions for the Mexican Pacific Coast”, Earthquake Spectra, 13 (3), pp. 505-532.

Tena-Colunga A. and Osornia M.A.P., 2006, “Design Displacements for Base Isolators Considering Bidirectional Seismic Effects”, Earthquake Spectra, 22(3), pp. 803-825.

Theodossiou D. and Constantinou M.C., 1991, “Evaluation of SEAOC Design Requirements for Sliding Isolated Structures”, Technical Report NCEER 91-0015, National Center for Earthquake Engineering Research, University at Buffalo, State University of New York, Buffalo, NY, 1991.

Tsopelas P., Constantinou M.C., Kircher C.A. and Whittaker A.S., 1997, “Evaluation of Simplified Methods of Analysis for Yielding Structures”, Technical Report NCEER 97-0012, National Center for Earthquake Engineering Research, University at Buffalo, State University of New York, Buffalo, NY.

Turkish Earthquake Code, 2007, “Specifications for the Buildings to be Constructed in Disaster Areas”, Ministry of Public Works and Settlement, Ankara, Turkey.

Vanmarcke E.H., 1979, “Representation of Earthquake Ground Motion: Scaled Accelerograms and Equivalent Response Spectra”, State-of-the-Art for Assessing Earthquake Hazards in the United States, Report 14, Miscellaneous Paper S-73-1. US Army Corps of Engineers, Vicksburg, Mississippi.

Wald D., 1997, “Surfing the Internet for Strong-Motion Data”, Seismological Research Letters, 68(5), pp. 766-769.

Warn G.P. and Whittaker A.S., 2004, “Performance Estimates in Seismically Isolated Bridge Structures”, Engineering Structures, 26, pp 1261-1278.

Winters C.W. and Constantinou M.C., 1993, “Evaluation of Static and Response Spectrum Analysis Procedures of SEAOC/UBC for Seismic Isolated Structures”, Technical Report NCEER 93-0004, National Center for Earthquake Engineering Research, University at Buffalo, State University of New York, Buffalo, NY.

Yakut A., 2008, “Capacity Related Properties of RC Frame Buildings in Turkey”, Journal of Earthquake Engineering, 12, pp. 265-272.

Zayas V.A., Low S.S. and Mahin S.A., 1990, “A Simple Pendulum Technique for Achieving Seismic Isolation”, Earthquake Spectra, 6, pp. 317-334.

Zeng Y., Anderson J.G. and Yu G., 1994, “A Composite Source Model for Computing Realistic Synthetic Strong Ground Motions”, Geophysical Research Letters, 21(8), pp. 725-728.

APPENDIX A

SOURCE CODE FOR COUPLED MATERIAL MODEL

```
void logMeNicely(CoupledMaterial* nane,char *str,...)
{
      va_list args;
      va_start (args, str);
      double d=0;
      #ifdef LOG_ALOT
      #endif
      va_end (args);
}


void genericRungeKutta(void (*f)(double *X,double *V,double
*k,double D_y), double *X, double *V, double h,double
*Xprime,double D_y)
{

      double k1[2],k2[2],k3[2],k4[2];
      double Xp[2];
      double k[2];

      f(X,V,k,D_y);
      k1[0]=h*k[0];
      k1[1]=h*k[1];

      Xp[0]=X[0]+k1[0]/2;
      Xp[1]=X[1]+k1[1]/2;
      f(Xp,V,k,D_y);
      k2[0]=h*k[0];
      k2[1]=h*k[1];

      Xp[0]=X[0]+k2[0]/2;
      Xp[1]=X[1]+k2[1]/2;
      f(Xp,V,k,D_y);
      k3[0]=h*k[0];
      k3[1]=h*k[1];

      Xp[0]=X[0]+k3[0];
      Xp[1]=X[1]+k3[1];
      f(Xp,V,k,D_y);
      k4[0]=h*k[0];
      k4[1]=h*k[1];
```

```
      Xprime[0]=(k1[0]/6+k2[0]/3+k3[0]/3+k4[0]/6)/h;
      Xprime[1]=(k1[1]/6+k2[1]/3+k3[1]/3+k4[1]/6)/h;

}


double sign(double x)
{

      if (x>0)
            return 1;
      else if (x==0)
            return 0;
      else
            return -1;

}


void getZdot(double *Z,double *Udot, double *Zdot,double D_y)
{

      double A[2][2];
      double B[2][2];
      double prod[2];

      B[0][0]=Z[0]*Z[0]*(sign(Udot[0]*Z[0])+1);

      B[0][1]=Z[0]*Z[1]*(sign(Udot[1]*Z[1])+1);

      B[1][0]=Z[0]*Z[1]*(sign(Udot[0]*Z[0])+1);

      B[1][1]=Z[1]*Z[1]*(sign(Udot[1]*Z[1])+1);

      A[0][0]=1-0.5*B[0][0];
      A[0][1]=0-0.5*B[0][1];
      A[1][0]=0-0.5*B[1][0];
      A[1][1]=1-0.5*B[1][1];

      prod[0]=A[0][0]*Udot[0]+A[0][1]*Udot[1];
      prod[1]=A[1][0]*Udot[0]+A[1][1]*Udot[1];

      Zdot[0]=prod[0]/D_y*1000;
      Zdot[1]=prod[1]/D_y*1000;

}

CoupledMaterial * CoupledMaterial::hitPointers[100000];
int CoupledMaterial::hitCount=0;

CoupledMaterial::CoupledMaterial
(int tag, double FY, double E, double B,
 double A1, double A2, double A3, double A4, int pairMaterialTag):
   UniaxialMaterial(tag,MAT_TAG_CoupledMaterial)
{
```

```
	this->fy=FY
	this->E0=E
	this->b=B
	this->a1=A1
	this->a2=A2
	this->a3=A3
	this->a4=A4
	this->pairMaterialTag=pairMaterialTag
	this->pairMaterial=NULL;
	this->isMasterMaterial=false;

	CminStrain = 0.0;
	CmaxStrain = 0.0;
	CshiftP = 1.0;
	CshiftN = 1.0;
	Cloading = 0;

	TminStrain = 0.0;
	TmaxStrain = 0.0;
	TshiftP = 1.0;
	TshiftN = 1.0;
	Tloading = 0;

	Cstrain = 0.0;
	Cstress = 0.0;
	Ctangent = E0;

	Tstrain = 0.0;
	Tstress = 0.0;
	Ttangent = E0;

	parameterID = 0;
	SHVs = 0;

	z=0;
	hitPointers[hitCount]=this;
	hitCount++;

	this->bidirZ[0]=0;
	this->bidirZ[1]=0;
	this->lastStrain=0;
	this->lastStrainRate=0;
	this->lastStrainUpdateTime=0;

}


CoupledMaterial::CoupledMaterial
 ():UniaxialMaterial(0,MAT_TAG_CoupledMaterial)
{
	this->fy=FY
	this->E0=E
	this->b=B
	this->a1=A1
	this->a2=A2
	this->a3=A3
```

```
      this->a4=A4
      this->pairMaterialTag=-1
      this->pairMaterial=NULL;
      this->isMasterMaterial=false;
      hitPointers[hitCount]=this;
      hitCount++;

      parameterID = 0;
      SHVs = 0;

}


CoupledMaterial::~ CoupledMaterial ()
{

      if (SHVs != 0)
             delete SHVs;

}


int CoupledMaterial::setTrialStrain (double strain, double
strainRate)
{

      logMeNicely(this,"setTrialStrain strain=%+9.8lf
strainRate=%+9.8lf\n",strain,strainRate);
      for (int i=hitCount-1;i>=0;i--)
      {

            if (hitPointers[i]->getTag()==pairMaterialTag &&
hitPointers[i]->lastStrainUpdateTime>0)
            {

                  pairMaterial=hitPointers[i];
                  isMasterMaterial=true;
                  pairMaterial->pairMaterial=this;
                  pairMaterial->isMasterMaterial=false;

            }
      }

      if (ops_TheActiveDomain!=NULL)
            lastStrainUpdateTime=ops_TheActiveDomain-
>getCurrentTime();
      else
             lastStrainUpdateTime=0;


      TminStrain = CminStrain;
      TmaxStrain = CmaxStrain;
      TshiftP = CshiftP;
      TshiftN = CshiftN;
      Tloading = Cloading;
      Tstrain = Cstrain;
```

```
	Tstress = Cstress;
	Ttangent = Ctangent;

	double dStrain = strain - Cstrain;
	lastStrain=strain;
	lastStrainRate=(dStrain/(ops_Dt*1000));

	if (fabs(dStrain) > DBL_EPSILON) {

		Tstrain = strain;
		determineTrialState (dStrain);

	}

	return 0;

}


int CoupledMaterial::setTrial (double strain, double &stress,
double &tangent, double strainRate)
{
	logMeNicely(this,"setTrial strain=%+9.8lf stress=%+9.8lf
tangent=%+9.8lf strainRate=%+9.8lf\n",strain,stress,tangent,
strainRate);

	if (ops_TheActiveDomain!=NULL)
		lastStrainUpdateTime=ops_TheActiveDomain-
>getCurrentTime();
	else
		 lastStrainUpdateTime=0;

	TminStrain = CminStrain;
	TmaxStrain = CmaxStrain;
	TshiftP = CshiftP;
	TshiftN = CshiftN;
	Tloading = Cloading;
	Tstrain = Cstrain;
	Tstress = Cstress;
	Ttangent = Ctangent;

	double dStrain = strain - Cstrain;
	lastStrain=strain;
	lastStrainRate=(dStrain/(ops_Dt*1000));

	if (fabs(dStrain) > DBL_EPSILON) {

		Tstrain = strain;
		determineTrialState (dStrain);
	}
	stress = Tstress;
	tangent = Ttangent;

	return 0;

}
```

```
void CoupledMaterial::updateBidirectionalZ()
{

	logMeNicely(this,"updateBidirectionalZ()\n");
	double Zdot[2];
	double udot[2];

	if (isMasterMaterial)
	{
		udot[0]=pairMaterial->lastStrainRate;
		udot[1]=this->lastStrainRate;
	}

	else
	{
		udot[0]=this->lastStrainRate;
		udot[1]=pairMaterial->lastStrainRate;
	}

	double h=ops_Dt;
	genericRungeKutta(getZdot,this->bidirZ,udot,h,Zdot,D_y);
	this->bidirZ[0]+=Zdot[0]*h;
	this->bidirZ[1]+=Zdot[1]*h;

	logMeNicely(this,"bidirz=[%9.7lf,%9.7lf]\n",bidirZ[0],bidirZ[
1]);

}


double CoupledMaterial::getZ()
{

	logMeNicely(this,"getZ()\n");
	if (pairMaterial->lastStrainUpdateTime!=lastStrainUpdateTime)
	{
		logMeNicely(this,"Houston our problems span the
space\n");
	}

	if (isMasterMaterial)
		return bidirZ[1];
	else
		return pairMaterial->bidirZ[0];

}


void CoupledMaterial::determineTrialState (double dStrain)
{

	double fyOneMinusB = fy * (1.0 - b);

	double Esh = b*E0;

	double epsy = fy/E0;
```

```
        double c1 = Esh*Tstrain;

        double c2 = TshiftN*fyOneMinusB;

        double c3 = TshiftP*fyOneMinusB;

        double c = Cstress + E0*dStrain;

        double c1c3 = c1 + c3;


        if (c1c3 < c)
                Tstress = c1c3;
        else
                Tstress = c;


        double c1c2 = c1-c2;


        if (c1c2 > Tstress)
                Tstress = c1c2;


        if (fabs(Tstress-c) < DBL_EPSILON)
                Ttangent = E0;
        else
                Ttangent = Esh;


        if (Tloading == 0 && dStrain != 0.0)
        {
                if (dStrain > 0.0)
                        Tloading = 1;
                else
                        Tloading = -1;
        }

        if (Tloading == 1 && dStrain < 0.0)
        {
                Tloading = -1;
                if (Cstrain > TmaxStrain)
                        TmaxStrain = Cstrain;
                        TshiftN = 1 + a1*pow((TmaxStrain-
                        TminStrain)/(2.0*a2*epsy),0.8);
        }
        if (Tloading == -1 && dStrain > 0.0)
        {
                Tloading = 1;

                if (Cstrain < TminStrain)
                        TminStrain = Cstrain;
                        TshiftP = 1 + a3*pow((TmaxStrain-
                        TminStrain)/(2.0*a4*epsy),0.8);
        }
}
```

```
void CoupledMaterial::detectLoadReversal (double dStrain)
{

      if (Tloading == 0 && dStrain != 0.0)
      {
             if (dStrain > 0.0)
                    Tloading = 1;
             else
                    Tloading = -1;
      }

      double epsy = fy/E0;


      if (Tloading == 1 && dStrain < 0.0)
      {
             Tloading = -1;

             if (Cstrain > TmaxStrain)
                    TmaxStrain = Cstrain;
                      TshiftN = 1 + a1*pow((TmaxStrain-
                      TminStrain)/(2.0*a2*epsy),0.8);
      }


      if (Tloading == -1 && dStrain > 0.0)
      {
             Tloading = 1;

             if (Cstrain < TminStrain)
               TminStrain = Cstrain;
                      TshiftP = 1 + a3*pow((TmaxStrain-
                      TminStrain)/(2.0*a4*epsy),0.8);
      }
}


double CoupledMaterial::getStrain ()
{
      logMeNicely(this,"getStrain -> %+9.8lf\n",Tstrain);
      return Tstrain;
}


double CoupledMaterial::getStress ()
{
      logMeNicely(this,"getStress -> %+9.8lf\n",Tstress);
      return Tstress;
}


double CoupledMaterial::getTangent ()
{
      logMeNicely(this,"getTangent -> %+9.8lf\n",Ttangent);
      return Ttangent;
}
```

```
int CoupledMaterial::commitState ()
{

      CminStrain = TminStrain;
      CmaxStrain = TmaxStrain;
      CshiftP = TshiftP;
      CshiftN = TshiftN;
      Cloading = Tloading;

      Cstrain = Tstrain;
      Cstress = Tstress;
      Ctangent = Ttangent;

      return 0;
}


int CoupledMaterial::revertToLastCommit ()
{

      logMeNicely(this,"revertToLastCommit ()\n");

      TminStrain = CminStrain;
      TmaxStrain = CmaxStrain;
      TshiftP = CshiftP;
      TshiftN = CshiftN;
      Tloading = Cloading;

      Tstrain = Cstrain;
      Tstress = Cstress;
      Ttangent = Ctangent;

      return 0;
}


int CoupledMaterial::revertToStart ()
{

      logMeNicely(this,"revertToStart \n");

      CminStrain = 0.0;
      CmaxStrain = 0.0;
      CshiftP = 1.0;
      CshiftN = 1.0;
      Cloading = 0;

      TminStrain = 0.0;
      TmaxStrain = 0.0;
      TshiftP = 1.0;
      TshiftN = 1.0;
      Tloading = 0;

      Cstrain = 0.0;
      Cstress = 0.0;
      Ctangent = E0;
```

```
	Tstrain = 0.0;
	Tstress = 0.0;
	Ttangent = E0;

	if (SHVs != 0)
		SHVs->Zero();

	return 0;
}


UniaxialMaterial* CoupledMaterial::getCopy ()
{

	CoupledMaterial * theCopy = new CoupledMaterial (this-
>getTag(), fy, E0, b, a1, a2, a3, a4);

	theCopy->CminStrain = CminStrain;
	theCopy->CmaxStrain = CmaxStrain;
	theCopy->CshiftP = CshiftP;
	theCopy->CshiftN = CshiftN;
	theCopy->Cloading = Cloading;

	theCopy->TminStrain = TminStrain;
	theCopy->TmaxStrain = TmaxStrain;
	theCopy->TshiftP = TshiftP;
	theCopy->TshiftN = TshiftN;
	theCopy->Tloading = Tloading;

	theCopy->Cstrain = Cstrain;
	theCopy->Cstress = Cstress;
	theCopy->Ctangent = Ctangent;

	theCopy->Tstrain = Tstrain;
	theCopy->Tstress = Tstress;
	theCopy->Ttangent = Ttangent;

	theCopy->z=z;
	theCopy->pairMaterial=this->pairMaterial;
	theCopy->pairMaterialTag=this->pairMaterialTag;
	theCopy->isMasterMaterial=this->isMasterMaterial;
	return theCopy;
}


int CoupledMaterial::sendSelf (int commitTag, Channel& theChannel)
{

	int res = 0;
	static Vector data(16);
	data(0) = this->getTag();

	data(1) = fy;
	data(2) = E0;
	data(3) = b;
	data(4) = a1;
```

```
	data(5) = a2;
	data(6) = a3;
	data(7) = a4;

	data(8) = CminStrain;
	data(9) = CmaxStrain;
	data(10) = CshiftP;
	data(11) = CshiftN;
	data(12) = Cloading;

	data(13) = Cstrain;
	data(14) = Cstress;
	data(15) = Ctangent;

	res = theChannel.sendVector(this->getDbTag(), commitTag,
data);

	if (res < 0)
		opserr << "Steel01::sendSelf() - failed to send
		data\n";

	return res;
}


int CoupledMaterial::recvSelf (int commitTag, Channel& theChannel,
FEM_ObjectBroker& theBroker)
{
	int res = 0;
	static Vector data(16);
	res = theChannel.recvVector(this->getDbTag(), commitTag,
data);

	 if (res < 0)
	 {
		opserr << "Steel01::recvSelf() - failed to receive
		data\n";
		this->setTag(0);
	 }
	 else
	 {
		this->setTag(int(data(0)));
		fy = data(1);
		E0 = data(2);
		b = data(3);
		a1 = data(4);
		a2 = data(5);
		a3 = data(6);
		a4 = data(7);

		CminStrain = data(8);
		CmaxStrain = data(9);
		CshiftP = data(10);
		CshiftN = data(11);
		Cloading = int(data(12));
```

```
            TminStrain = CminStrain;
            TmaxStrain = CmaxStrain;
            TshiftP = CshiftP;
            TshiftN = CshiftN;
            Tloading = Cloading;

            Cstrain = data(13);
            Cstress = data(14);
            Ctangent = data(15);

            Tstrain = Cstrain;
            Tstress = Cstress;
            Ttangent = Ctangent;
      }

      return res;
}


void CoupledMaterial::Print (OPS_Stream& s, int flag)
{

      s << " CoupledMaterial tag: " << this->getTag() << endln;
      s << "  fy: " << fy << " ";
      s << "  E0: " << E0 << " ";
      s << "  b:  " << b << " ";
      s << "  a1: " << a1 << " ";
      s << "  a2: " << a2 << " ";
      s << "  a3: " << a3 << " ";
      s << "  a4: " << a4 << " ";

}


int
CoupledMaterial::setParameter(const char **argv, int argc,
Parameter &param)
{

      if (strcmp(argv[0],"sigmaY") == 0 || strcmp(argv[0],"fy") ==
0)
            return param.addObject(1, this);

      if (strcmp(argv[0],"E") == 0)
            return param.addObject(2, this);

      if (strcmp(argv[0],"b") == 0)
            return param.addObject(3, this);

      if (strcmp(argv[0],"a1") == 0)
            return param.addObject(4, this);

      if (strcmp(argv[0],"a2") == 0)
            return param.addObject(5, this);

      if (strcmp(argv[0],"a3") == 0)
```

```
		return param.addObject(6, this);

	if (strcmp(argv[0],"a4") == 0)
		return param.addObject(7, this);

	return -1;
}


int
CoupledMaterial::updateParameter(int parameterID, Information
&info)
{
	switch (parameterID) {
	case -1:
		return -1;
	case 1:
		this->fy = info.theDouble;
		break;
	case 2:
		this->E0 = info.theDouble;
		break;
	case 3:
		this->b = info.theDouble;
		break;
	case 4:
		this->a1 = info.theDouble;
		break;
	case 5:
		this->a2 = info.theDouble;
		break;
	case 6:
		this->a3 = info.theDouble;
		break;
	case 7:
		this->a4 = info.theDouble;
		break;
	default:
		return -1;
	}

	Ttangent = E0;          // Initial stiffness
	return 0;
}


int
CoupledMaterial::activateParameter(int passedParameterID)
{
	parameterID = passedParameterID;

	return 0;
}
```

```
double
CoupledMaterial::getStressSensitivity(int gradIndex, bool
conditional)
{
	double gradient = 0.0;

	double CstrainSensitivity = 0.0;
	double CstressSensitivity = 0.0;
	if (SHVs != 0)
	{
		CstrainSensitivity = (*SHVs)(0,gradIndex);
		CstressSensitivity = (*SHVs)(1,gradIndex);
	}


	double fySensitivity = 0.0;
	double E0Sensitivity = 0.0;
	double bSensitivity = 0.0;

	if (parameterID == 1)
	{
		fySensitivity = 1.0;
	}
	else if (parameterID == 2)
	{
		E0Sensitivity = 1.0;
	}
	else if (parameterID == 3)
	{
		bSensitivity = 1.0;
	}


	double Tstress;
	double dStrain = Tstrain-Cstrain;
	double sigmaElastic = Cstress + E0*dStrain;
	double fyOneMinusB = fy * (1.0 - b);
	double Esh = b*E0;
	double c1 = Esh*Tstrain;
	double c2 = TshiftN*fyOneMinusB;
	double c3 = TshiftP*fyOneMinusB;
	double sigmaMax = c1+c3;
	double sigmaMin = c1-c2;
	if ( (sigmaMax < sigmaElastic) && (fabs(sigmaMax-
sigmaElastic)>1e-5) )
	{
		Tstress = sigmaMax;
		gradient = E0Sensitivity*b*Tstrain
			+ E0*bSensitivity*Tstrain
			+ TshiftP*(fySensitivity*(1-b)-
			fy*bSensitivity);
	}
	else
	{
		Tstress = sigmaElastic;
		gradient = CstressSensitivity
```

```
                    + E0Sensitivity*(Tstrain-Cstrain)
                    - E0*CstrainSensitivity;
        }

        if (sigmaMin > Tstress) {
                gradient = E0Sensitivity*b*Tstrain
                        + E0*bSensitivity*Tstrain
                        - TshiftN*(fySensitivity*(1-b)-
                        fy*bSensitivity);
        }

          return gradient;
}


double
CoupledMaterial::getInitialTangentSensitivity(int gradIndex)
{

        if (parameterID == 2) {
                return 1.0;
        }
        else
        {
                return 0.0;
        }
}


int
CoupledMaterial::commitSensitivity(double TstrainSensitivity, int
gradIndex, int numGrads)
{

        if (SHVs == 0) {
                SHVs = new Matrix(2,numGrads);
        }

        double gradient = 0.0;
        double CstrainSensitivity = 0.0;
        double CstressSensitivity = 0.0;
        if (SHVs != 0) {
                CstrainSensitivity = (*SHVs)(0,gradIndex);
                CstressSensitivity = (*SHVs)(1,gradIndex);
        }


        double fySensitivity = 0.0;
        double E0Sensitivity = 0.0;
        double bSensitivity = 0.0;

        if (parameterID == 1)
        {
                fySensitivity = 1.0;
        }
```

```
	else if (parameterID == 2)
	{
		E0Sensitivity = 1.0;
	}
	else if (parameterID == 3)
	{
		bSensitivity = 1.0;
	}


	double Tstress;
	double dStrain = Tstrain-Cstrain;
	double sigmaElastic = Cstress + E0*dStrain;
	double fyOneMinusB = fy * (1.0 - b);
	double Esh = b*E0;
	double c1 = Esh*Tstrain;
	double c2 = TshiftN*fyOneMinusB;
	double c3 = TshiftP*fyOneMinusB;
	double sigmaMax = c1+c3;
	double sigmaMin = c1-c2;


	if ( (sigmaMax < sigmaElastic) && (fabs(sigmaMax-
sigmaElastic)>1e-5) )
	{
		Tstress = sigmaMax;
		gradient = E0Sensitivity*b*Tstrain
			+ E0*bSensitivity*Tstrain
			+ E0*b*TstrainSensitivity
			+ TshiftP*(fySensitivity*(1-b)-
			fy*bSensitivity);
	}
	else
	{
		Tstress = sigmaElastic;
		gradient = CstressSensitivity
			+ E0Sensitivity*(Tstrain-Cstrain)
			+ E0*(TstrainSensitivity-CstrainSensitivity);
	}

	if (sigmaMin > Tstress)
	{
		gradient = E0Sensitivity*b*Tstrain
			+ E0*bSensitivity*Tstrain
			+ E0*b*TstrainSensitivity
			- TshiftN*(fySensitivity*(1-b)-
			fy*bSensitivity);
	}


	(*SHVs)(0,gradIndex) = TstrainSensitivity;
	(*SHVs)(1,gradIndex) = gradient;

	return 0;
}
```

CURRICULUM VITAE

PERSONAL INFORMATION

Surname, Name: Özdemir, Gökhan
Nationality: Turkish (TC)
Date and Place of Birth: 01.05.1981, Gaziantep
Marital Status: Married
Phone: +90 (312) 210 5465
Fax: +90 (312) 287 8951
Email: ogokhan@metu.edu.tr

EDUCATION

2005-2010	Ph.D., Civil Engineering, METU
02–11.2009	Research Fellowship at State University of New York at Buffalo
2002-2005	MS, Civil Engineering, METU
1998-2002	BS, Civil Engineering, Gazi University
1991-1998	Fitnat Nuri Tekerekoğlu Anatolian High School

WORK EXPERIENCE

2004-Present	Research Assistant, Department of Civil Engineering, METU

PUBLICATIONS

1. **Ozdemir G.** and Constantinou M.C., "Evaluation of Equivalent Lateral Force Procedure in Estimating Seismic Isolator Displacements", Soil Dynamics and Earthquake Engineering, doi:10.1016/j.soildyn.2010.04.015, 2010.

2. Kalpakidis I.V., **Ozdemir G.**, Constantinou M.C. and Dargush G.F., "Lead-Rubber Bearing User Element with Strength Degradation", Computers and Structures, 2010, (to appear).

3. **Ozdemir G.** and Akyuz U., "Response of Isolated Buildings Under Bi-directional Near-Fault Ground Motions", 9th U.S. National and 10th Canadian Conference on Earthquake Engineering, 2010 (accepted).

4. **Ozdemir G.**, "Response of an Isolated Structure with Deteriorating Hysteretic Isolator Model", 14th European Conference on Earthquake Engineering, Skopje-Ohrid, Macedonia, 2010 (accepted).

5. **Ozdemir G.**, Yakut A. and Akyuz U., "Comparison of Responses of Existing 5-story Isolated RC Frame Under Two Different Isolator Models", Sakarya International Symposium on Earthquake Engineering, paper no: 1402, Sakarya, Turkey, 2009.

6. Pinarbasi S., Akyuz U. and **Ozdemir G.**, "An Experimental Study on Low Temperature Behavior of Elastomeric Bridge Bearings", 10th World Conference on Seismic Isolation, Energy Disspation and Active Vibrations Control of Structures, Istanbul, Turkey, 2007.

7. **Ozdemir G.** and Akyuz U., "Tensile Capacities of CFRP Anchors", Seismic Assessment and Rehabilitation of Existing Buildings", ed. Wasti S.T. and Ozcebe G., 2006.

8. Pinarbasi S, **Ozdemir G.** and Akyuz U., "An Experimental Study on Behavior of Low Shape Factor Rubber Bearings Under Large Compressions", International Conference on Earthquake Engineering, paper no: E178, Skopje-Ohrid, Macedonia, 2005.

9. **Ozdemir G.** and Akyuz U., "Tensile Capacities of CFRP Anchors", ACI Special Publication, Vol. 230, pp 39-56, USA, 2005.

10. **Ozdemir G.**, "Mechanical Properties of CFRP Anchorages", M.S. Thesis, Middle East Technical University, 2005.

11. Akyuz U. and **Ozdemir G.**, "Mechanical Properties of CFRP Anchorages", 13th World Conference on Earthquake Engineering, paper no: 3349, Vancouver, Canada, 2004.

12. Akyuz U. and **Ozdemir G.**, "CFRP Ankrajların Mekanik Özelliklerinin Belirlenmesi", TÜBİTAK – Yapı Mekaniği Laboratuvarları Toplantısı II, 159-162, Konya, 2003.